

Copyright

by

Michael Joseph Murphy

2012

**The Thesis Committee for (Michael Joseph Murphy)
Certifies that this is the approved version of the following thesis:**

**Experimental Analysis of Electrostatic and Hydrodynamic Forces Affecting
Nanoparticle Retention in Porous Media**

**APPROVED BY
SUPERVISING COMMITTEE:**

Supervisor:

Steven Bryant

Chun Huh

**Experimental Analysis of Electrostatic and Hydrodynamic Forces Affecting
Nanoparticle Retention in Porous Media**

by

Michael Joseph Murphy, BS PE

Thesis

Presented to the Faculty of the Graduate School of
The University of Texas at Austin
in Partial Fulfillment
of the Requirements
for the Degree of

Master of Science in Engineering

The University of Texas at Austin

May, 2012

Dedication

To my parents from whom I see the best of myself reflected.

Acknowledgements

I'd like to thank Dr. Bryant for his guidance and incredible attitude these past 2 years. His enthusiasm for scientific discovery was contagious and I'm very grateful to have been part of his research team. Glen Baum for his invaluable aid in setting up and frequently repairing my experimental equipment. Federico Caldelas for introducing me to graduate school and research work. Dr. Huh for his helpful contributions to my research. Andrew Worthen and Ki Youl Yoon for their generous assistance with laboratory measurements. Tina Zhang for her modeling work and her saintly patience. Dr. Jim Baran provided samples for many of the nanoparticles used in this research. Finally, I'd like to thank the Advanced Energy Consortium for its sponsorship that made this work possible.

Abstract

Experimental Analysis of Electrostatic and Hydrodynamic Forces Affecting Nanoparticle Retention in Porous Media

Michael Joseph Murphy, M.S.E.

The University of Texas at Austin, 2012

Supervisor: Steven Bryant

There have been significant advances in the research of nanoparticle technologies for formation evaluation and reservoir engineering operations. The target applications require a variety of different retention characteristics ranging from nanoparticles that adsorb near the wellbore to nanoparticles that can travel significant distances within the porous medium with little or no retention on the grain substrate. A detailed understanding of the underlying mechanisms that cause nanoparticle retention is necessary to design these applications. In this thesis, experiments were conducted to quantify nanoparticle retention in unconsolidated columns packed with crushed Boise sandstone and kaolinite clay. Experimental parameters such as flow rate, injected concentration and sandpack composition were varied in a controlled fashion to test hypotheses concerning retention mechanisms and enable development and validation of a mathematical model of nanoparticle transport. Results indicate nanoparticle retention, defined as the

concentration of nanoparticles remaining attached to grains in the porous medium after a volume of nanoparticle dispersion is injected through the medium and then displaced with brine, is a function of injected fluid velocity with higher injected velocities leading to lower retention. In many cases nanoparticle retention increased nonlinearly with increasing concentration of nanoparticles in the injected dispersion. Nanoparticle retention concentration was found to exhibit an upper bound beyond which no further adsorption from the nanoparticle dispersion to the grain substrate occurred. Kaolinite clay was shown to exhibit lower retention concentration [mg/m^2] than Boise sandstone suggesting DLVO interactions do not significantly influence nanoparticle retention in high salinity dynamic flow environments.

Table of Contents

Chapter: 1	Introduction.....	1
1.1	Nanotechnology Research for Application in Petroleum Engineering..	1
1.2	Transport Mechanisms.....	2
1.3	Research Objectives.....	4
Chapter: 2	Experimental Procedure to Measure Nanoparticle Transport and Retention	6
2.1	Materials	6
2.2	Apparatus	7
2.2.1	Vacuum Saturation.....	8
2.2.1.1	Injection Apparatus (Setup 1)	9
2.2.1.2	Injection Apparatus (Setup 2)	11
2.2.2	Injection Apparatus (Setup 3)	12
2.2.3	Definitions of Important Quantities and Methods Used to Calculate Them	13
Chapter: 3	Results.....	18
3.1	The Effect of Air Saturation on Nanoparticle Transport	20
3.2	Effect of Injected Nanoparticle Concentration On Retention Concentration	24
3.2.1	The Effect of Injected Concentration of Nexsil DP Nanoparticle at Low Velocities without Clay	25
3.2.2	The Effect of Injected Concentration on Nexsil DP Nanoparticle Transport at High Velocities with Clay	26
3.2.3	The Effect of Injected Concentration of Nexsil DP Nanoparticle at Low Velocity with Clay.....	28
3.2.4	The Effect of Injected Concentration of Fluorescently Tagged Silica Nanoparticle	30
3.3	Quantifying the Retention Concentration of Kaolinite.....	32
3.3.1	The Effect of Kaolinite Content on Retention Concentration of Salt Tolerant 3M particles	33
3.3.2	The Effect of Kaolinite Content on Retention Concentration of Nexsil DP Particles	35

3.4	The Effect of Constant Flow Rate on Retention Concentration	39
3.5	The Effect of Step Change Flow Rate on Retention Concentration	44
3.6	The Effect of Dispersion Reinjection and Secondary Slug Injections on Retention Concentration	48
3.6.1	Injection of Fresh Dispersion Into Postflushed Sandpack	48
3.6.2	Injection of Fresh Dispersion at Lower Flow Rate After Postflush	50
3.6.3	Injection of Effluent Dispersion from One Sandpack Into Fresh Sandpack	51
3.7	The Effect of Temporary Flow Cessation on Nanoparticle Transport	56
3.8	The Effect of Injected Slug Size on Retention Concentration	61
Chapter: 4	Conclusions	65
4.1	Experimental Findings	65
4.2	Future Work	66
A	Appendix	71
A.1	Experimental	71
A.1.1	Nanoparticle Dispersion Dilution	71
A.1.2	Sand Acquisition and Washing	76
A.1.3	Sandpack Preparation and Packing	79
A.1.4	Sandpack Vacuum Saturation	80
A.1.5	Sandpack Characterization	81
A.1.6	Zeta Potential	82
A.1.7	Tracer Test	83
A.1.8	Effluent Concentration Using Refractometer	85
A.1.9	Effluent Concentration Using UV Detector	87
A.2	Procedure	89
A.2.1	Sand Acquisition	89
A.2.2	Sand Packing and Saturation	90
A.2.3	Experimental Apparatus Setup (for Setup 1, 2 and 3)	91
A.2.4	Brine Tracer Experiment	92
A.2.5	Nanoparticle Injection (For Experimental Apparatus Setup 1) ..	92

A.2.6 Nanoparticle Injection (For Experimental Apparatus Setup 2 and 3)	93
A.3 Runs	95
A.3.1 Experimental Parameters	95
A.3.2 Results Summary	96
A.3.3 Effluent Histories	104
A.3.3.1 Experiment 59*	104
A.3.3.2 Experiment 60	105
A.3.3.3 Experiment 61*	106
A.3.3.4 Experiment 62	107
A.3.3.5 Experiment 63	108
A.3.3.6 Experiment 64	109
A.3.3.7 Experiment 65	110
A.3.3.8 Experiment 66	111
A.3.3.9 Experiment 67	112
A.3.3.10 Experiment 68	113
A.3.3.11 Experiment 69	114
A.3.3.12 Experiment 70	115
A.3.3.13 Experiment 71	116
A.3.3.14 Experiment 72	117
A.3.3.15 Experiment 73	118
A.3.3.16 Experiment 74	119
A.3.3.17 Experiment 75	120
A.3.3.18 Experiment 76	121
A.3.3.19 Experiment 77	122
A.3.3.20 Experiment 78	123
A.3.3.21 Experiment 79	124
A.3.3.22 Experiment 80	125
A.3.3.23 Experiment 81	126
A.3.3.24 Experiment 82	127
A.3.3.25 Experiment 83	128

A.3.3.26	Experiment 84	129
A.3.3.27	Experiment 85	130
A.3.3.28	Experiment 86	131
A.3.3.29	Experiment 91	133
A.3.3.30	Experiment 92	134
A.3.3.31	Experiment 93	135
A.3.3.32	Experiment 94 (Part 1)	136
A.3.3.33	Experiment 94 (Part 2)	137
A.3.3.34	Experiment 95	137
A.3.3.35	Experiment 96	138
A.3.3.36	Experiment 97	139
A.3.3.37	Experiment 98	140
A.3.3.38	Experiment 99 (Part 1)	141
A.3.3.39	Experiment 99 (Part 2)	142
A.3.3.40	Experiment 100	143
A.3.3.41	Experiment 101	144
A.3.3.42	Experiment 102	145
A.3.3.43	Experiment 103	146
A.3.3.44	Experiment 104	147
Nomenclature		148
References		150
VITA		153

List of Tables

Table 3.1: Summary of Experimental Parameters Explored	19
Table 3.2: Data for Air Saturation Sensitivity Data (Salt Tolerant 3M).....	23
Table 3.3: Data for Injection Concentration Sensitivity (No Clay at Low Flow Rate) For Nexsil DP Nanoparticles	25
Table 3.4: Data for Injection Concentration Sensitivity (Nexsil DP with Clay at High Flow Rate).....	27
Table 3.5 : Data for Injection Concentration Sensitivity (Nexsil DP with Clay at Low Flow Rate).....	28
Table 3.6: Data for Fluorescently Tagged 3M Injection Concentration Sensitivity	31
Table 3.7: Data for Kaolinite Content Sensitivity (Salt Tolerant 3M)	34
Table 3.8: Data for Kaolinite Content Sensitivity (Nexsil DP)	36
Table 3.9: Data for Constant Flow Rate Sensitivity	41
Table 3.10: Data for Step Change Flow Rate Experiments	46
Table 3.11: Data For Reinjection Experiments (100% Boise Sandstone Packs)	53
Table 3.13: Data for Pump Stop Experiments (3M Fluorescent Nanoparticles Injected into Boise Sandstone Packs)	57
Table 3.14: Data for Injected Slug Size Sensitivity Study (Salt Tolerant 3M Nanoparticles)	62
Table A.1: Diluting 20.11 wt% Salt Tolerant 3M to 5 wt% Salt Tolerant 3M with 3 wt% NaCl.....	71
Table A.2: Diluting 5 wt% Nexsil DP to 5 wt% Nexsil DP with 3 wt% NaCl	72

Table A.3: Diluting 30 wt% Nexsil DP to 3.5 wt% Nexsil DP with 3 wt% NaCl	72
Table A.4: Diluting 30 wt% Nexsil DP to 2.6 wt% Nexsil DP with 3 wt% NaCl	73
Table A.5: Diluting 30 wt% Nexsil DP to 1.5 wt% Nexsil DP with 3 wt% NaCl.....	73
Table A.6: Diluting 30 wt% Nexsil DP to 1.4 wt% Nexsil DP with 3 wt% NaCl	74
Table A.7: Diluting 20.6 wt% Fluorescent PEG 3M to 5 wt% Fluorescent PEG 3M with 3wt% NaCl.....	74
Table A.8: Diluting 20.6 wt% Fluorescent PEG 3M to 1 wt% Fluorescent PEG 3M with 3 wt% NaCl.....	75
Table A.9: Diluting 20.6 wt% Fluorescent PEG 3M to 0.1 wt% Fluorescent PEG 3M with 3 wt% NaCl.....	75
Table A.10: BET Measurements.....	82
Table A.11: Zeta Potential Measurements.....	83
Table A.12: Results Summary	103

List of Figures

Figure 2.1: Vacuum Saturation Apparatus.....	9
Figure 2.2: Injection Apparatus Schematic (Setup 1):.....	11
Figure 2.3: Injection Apparatus Schematic (Setup 2):.....	12
Figure 2.4: Apparatus Schematic (Setup 3):.....	13
Figure 3.1: Calculated Air Filled Porosity.....	22
Figure 3.4: Sensitivity of Nexsil DP Retention Concentration to Injection Concentration (with Clay at High Flow Rate).....	27
Figure 3.5: Sensitivity of Retention Concentration to Injection Concentration (All Nexsil DP Cases).....	29
Figure 3.7: Retention Concentration vs. Kaolinite Content (Salt Tolerant 3M)....	33
Figure 3.8: Incremental Nanoparticle Retention Concentration (mg/m^2) vs. Kaolinite Content for (Salt Tolerant 3M Nanoparticles Injected at 5 wt%).....	35
Figure 3.9: Retention Concentration vs. Kaolinite Content (Nexsil DP).....	36
Figure 3.10: Incremental Nanoparticle Retention Concentration vs. Kaolinite Content (Nexsil DP).....	37
Figure 3.11: Sensitivity of Effluent Concentration History to Constant Flow Rate (Iron Oxide) [Experiments 91 and 92].....	39
Figure 3.12 Sensitivity of Effluent Concentration History to Constant Flow Rate (Nexsil DP) [Experiments 68 and 80].....	40
Figure 3.13: Sensitivity of Effluent Concentration History to Constant Flow Rate (Salt Tolerant 3M) [Experiments 66 and 67].....	40
Figure 3.14: Step Change Flow Rate Effluent History ($q = 9.3 \text{ mL}/\text{min}$ for $t_p < 2.7$ PV , $q = 1.07 \text{ mL}/\text{min}$ for $t_p > 2.7 PV$).....	45

Figure 3.15: Step Change Flow Rate Effluent History ($q = 0.87$ mL/min for $t_p < 4.4$ PV, $q = 10$ mL/min for $t_p > 4.4$ PV).....	45
Figure 3.16: Effluent History of Second Nanoparticle Slug Injection for Experiment 94.....	49
Figure 3.17: Sensitivity of Transport of Fluorescent 3M Nanoparticles to Nanoparticle History; Effluent Nanoparticles from Experiment 96 Were Injected Into New Sandpack in Experiment 97	52
Figure 3.18: Effluent ReInjection Sensitivity Study (Salt Tolerant Silica)	55
Figure 3.19: Pump Stop Sensitivity Study Effluent Histories	57
Figure 3.20: Extrapolated Effluent Histories for Pump Stop Experiments	58
Figure 3.21: Summarized Results from Pump Stop Sensitivity	59
Figure 3.22: Injected Slug Size Sensitivity Study	62
Figure 3.23: Experiment 65 Data Extrapolated to $C_D = 1$	64
Figure A.1: Boise Sandstone Source Block (1 Foot Tape Measure for Scale).....	76
Figure A.2: Mortar and Pestle.....	77
Figure A.3: Cuisinart Blender.....	77
Figure A.4: Mesh Sieves loaded into Ro-Tap Sieve Shaker.....	77
Figure A.5: Blue M Series Oven.....	78
Figure A.6: 1 ft Slim-Tube Column.....	79
Figure A.8: Orion 3Star Conductivity Probe	84
Figure A.9: Nexsil DP Refractive Index Calibration Curve	85
Figure A.10: Salt Tolerant 3M Refractive Index Calibration Curve	86
Figure A.11: Leica Mark II Plus Refractometer	87
Figure A.12: Fluorescent 3M PEG UV Calibration Curve.....	88
Figure A.13: Ultimate 3000 UV-Vis detector.....	89

Figure A.14: Experiment 59 Effluent History	104
Figure A.15: Experiment 32 Effluent History	104
Figure A.16: Experiment 60 Effluent History	105
Figure A.17: Experiment 61 Effluent History	106
Figure A.18: Experiment 62 Effluent History	107
Figure A.19: Experiment 63 Effluent History	108
Figure A.20: Experiment 64 Effluent History	109
Figure A.21: Experiment 65 Effluent History	110
Figure A.22: : Experiment 66 Effluent History	111
Figure A.23: Experiment 67 Effluent History	112
Figure A.24: Experiment 68 Effluent History	113
Figure A.25: Experiment 69 Effluent History	114
Figure A.26: Experiment 70 Effluent History	115
Figure A.27: Experiment 71 Effluent History	116
Figure A.28: Experiment 72 Effluent History	117
Figure A.29: Experiment 73 Effluent History	118
Figure A.30: Experiment 74 Effluent History	119
Figure A.31: Experiment 75 Effluent History	120
Figure A.32: Experiment 76 Effluent History	121
Figure A.33: Experiment 77 Effluent History	122
Figure A.34: Experiment 78 Effluent History	123
Figure A.35: Experiment 79 Effluent History	124
Figure A.36: Experiment 80 Effluent History	125
Figure A.37: Experiment 81 Effluent History	126
Figure A.38: Experiment 82 Effluent History	127

Figure A.39: Experiment 84 Effluent History	129
Figure A.40: Experiment 85 Effluent History	130
Figure A.41: Experiment 86 Effluent History	131
Figure A.42: Experiment 91 Effluent History	133
Figure A.43: Experiment 92 Effluent History	134
Figure A.44: Experiment 93 Effluent History	135
Figure A.45: Experiment 94 (Part 1) Effluent History	136
Figure A.46: Experiment 94 (Part 2) Effluent History	137
Figure A.47: Experiment 96 Effluent History	138
Figure A.48: Experiment 97 Effluent History	139
Figure A.49: Experiment 98 Effluent History	140
Figure A.50: Experiment 99 Part 1 Effluent History	141
Figure A.51: Experiment 99 Part 2 Effluent History	142
Figure A.52: Experiment 100 Effluent History	143
Figure A.53: Experiment 101 Effluent History	144
Figure A.54: Experiment 102 Effluent History	145
Figure A.55: Experiment 103 Effluent History	146
Figure A.56: Experiment 104 Effluent History	147

Chapter: 1 Introduction

This thesis is divided into four chapters. In this first chapter, a literature review describing current research into nanoparticle technology details potential uses for nanotechnology in upstream operations; and describes current understanding on mechanisms for nanoparticle transport through porous media. The second chapter describes the experimental apparatus built for the experiments described in this thesis. The third chapter elucidates our findings and proposes likely implications. The fourth chapter summarizes the findings from this thesis and recommends future work to be undertaken. Finally the Appendix describes the experimental apparatus and procedure in detail and lists experimental variables and results for each run undertaken.

1.1 NANOTECHNOLOGY RESEARCH FOR APPLICATION IN PETROLEUM ENGINEERING

Nanotechnology is currently used in a broad range of applications from cutting edge drug delivery to surface coatings on photovoltaic solar panels. Recent investments in petroleum engineering-specific nanotechnology research from organizations such as the Advanced Energy Consortium have spurred efforts to apply existing use in the energy industry. A nanotechnology of particular interest is the synthesis of nanoparticles with engineered surface coatings.

Drilling applications include new nanoparticle-enhanced drilling fluids capable of significant reduction of wear on the drill bit and increased drilling speeds (Krishnamoorti,

2006). Mixing cement with nanosilica and nano iron oxide components can enhance compressive and flexural strengths satisfying the need for robust cement in deep offshore wells. (Li, H et al., 2004). Nanotechnology can also be applied in the form of corrosion-resistant coatings on piping and drilling equipment, significantly extending their useful life in harsh environments (P. Pourafshary, 2009).

In production and EOR applications fluorescently tagged nano beads have shown promise as the base for a next generation tracer (Agenet, 2012). Nano iron oxide and copper particles have proven to be excellent catalysts helping to break carbon-sulfur bonds within asphaltenes, significantly reducing the viscosity of heavy oils (Greff, 2011). Nano-sized silica dispersion has been successfully applied to laboratory proppant packs to mitigate fines migration (Huang et al., 2008). Research has also shown that low concentrations of nanoparticles used in viscoelastic surfactant floods can significantly enhance fluid viscosity and increase thermal stability of the chemical flood (Huang et al., 2008).

1.2 TRANSPORT MECHANISMS

Use of nanoparticles for tasks such as chemical flooding and tracers require that the nanoparticle dispersion be able to travel significant distance within the porous medium. A detailed understanding of the transport mechanisms and variables which affect nanoparticle retention will be necessary to confirm such applications are possible. A literature review of the currently available publications on nanoparticle transport mechanisms follows.

Well established models exist to explain the transport of colloidal particles size ($\sim 10^{-6}m$) and molecules ($\sim 10^{-10}m$) in a porous medium. Nanoparticles, sized around ($\sim 10^{-8}m$), fall between colloidal particles and molecules and share characteristics from both in their transport behavior. Colloidal particle transport through porous media is dominated by particle straining and retention on the grain surface. As particles flow through the porous medium some particles become trapped behind pore throats too small to allow passage (straining) while attractive interactions between particle and grain surface cause other particles to become irreversibly adsorbed onto the porous medium grain surface (filtration). The classical filtration theory was used by Benamar et al. (2007) to describe colloidal transport and has been adapted by Wang et al. (2008) to describe nanoparticle transport and capture the effects of fluid velocity and dispersivity on nanoparticle retention characteristics. In batch experiments (Shahavi, 2011) nanoparticle retention data were successfully fit to a Langmuirian isotherm suggesting nanoparticle retention accompanying flow of dispersions in porous media will be a function of injected concentration.

A significant body of research has developed to describe variables that affect nanoparticle retention in porous media. Alaskar et al. (2011) found nanoparticle shape to significantly affect retention. The small size of nanoparticles allows most nanoparticle dispersions to slip through pore throats with minimal straining. This was found to be particularly true for spherically shaped nanoparticles. Conversely, experiments involving dispersed nanowire exhibited significant straining with no significant transport through the sandstone core. Saleh et al. (2006) found the electrostatically stabilizing effects of

some surfactant coatings significantly enhanced the transport of nanoiron particles through porous media. Aggregation of bare nanoiron particles increased mean cluster size and led to significant particle straining. PMAA-PMMA-PSS triblock copolymers significantly enhanced the ability of nano-iron to transport reducing the tendency of particles to aggregate and reducing electrostatic interactions between particle clusters and the grain substrate with the porous medium. Lecoanet et al. (2004) injected nano-sized anatase clusters and silica nanoparticles through glass bead porous media and found retention was closely linked to the Darcy velocity of injected fluid with slow velocities leading to larger retentions. Finally, Caldelas et al. (2010) performed extensive set of columnflood experiments which indicated nanoparticle retention was most strongly linked to the surface area of the porous medium. Those experiments also suggested brine salinity and composition could affect nanoparticle retention. Specifically, porous media saturated with API brine (8 wt% NaCl and 2 wt% CaCl₂) rather than 3 wt% NaCl brine exhibited significantly higher nanoparticle retention.

1.3 RESEARCH OBJECTIVES

This thesis expands on research started by Caldelas (2010) documenting nanoparticle retention in slim tube sand packs. The focus is on nanoparticles that exhibit minimal attraction to the surfaces of grains in sedimentary rocks. Examples of such nanoparticles include those with the same charge as the rock grains (e.g. charge-stabilized dispersions of uncoated nanoparticles) and nanoparticles with suitable polymer chains attached to their surface (e.g. PEG-coated silica nanoparticles). The overall objective is to determine how far and at what concentration such nanoparticles could be propagated

through reservoir rocks. The research objective is to identify and quantify the mechanisms of interaction between weakly attracted nanoparticles and typical rock grain surfaces as a nanoparticle dispersion flows past the grains. Thus experiments were conducted to explore the effect of parameters such as fluid velocity, injected nanoparticle dispersion concentration, surface area of the porous medium, and composition of the porous medium substrate on nanoparticle retention; and thereby to develop a better understanding of the mechanisms affecting their transport through porous media. Comprehensive characterization of the injected nanoparticle dispersions and slim tube sandpacks was performed to ensure that results could be used to test transport models as rigorously as possible. In this thesis a key measure of transportability is the retention concentration defined in Chapter 2. This corresponds to the mass of nanoparticles per unit surface area of sand that remain in the sandpack after an extensive postflush with brine. Such particles can be considered “permanently” retained at least at the conditions of the experiment. This measure is of particular relevance to field applications that are likely to involve injection of a finite volume (a slug) of nanoparticle dispersion, which is then displaced with another fluid.

Chapter: 2 Experimental Procedure to Measure Nanoparticle Transport and Retention

2.1 MATERIALS

Silica nanoparticles with a polyethylene glycol coating were received from 3M® as 20.6 wt% aqueous dispersions. These particles were fluorescently tagged, so that their concentration in brine could be accurately measured with a UV-spectrometer. The silica core was 5 nm in diameter and the PEG coating brings the particle to a nominal 10 nm diameter. Computed monolayer coverage, Equation 2.6, for this particle is $0.099041 * R_{conc}$, where R_{conc} is the retention concentration, Equation 2.3.

“Salt Tolerant 3M” with an undisclosed Salt Tolerant coating was received from 3M® as 20.11 wt% aqueous dispersions. The particles had a nominal diameter of 15 nm as measured via dynamic light scattering. The dispersion had a zeta potential of -3.22 ± 3.05 mV in the presence of 3 wt% NaCl. Both measurements are courtesy of Andrew Worthen (UT Chemical Engineering). Computed monolayer coverage for this particle is $0.066027 * R_{conc}$, where R_{conc} is the retention concentration, Equation 2.3.

“Nexsil DP” nanoparticles with an undisclosed coating were received from Nyalcol Nano Technologies® in 30 wt% dispersions. The particles had a nominal diameter of 27 nm as measure by Andrew Worthen via dynamic light scattering. The dispersion had a zeta potential of -3.91 ± 2.01 mV in the presence of 3 wt% NaCl. Computed monolayer coverage, Equation 2.6, for this particle is $0.036682 * R_{conc}$, where R_{conc} is the retention concentration, Equation 2.3.

“NexSil 20” silica nanoparticles with no surface-coating were received from Nyalcol Nano Technologies® in a 30 wt% aqueous dispersion. These particles were charge stabilized and were not Salt Tolerant. All experiments run with NexSil 20 were performed without NaCl added to the dispersion, saturating fluid or flushed fluid to avoid excessive aggregation of nanoparticles or solidification of the dispersion fluid. The

nominal diameter for this particle as reported by Nyacol Nano Technologies® is 20 nm. The dispersion had a zeta potential of -50.51 ± 2.26 mV when diluted to 5 wt% with deionized water. Computed monolayer coverage, Equation 2.6, for this particle is $0.049521 * R_{conc}$ mg/m², where R_{conc} is the retention concentration, Equation 2.3.

Iron oxide particles with various coatings were provided by Dr. Hitesh Bagaria of the University of Texas at Austin. Each batch consisted of approximately 1 wt% iron oxide dispersed in deionized water. Aggregate particle size was determined using dynamic light scattering and varied between batches. The iron oxide particle density is approximated as 2.52 g/cm³ and the average nominal diameter of the particle clusters is 150 nm. With these values the computed monolayer coverage, Equation 2.6, for this particle is $0.004376 * R_{conc}$, where R_{conc} is the retention concentration, Equation 2.3.

Dispersions were diluted with deionized water (Nanopure) and mixed with laboratory grade sodium chloride (NaCl, Fisher Scientific) to obtain the desired salinity using a process described in section A.1.1 of the Appendix. The remains of large Boise sandstone rocks used to cut cores for other projects were crushed and sieved to separate the different grain sizes in a process described in section A.1.2 of the Appendix. Kaolinite (Wards Scientific) was used as received in powdered form. Mesoporous silica (Grace) was used as received.

2.2 APPARATUS

The experimental apparatus was purposely built for the experiments described in this thesis. Early experiments used a refractometer to measure effluent concentrations, as implemented by Caldelas (2010). The effluent was collected as 2 to 3 mL samples in borosilicate glass test tubes by a fraction collector (Injection Apparatus Setup 1 of Figure 2.2). Later experiments run at lower injected concentrations required a more sensitive instrument to measure effluent concentrations and the refractometer was replaced with a

UV spectrometer (Injection Apparatus Setup 2 of Figure 2.3). Flow experiments were run through slim tubes packed with unconsolidated Boise sandstone and kaolinite clay. The slim tubes were stainless steel, 1 foot in length, with an inner diameter of 0.43 inches. Ground and sieved Boise sandstone and kaolinite were loaded into the slim tubes with a funnel. A detailed description of the components used in both these setups follows below.

A few of the earliest experiments in this thesis involved saturating the sandpack by simply flowing several pore volumes of brine through the slim tube after packing. Most of the sandpacks used in this research were saturated using a vacuum pump as described below. A complete list of the saturation methods used for each experiment can be found in section A.3 of the Appendix.

2.2.1 Vacuum Saturation

To ensure the sand pack was 100% brine saturated before the injection of nanoparticle dispersion, an Edwards E2M2 vacuum pump was used to evacuate all air from the packed column. Two-way Swagelok valves were used to shut off the columns connection to the vacuum pump downstream and open the connection to a brine-filled graduated cylinder upstream. The near-vacuum pressure in the column pulled brine from the graduated cylinder into the sand pack when the upstream valve was opened. The column was connected to this saturation apparatus with 1/8th inch stainless steel Swagelok® quick connects. These quick connects ensure no fluid loss occurred when the column was removed from the saturation apparatus. A labeled illustration of the saturation apparatus can be found in Figure 2.1 below.

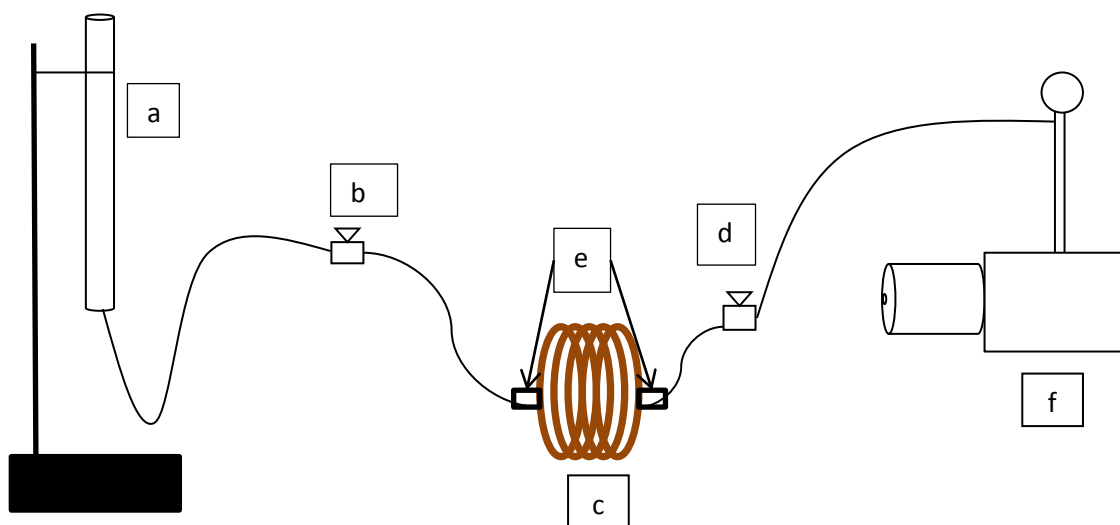


Figure 2.1: Vacuum Saturation Apparatus: (a) Graduated Cylinder Containing Brine (b) Upstream 2-way valve (c) Slim Tube Sandpack (d) Downstream Valve (e) Swagelok Quick Connects (f) Edwards vacuum pump

2.2.1.1 Injection Apparatus (Setup 1)

Injection Apparatus (Setup 1) was designed specifically for these experiments. Figure 2.2 shows a schematic of the apparatus. The pump used is a Lab Alliance 3000 capable of a 12 ± 0.05 mL/min flow rate. During brine injection fluid flowed directly from the pump to the sand pack. For nanoparticle injection, 3-way Swagelok valves were used to direct flow from the pump to the upstream end of the accumulator. Pressure from the pump moved the accumulator piston which in turn propelled nanoparticle dispersion fluid, previously loaded into the accumulator downstream of the accumulator piston, into the sand pack. The Refractive Index (RI) of each of the effluent samples was measured using a Leica Mark II Plus Refractometer. The relationship between nanoparticle concentration and refractive index was found to be linear for the range of concentrations used; calibration curves for nanoparticle dispersions examined with this approach can be

found in section A.1.8 of the Appendix. Using the trapezoid rule, the area under the concentration vs. pore volume injected curve (effluent concentration history) was calculated. This provides a value for the mass of nanoparticles recovered in pore volumes at the injected concentration. Dividing this value by mass of nanoparticles injected, which is the number of pore volumes injected (PVI) multiplied by the concentration of nanoparticles in the injected dispersion, gives the nanoparticle recovery as a fraction of nanoparticle pore volume injected (R_{NP}) as shown in Equation 2.1. A small number of experiments also made use of a Cray 500 UV spectrometer to compare concentration measurements using UV spectroscopy with those measured using a refractometer in order to validate that a UV spectrometer could be used to accurately measure nanoparticle concentration.

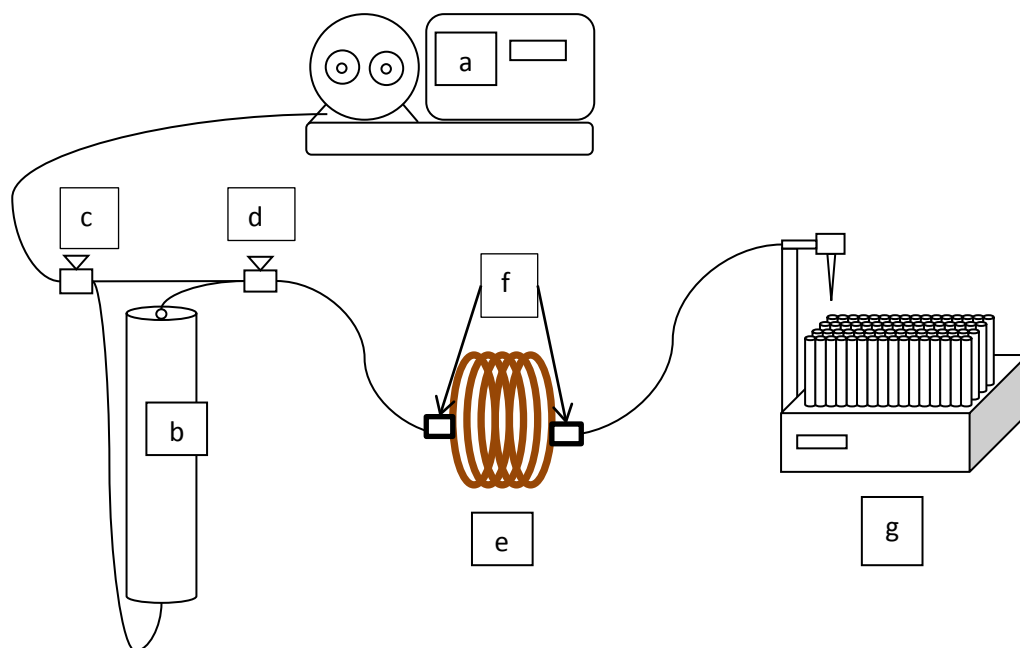


Figure 2.2: Injection Apparatus Schematic (Setup 1): (a) Pump, (b) Accumulator, (c) Upstream valve (d) Downstream Valve, (e) Slim Tube Sandpack, (f) Swagelok Quick Connects, (g) Fraction Collector.

2.2.1.2 Injection Apparatus (Setup 2)

In later experiments, Injection Apparatus (Setup 1) was adapted to create Injection Apparatus (Setup 2). The fraction collector and refractometer were replaced with an UltiMate 3000 Variable Wavelength Detector. The UV detector was a significantly more sensitive instrument allowing for accurate readings in experiments with low injected concentrations. The examination wavelength for these experiments was adjusted so measured absorbance and nanoparticle concentration maintained a linear relationship. Representative calibration curves and a detailed description of other factors affecting accuracy which are specific to the UV detector can be found in the Appendix. A graduated cylinder was added to collect effluent and track volume of effluent produced as

a function of time. In all other respects, Apparatus (Setup 1) and Apparatus (Setup 2) are identical.

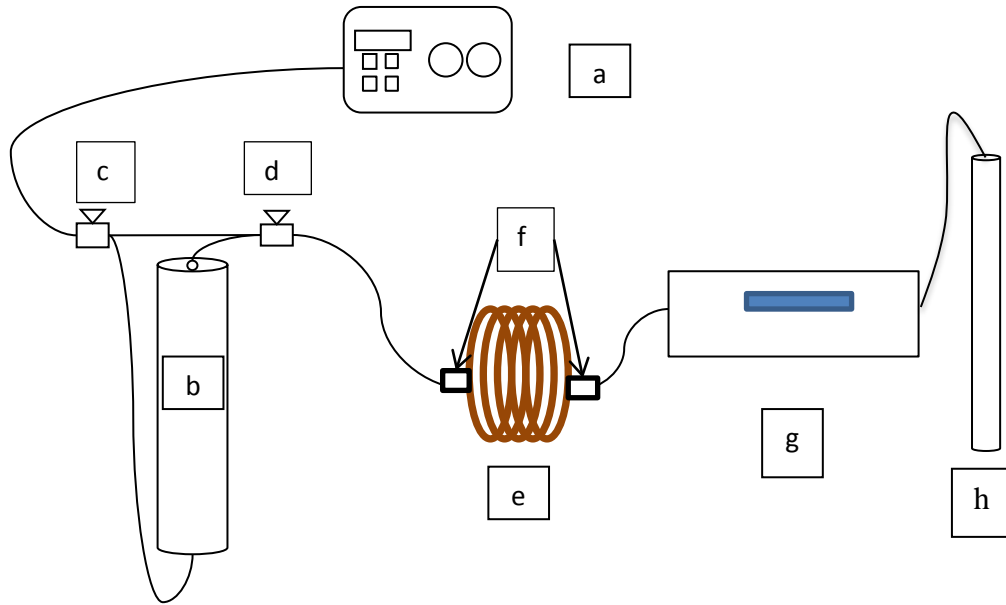


Figure 2.3: Injection Apparatus Schematic (Setup 2): (a) Pump, (b) Accumulator, (c) Upstream 3-Way Valve, (d) Downstream 3-Way Valve, (e) Slim Tube Sandpack, (f) Swagelok Quick Connects, (g) UltiMate 3000 UVD (h) 100 mL Graduated Cylinder

2.2.2 Injection Apparatus (Setup 3)

A New Classic MS Precision balance was added to Apparatus (Setup 2) to form Apparatus (Setup 3). The addition of the balance allowed fluid injection to be measured with high accuracy as a function of time allowing experiments with high injection concentrations to be performed with more accurately measured effluent histories and thus more accurately measured retention.

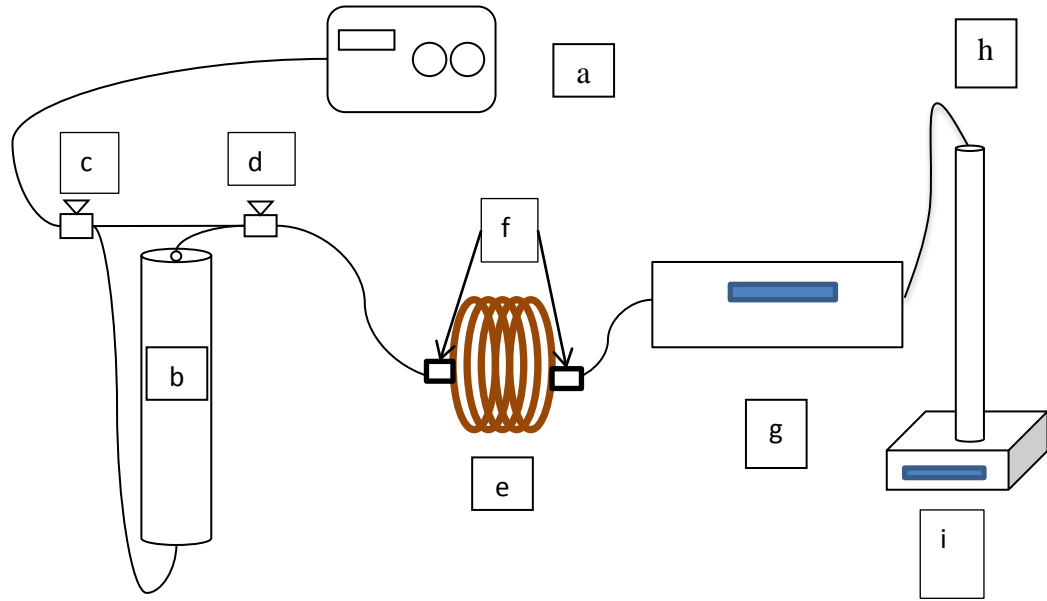


Figure 2.4: Apparatus Schematic (Setup 3): (a) Pump, (b) Accumulator, (c) Upstream 3-way valve, (d) Downstream 3-way valve, (e) Slim tube sandpack, (f) Swagelok Quick Connects, (g) UltiMate 3000 UVD (h) 100 mL graduated cylinder (i) MS precision balance

Each experiment was preceded by a passive tracer test to characterize the dispersivity of the packed slim tube. In-depth descriptions of these tracer tests and process for measuring effluent concentration by refractive index (Injection Apparatus Setup 1) and UV spectroscopy can be found in section A.1 of the Appendix.

2.2.3 Definitions of Important Quantities and Methods Used to Calculate Them

- Nanoparticle Recovery, R_{NP} : Refers to the fraction of nanoparticles injected that are recovered in the effluent. The nanoparticle recovery was calculated by integrating the area under the effluent history curve using the trapezoidal approximation giving a value of equivalent recovered in pore volumes of

dispersion at injected concentration. Dividing the nanoparticle recovery by volume of nanoparticles injected (PVI) gives the fraction of injected nanoparticles that were recovered (R_{NP}) as shown in Equation 2.1.

$$R_{NP} = \frac{\sum_i (PVI_i - PVI_{i+1}) * \frac{(C_{Di} + C_{Di+1})}{2}}{PVI} \quad \text{Equation 2.1}$$

where $C_D = \frac{C_{effluent}}{C_{injected}}$, is the dimensionless effluent concentration

- Retained Mass, R_M : Refers to the calculated retention of nanoparticles within the sand pack following postflush in [mg] calculated from R_{NP} .

$$R_M = (1 - R_{NP}) * PVI * C_{inj} * V_p \quad \text{Equation 2.2}$$

- Retention Concentration, R_{Conc} : Retention of nanoparticles following brine flush normalized by the surface area of the porous medium. Calculated as the Retained Mass (R_M) divided by the calculated surface area of the sand pack (S_A) as shown in Equation 2.3 in [mg/m^2].

$$R_{Conc} = \frac{R_M}{S_A} \quad \text{Equation 2.3}$$

- Retention Capacity, R_{Cap} : Mass of nanoparticles a porous medium is capable of retaining per unit surface area of the porous medium in [mg/m^2]. For cases in which the effluent concentration reached the injected concentration all sites in the porous medium capable of nanoparticle retention had been filled. In these cases, if no nanoparticles are detached during the postflush then the Retention Concentration (R_{Conc}) is equal to the Retention Capacity (R_{Cap}).

- Nanoparticle Arrival Time, $t_{arrival}$: Refers to the dimensionless time, in pore volumes injected, when the effluent dimensionless nanoparticle concentration reaches 0.50 i.e. half of the injected concentration. For tracer-like flow the arrival time should be 1 pore volume. For cases in which the refractometer was used to measure nanoparticle concentration, the time resolution of the effluent history is relatively coarse, the arrival time is interpolated from the measurements using Equation 2.4, where i and $i+1$ bracket $C_D = 0.50$.

$$t_{arrival} = PVI_i + (0.5 - C_{Di}) \left[\frac{PVI_{i+1} - PVI_i}{C_{Di+1} - C_{Di}} \right] \quad \text{Equation 2.4}$$

The arrival time is related to the retention capacity if the rate of nanoparticle attachment to the sandpack grains is sufficiently fast. This enables an estimate of retention capacity.

$$t_{arrival} = 1 + D = 1 + \frac{R_{cap}\alpha}{\phi C_{inj}} \quad \text{Equation 2.5}$$

where α is the specific surface area of the sandpack in m^2 per m^3 of pore volume, ϕ is the porosity, and C_I is the injected nanoparticle concentration in mg/m^3 .

- Monolayer Coverage: the nanoparticle percent monolayer coverage ($R_{monolayer}$) represents the fraction of the grain surface covered with nanoparticles following nanoparticle injection and a brine flush. The monolayer coverage was calculated from the Retention Concentration (R_{conc}), the particle nominal diameter (D_p), and the nanoparticle density.

$$R_{monolayer} = \frac{R_{Conc} * 3 * \sqrt{3}}{\pi * D_p * \rho_p} \quad \text{Equation 2.6}$$

The nanoparticle density ρ_p is taken to be 1.67 g/cm³ for silica and 2.52 g/cm³ for iron oxide

- Incremental Retained Mass $R_{M(Inc)}$: Incremental change in calculated nanoparticle Retained Mass (R_M) between two experiments i and $i+1$ as described in Equation 2.7.

$$R_{M(Inc)} = R_{Mi+1} - R_{Mi} \quad \text{Equation 2.7}$$

- Incremental Surface Area, $S_{A(Inc)}$: Incremental change in surface area between two experiments i and $i+1$ with different amounts of kaolinite.

$$S_{A(Inc)} = S_{Ai+1} - S_{Ai} \quad \text{Equation 2.8}$$

- Incremental Retention Concentration, $R_{Conc(Inc)}$: Incremental change in calculated retention concentration between two experiments. For example calculating the incremental concentration between an experiment with kaolinite and Boise sandstone and one with only Boise sandstone effectively calculates the retention concentration of the added kaolinite. The incremental retention capacity is calculated with the incremental retained mass and the incremental surface area as shown in Equation 2.9.

$$R_{Conc(inc)} = \frac{R_{M(inc)}}{S_{A(inc)}} \quad \text{Equation 2.9}$$

- Extrapolated Retention Capacity: Refers to estimating the retention capacity for a porous medium. Experiments in which the effluent concentration never reached the injected concentration did not fill the retention capacity of the medium with nanoparticles. By extrapolating the effluent concentration history trend to the time at which the effluent concentration would have reached the injected concentration, it is possible to estimate the retention capacity for the porous

medium. Effluent concentration vs. dimensionless time (PVI) is extrapolated logarithmically, by fitting the 0.5 pore volume of effluent history prior to postflush breakthrough to a logarithmic trend line, and interspersing the extrapolation within the experimental data. The retention capacity is then calculated using Equation 2.3 with the assumption that the postflush does not detach any nanoparticles (see definition of retention capacity above). The logarithmic fits for experiments 98, 100, and 65 are shown in Equations 2.10, 2.11, and 2.12 respectively.

$$C_D = 0.114698 * \ln(PV) + 0.2495 \quad \text{Equation 2.10}$$

$$C_D = 0.344 * \ln(PV) + 0.692 \quad \text{Equation 2.11}$$

$$C_D = 0.1648 * \ln(PV) + 0.7794 \quad \text{Equation 2.12}$$

Chapter: 3 Results

Experiments in this thesis focused on experimental parameters that influenced the transport of nanoparticles through the slim tube sandpack. Variables such as air saturation, injected concentration, flow velocity, nanoparticle type, slug size, and the number of slugs injected were varied to gain a better understanding of the dominant retention mechanisms for nanoparticle transport. A summary of the results from these sensitivity studies follows in the chapter below. Table 3.1 organizes the variables studied in this thesis into sections and lists the pertinent experiments.

As described in Chapter 1, the retention concentration (R_{Conc}) is the main measure of nanoparticle migration used in this research. This corresponds to the mass of nanoparticles per unit surface area of porous medium remaining in the sandpack after injecting and postflushing a slug of nanoparticle dispersion through the sandpack.

Variable	Number and Title of Section of Chapter 3	Experiments (See Table A.12: Results Summary in Section A.2 of the Appendix) *
Air Saturation	3.1. The Effect of Air Saturation on Nanoparticle Transport	60 and 61
Injection Concentration	3.2.1. The Effect of Injected Concentration on Nexsil DP Nanoparticle Transport at Low Velocities without Clay	73, 75 and 76
	3.2.2. The Effect of Injected Concentration on Nexsil DP Nanoparticle Transport at High Velocities with Clay	78, 79 and 80
	3.2.3. The Effect of Inject Concentration on Nexsil DP Nanoparticle Transport at Low Velocities with Clay	68 and 86
	3.2.4. The Effect of Injected Concentration on Fluorescently tagged Silica Nanoparticle Transport	96, 103 and 104
Kaolinite Retention Capacity	3.3.1. The Effect of Kaolinite Content on Retention of Salt Tolerant 3M Particles	60, 62 and 67
	3.3.2. The Effect of Kaolinite Content on Retention of Nexsil DP Particles	68, 72, and 73
Velocity	3.4. The Effect of Constant Flow Rate on Nanoparticle Transport	66, 67, 68, 80, 91, and 92
	3.5. The Effect of Step Change Flow Rate on Nanoparticle Transport	93, 94 (part 1),
	3.7. The Effect of Temporary Flow Cessation on Nanoparticle Transport	96, 97, 99 (parts 1 and 2), 69 and 70
Residence Time	3.6. The Effect of Dispersion Reinjection and Secondary Slug Injections on Nanoparticle Transport	98, 99 (part 1), 100, and 101
	3.8. The Effect of Injected Slug Size on Nanoparticle Transport	65 and 66
Retention Capacity	3.6. The Effect of Dispersion Reinjection and Secondary Slug Injections on Nanoparticle Transport	94 (parts 1 and 2)

* The experiments are numbered from 57, to compare with Caldelas (2010) who presented experiments numbered 1 through 56.

Table 3.1: Summary of Experimental Parameters Explored

Each section of this thesis will include a table of pertinent experimental parameters for the experiments discussed. Some sections also include figures illustrating the effluent histories of important experiments. Following standard scientific convention, experimental data are plotted as points. Data for tracer experiments are plotted as the convection-dispersion equation fit to measured tracer concentrations and drawn as continuous red lines. A full list of all available experimental parameters for experiments performed for this thesis can be found in the Appendix.

The numbering of the experiments reflects the fact that this research followed the related prior work of Caldelas (2010). His experiments, 1 through 56, are referenced for comparison occasionally within this thesis.

3.1 THE EFFECT OF AIR SATURATION ON NANOPARTICLE TRANSPORT

Nanoparticles and colloids generally have some affinity for fluid/solid and fluid/fluid interfaces. Thus when nanoparticle dispersion is injected through a sandpack not fully saturated with brine, there is a potential for nanoparticle retention at the air-water interface. The air saturation of a sand pack can be estimated by calculating the sandpack porosity as a function of the weight of sand loaded into the column using Equation 3.2 and the porosity as a function of the weight of brine loaded into the column using Equation 3.1 (note the 1.02 factor adjusts for the density of 3 wt% NaCl). The difference between Equation 3.1 and Equation 3.2 represents the porosity occupied by air, Equation 3.3. The air saturation S_{air} is the ratio $\frac{\phi_{air}}{\phi_{grain}}$. Both weights are available for all experiments reported in this thesis as well as for the experiments reported by Caldelas

(2010). For sand packs that include kaolinite the grain density is a weighted average of the masses of sand and kaolinite used, Equation 3.4.

$$\phi_{brine} = \frac{V_{brine}}{V_{bulk}} = \frac{W_{brine}}{1.02V_{bulk}} \quad \text{Equation 3.1}$$

$$\phi_{grain} = 1 - \frac{V_{sand}}{V_{bulk}} = 1 - \frac{W_{sand}}{\rho_{sand}V_{bulk}} \quad \text{Equation 3.2}$$

$$\phi_{air} = \phi_{grain} - \phi_{brine} \quad \text{Equation 3.3}$$

$$\rho_{sand} = \sum_i \rho_i y_i \quad \text{Equation 3.4}$$

where, ρ_i = density of grain type i and y_i = weight fraction of grain type i

In the first few experiments conducted in this research sandpacks were saturated by simply injecting several pore volumes of brine through freshly packed slim tubes. Calculating air-filled porosity from Equation 3.3 indicated significant air saturation was present in these sand packs. A new saturation method using the vacuum saturation apparatus detailed in the Experimental section of this thesis was employed to minimize the air saturation. Calculated air filled porosity values for experiment 20 onwards are plotted in Figure 3.1. Experiments 20 through 56 are described in Caldelas (2010); experiments 57 through 104 are described in this thesis. Clearly the use of the vacuum saturation apparatus from experiment 60 onwards has greatly reduced the air-filled porosity in the sandpacks. Small changes in the volume of the sandpacks due to changes in end cap placement result in a small error in the calculation of air-filled porosities. Air-

filled porosity values for the slim tubes saturated with the vacuum pump are within this margin of this error and can be assumed to have negligible air-filled porosity.

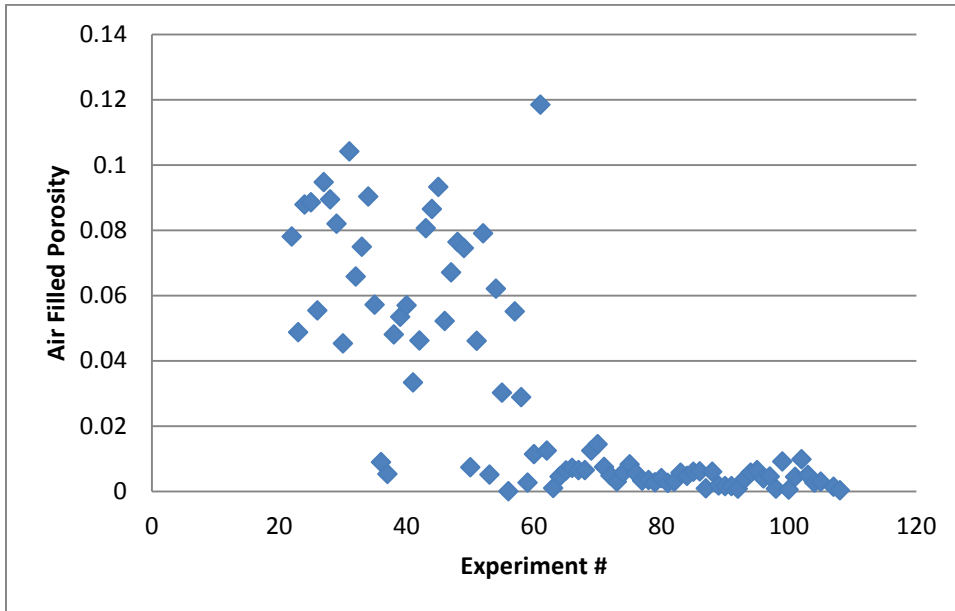


Figure 3.1: Calculated Air Filled Porosity for Experiments 20 through 56 (Caldelas 2010) Saturated via Brine Injection to Displace Air; Experiments 60 through 104 [Except 61] (This Work) Vacuum Saturated with Brine

Having developed a new system to eliminate residual saturations of air, it became possible to quantify the impact of an air-water interface on nanoparticle retention. Experiment 60 and 61 share very similar experimental parameters except experiment 60 was saturated using a vacuum pump and experiment 61 was saturated by simply flushing the sandpack with several pore volumes of brine at atmospheric pressure. The specific experimental parameters can be found in Table 3.2. The effluent concentration histories for these experiments can be found in Figure 3.2. Note that 3.3 pore volumes of nanoparticle dispersion were injected in experiment 61 and only 3 pore volumes were

injected in experiment 60 resulting in a later decline of effluent concentrations for experiment 61.

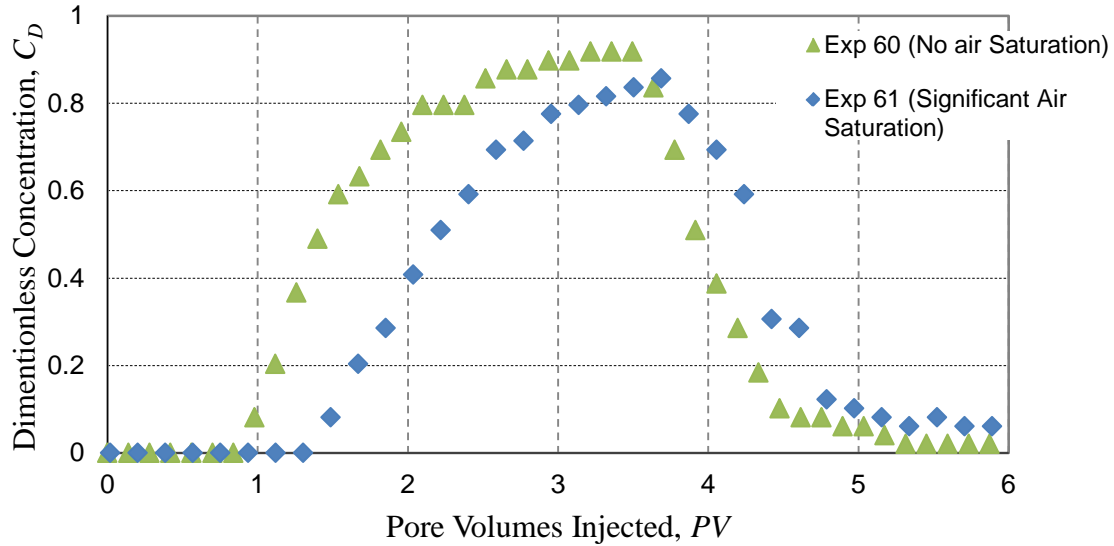


Figure 3.2: Air Saturation Sensitivity Effluent Histories

Exp	Air-Filled Porosity	Sand Type	S_A (m ²)	q (cc/min)	PVI (PVs)	R_{NP} (%)	R_{Conc} (mg/m ²)*	$R_{Monolayer}$ (%)	C_I (wt%)
60	0.14%	Boise + 10% Kao	165	1	3	78.00	2.83	18.68	5.00
61	11.4%	Boise + 10% Kao	159	1	3.3	60.50	4.46	29.41	5.00

*Assuming nanoparticles adsorbed only to the grain surfaces, and that all grain surfaces are in contact with aqueous phase

Table 3.2: Data for Air Saturation Sensitivity Data (Salt Tolerant 3M)

Results indicate air saturation leads to significantly larger retention. The delay of nanoparticle arrival is nearly a pore volume larger for the sandpack with significant air filled porosity ($t_{arrival} = 2.2$ PV vs $t_{arrival} = 1.4$ PV). From equation 2.5 this indicates a

retention capacity $(2.2 - 1)/(1.4 - 1)$ or 3 times greater. Since the sand and clay are the same in both columns the difference in capacity must correspond to the presence of air/water interfaces in experiment 61.

Table 3.2 shows retention concentration calculated assuming that all nanoparticles not recovered from the sandpack are attached to sand and clay grains, i.e. ignoring the air/water interface. The retention concentration computed this way is over 60% larger for the sand pack containing air-filled porosity. This confirms the conclusion from the delay in arrival of injected nanoparticles: a significant fraction of the nanoparticles must have attached to the air/water interface. Note the air-filled porosity of experiment 61 is 11.4% and represents the largest air-filled porosity measured among the 60 experiments saturated via brine injection at atmospheric pressure. The average air-filled porosity using this method was approximately 5% (see Figure 3.1) and would presumably have a proportionately smaller impact than this worst case example. Nevertheless this sensitivity indicates it is necessary to employ a vacuum pump for sand pack saturation in order to avoid confounding nanoparticle retention at air/water interfaces with retention at solid/brine interfaces, which are the main focus of this research. All the experiments used to demonstrate the effect of different operating conditions on retention in this thesis were vacuum-saturated.

3.2 EFFECT OF INJECTED NANOPARTICLE CONCENTRATION ON RETENTION CONCENTRATION

In this section, the concentration of nanoparticles in the injected dispersion is varied. In batch experiments nanoparticle retention can be fit to a Langmuir isotherm

indicating retention concentration in a porous medium should be a function of the nanoparticle concentration of the injected dispersion. Sensitivity studies were performed to test how injected concentration affects the nanoparticle retention concentration of the sandpack for steady flow of the nanoparticle dispersion. Several experimental sensitivities were performed to gauge the relative impact of injected concentration with different injection rates, porous medium composition (by adding kaolinite) and nanoparticle type (both Nexsil DP and Fluorescently Tagged 3M particles were tested).

3.2.1 The Effect of Injected Concentration of Nexsil DP Nanoparticle at Low Velocities without Clay

Experiments 73, 75 and 76 use 1 foot sandpacks filled with 100% Boise sandstone. Experiments 73 and 75 had an injection rate of 1 mL/min while experiment 76 had a somewhat smaller injection rate of 0.88 mL/min. The resulting retention concentrations were plotted as a function of injected concentration in Figure 3.3; the pertinent experimental parameters can be found in Table 3.3.

Exp	V_p (cc)	Sand Type	S_A (m ²)	q (cc/min)	C_I (wt%)	R_{Conc} (mg/m ²)	$R_{Monolayer}$ (%)
73	14.9	Boise	47.9	1	5.00	3.42	12.53
75	14.6	Boise	47.8	1	2.84	1.25	4.58
76	14.6	Boise	48	0.88	1.50	0.964	3.53

Table 3.3: Data for Injection Concentration Sensitivity (No Clay at Low Flow Rate) For Nexsil DP Nanoparticles

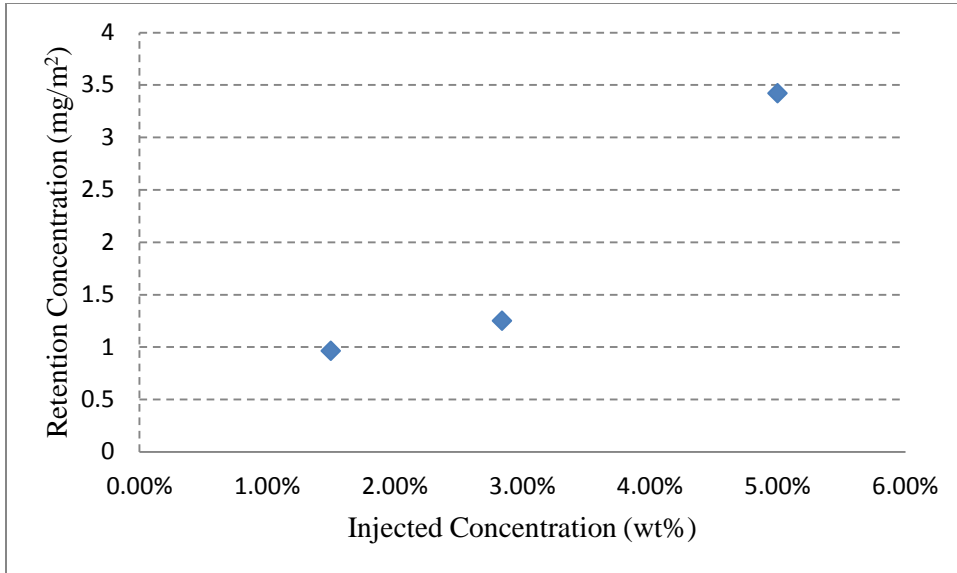


Figure 3.3: Sensitivity of Nexsil DP Retention Concentration to Injection Concentration (no Clay at Low Flow Rate)

Larger injected concentrations appear to result in higher retention. The trend is nonlinear with the relative change in retention between experiment 73 ($C_I = 5$ wt%) and experiment 75 ($C_I = 2.84$ wt%) being 6 times larger than the change in retention from experiment 75 ($C_I = 2.84$ wt%) and experiment 76 ($C_I = 1.5$ wt%).

3.2.2 The Effect of Injected Concentration on Nexsil DP Nanoparticle Transport at High Velocities with Clay

Experiments 78, 79, and 80 use 1 foot sandpacks filled with 95 wt% crushed Boise sandstone and 5 wt% kaolinite. Experiments 78 and 79 had an injection rate of 10 mL/min while experiment 80 had a somewhat smaller injection rate of 9.6 mL/min. The

resulting retention concentrations were plotted as a function of injected concentration in Figure 3.4 and the pertinent experimental parameters can be found in Table 3.4.

Exp	Sand Type	S_A (m^2)	q (cc/min)	C_I (wt%)	R_{Conc} (mg/m^2)	$R_{Monolayer}$ (%)
78	Boise + 5 wt% kaolinite	108	10	1.34	0.191	0.70
79	Boise + 5 wt% kaolinite	109	10	3.00	0.309	1.13
80	Boise + 5 wt% kaolinite	107	9.6	5.00	0.656	2.40

Table 3.4: Data for Injection Concentration Sensitivity (Nexsil DP with Clay at High Flow Rate)

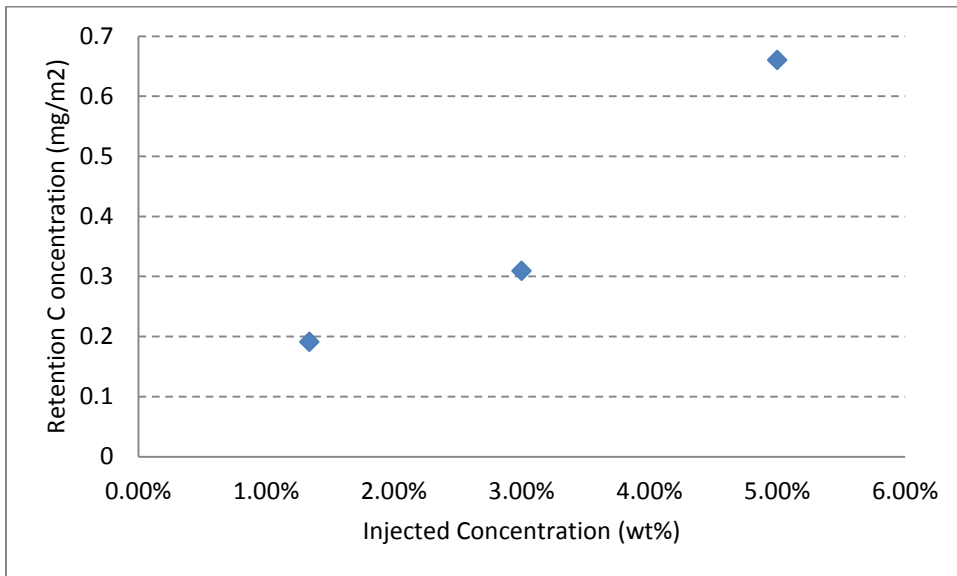


Figure 3.4: Sensitivity of Nexsil DP Retention Concentration to Injection Concentration (with Clay at High Flow Rate)

Here as in the experiments at smaller flow rates, there appears to be a large increase in retention concentration as the injected concentration is increased. The trends in the low flow rate / no clay case (experiments 73, 75, and 76) are very similar to the trends in the high flow rate / 5 wt% kaolinite case (experiments 78, 79, and 80).

3.2.3 The Effect of Injected Concentration of Nexsil DP Nanoparticle at Low Velocity with Clay

Experiments 68 and 86 were run with 1 foot sandpacks filled with 95 wt% crushed Boise sandstone and 5 wt% kaolinite. Nanoparticle dispersion was injected at 1 mL/min for both cases. Data for these runs can be found in Table 3.5 below and the retention as a function of injection concentration for all injected concentration sensitivity studies involving Nexsil DP are plotted in Figure 3.5.

Exp	Sand Type	S_A (m^2)	q (cc/min)	C_I (wt%)	R_{Conc} (mg/m^2)	$R_{Monolayer}$ (%)
86	Boise + 5 wt% kaolinite	110	1	1.20	0.49	1.79
68	Boise + 5 wt% kaolinite	108	1	5.00	1.84	6.74

Table 3.5 : Data for Injection Concentration Sensitivity (Nexsil DP with Clay at Low Flow Rate)

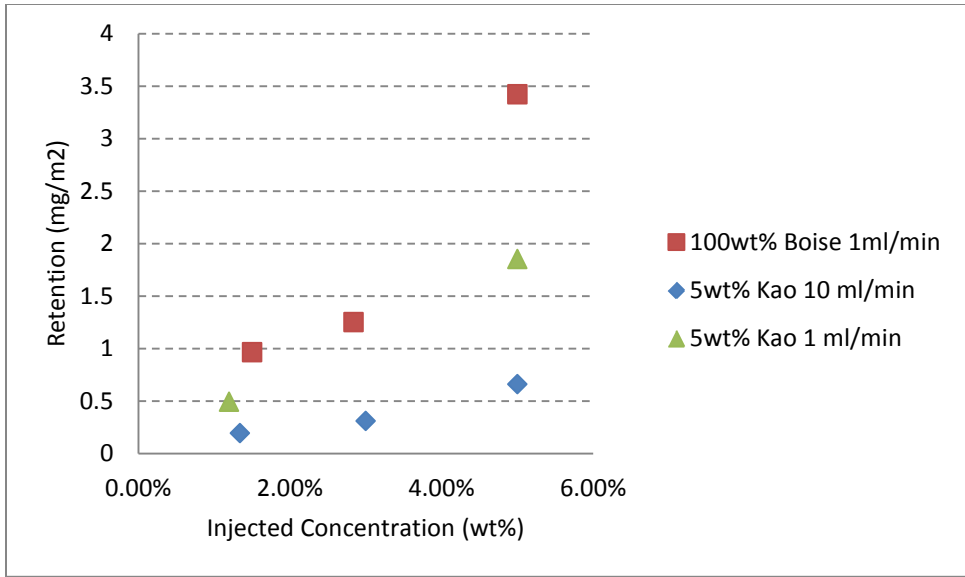


Figure 3.5: Sensitivity of Retention Concentration to Injection Concentration (All Nexsil DP Cases)

The relative similarity between all three sensitivity studies suggests that the effect of injected concentrations on retention concentration is qualitatively independent of flow rate and clay content. Also, in each case the absolute change in retention drops dramatically at lower injected concentrations suggesting the retention concentration might asymptotically approach a characteristic value for injected concentrations below a certain threshold. Note the reinjection sensitivity (experiments 96 and 97) described in section 3.6 provide independent support for this being the case.

At each injected concentration in Figure 3.5, the retention concentration for sandpacks with 5 wt% kaolinite measured at 1 mL/min is about half the value measured in sandpacks without kaolinite at the same flow rate. The surface area for the sandpacks

with kaolinite is about twice the surface area of the sandpack without kaolinite. Thus the retained mass of nanoparticles is about the same at each injected concentration. The influence of specific surface area on retention concentration is examined further in section 3.4.

At each injected concentration the retention concentration at large flow rate is smaller than at small flow rate. The effect of flow velocity on retention is an important factor that is examined further in section 3.4.

3.2.4 The Effect of Injected Concentration of Fluorescently Tagged Silica Nanoparticle

Experiments 96, 103 and 104 were run with 1 foot slim tube columns filled with 100% Boise sandstone. Fluorescently Tagged 3M nanoparticles were injected at approximately 1 mL/min in varying concentrations. Table 3.6 below includes a list of the pertinent experimental parameters for this sensitivity study. The resulting retention concentrations for these experiments were plotted as a function of the injected concentration in Figure 3.6 below.

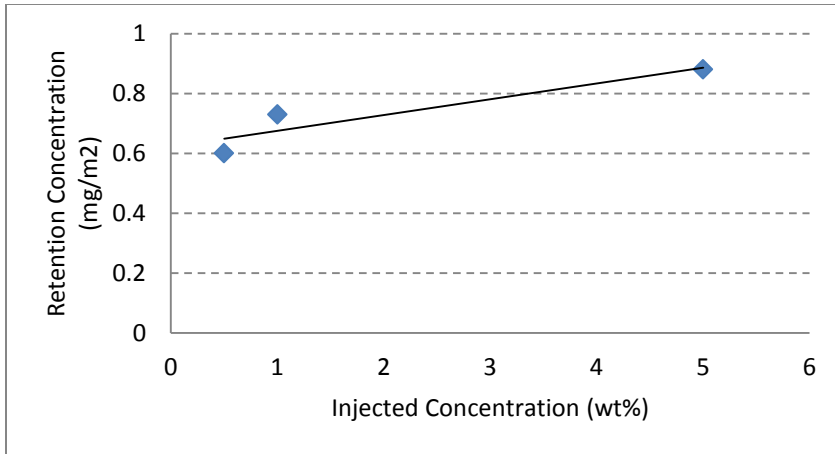


Figure 3.6 : Sensitivity of Fluorescently Tagged 3M Retention Concentration to Injected Concentration

Exp	ϕ_{brine} (%)	Sand Type	S_A (m ²)	q (cc/min)	R_{NP} (mg/m ²)	$R_{\text{Monolayer}}$ (%)	C_I (wt%)
96	54.2	Boise	48.2	1.05	0.73	7.22	1.00
103	48.7	Boise	51.3	1.02	0.876	8.66	5.00
104	48.5	Boise	48.2	1	0.605	5.98	0.50

Table 3.6: Data for Fluorescently Tagged 3M Injection Concentration Sensitivity

Much like the Nexsil DP, retention capacity for Fluorescently Tagged 3M nanoparticles appear to increase with increasing injected concentration, but while Nexsil DP particles exhibited a non-linear relationship between injected concentration and retention capacity for 3M's PEG particles the relationship appears somewhat linear with a drop-off at low concentrations. Very low concentration experiments ($C_I = 0.1$ wt%) such as experiment 98 were not included in this comparison because the pump stops performed during experiment 98 are believed to have affected the retention. Filtration theory predicts a linear relationship between retention and injected concentration, but the

data of Figure 3.6 and Figure 3.5 suggest that the sandpacks have a threshold capacity that gets filled even at small injected concentrations. It's possible that a non-linear section of the curve, like those observed between 3 wt% and 5 wt% injected concentration in Figure 3.5, would appear at still higher injected concentrations.

It is also interesting to consider the extrapolation of the trend in Figure 3.6 to small injected concentrations. There appears to be a nonzero capacity for permanent retention, around 0.5 mg/m^2 . That is characteristic of these sandpacks. That is, this capacity would be filled regardless of the injected concentration, if sufficient volumes of dispersion were injected. As shown in the Appendix, the effluent concentrations histories for experiments 96, 103 and 104 all reached or came close to the injected concentration. This indicates that all the sites in the porous medium capable of nanoparticle retention had been filled and the retention concentration values plotted in Figure 3.6 are also an accurate estimation of the retention capacities of the sandpacks for these three experiments.

3.3 QUANTIFYING THE RETENTION CONCENTRATION OF KAOLINITE

The experiments in this section vary kaolinite content in the sand pack to analyze the effect of clay content on nanoparticle retention concentration. The zeta potential for Boise sandstone ($-22.12 \pm 5.58 \text{ mV}$) is somewhat smaller than that of kaolinite clay ($-17.77 \pm 4.09 \text{ mV}$). The zeta potentials for both nanoparticle dispersions tested are negative suggesting that if DLVO interaction is the dominant interaction that controls retention the relatively larger repulsive forces from the Boise sandstone / nanoparticle interaction will lead to smaller retention concentration on Boise sandstone than on

kaolinite. Kaolinite content sensitivity studies were run for both Salt Tolerant 3M and Nexsil DP particles.

3.3.1 The Effect of Kaolinite Content on Retention Concentration of Salt Tolerant 3M particles

Experiments 60, 62 and 67 were run in 1 foot long sandpacks injecting Salt Tolerant 3M particles at a concentration of 5 wt% with a flowrate of 1 mL/min. Kaolinite content inside the sandpack was varied from 0 wt% to 5 wt% to 10 wt% in experiments 62, 67 and 60 respectively. The specific surface area for each column was determined from BET measurements as described in Appendix, Section A.1.5. The resulting nanoparticle retention concentrations for these runs are plotted in Figure 3.7 below and the specific experimental parameters for this sensitivity are listed in Table 3.7.

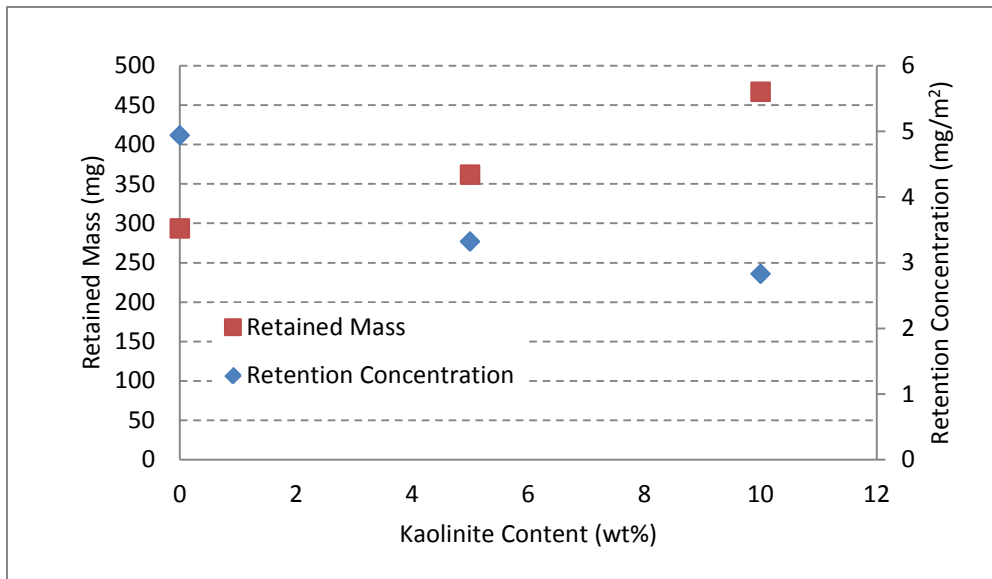


Figure 3.7: Retention Concentration vs. Kaolinite Content (Salt Tolerant 3M)

Exp	V_p (cc)	Sand Type	S_A (m ²)	R_M (mg)	R_{Conc} (mg/m ²)	$S_{A(Inc)}$ (m ²)	$R_{M(Inc)}$ (mg)	$R_{Conc(Inc)}$ (mg/m ²)
62	13.9	Boise	59.4	293	4.94	59.4	293	4.93
67	13.8	Boise + 5wt% kaolinite	109	362	3.32	49.8	68.4	1.37
60	14.3	Boise + 10 wt% kaolinite	165	467	2.83	56	105	1.88

Table 3.7: Data for Kaolinite Content Sensitivity (Salt Tolerant 3M)

Results show surface area increases with increasing clay content. As surface area increases the total mass of nanoparticles retained (R_M) also increases. Retained mass and surface area values of experiment 62 are subtracted from retained mass and surface area values of experiment 67 to estimate the incremental rise in retention concentration and surface area due to the addition of 5 wt% kaolinite to the sandpack. Values from experiment 67 are subtracted from experiment 60 in a similar fashion to determine the incremental values for a 10 wt% kaolinite sandpack. Equation 2.9 gives the incremental retention concentration for the sandpack as shown in Figure 3.8. Boise sandstone appears to have a higher retention concentration, about 5 mg/m², than kaolinite which is about 1.63 mg/m². The incremental retention capacities for the 5 wt% and 10 wt% kaolinite cases are very similar suggesting the retention concentration area of kaolinite is constant. While the retained mass of nanoparticles will increase linearly with increasing clay content the retention concentration (mg/m²) will decrease in a non-linear fashion as it

approaches the incremental retention concentration calculated in experiments 67 and 60 (approximately 1.8 mg/m^2).

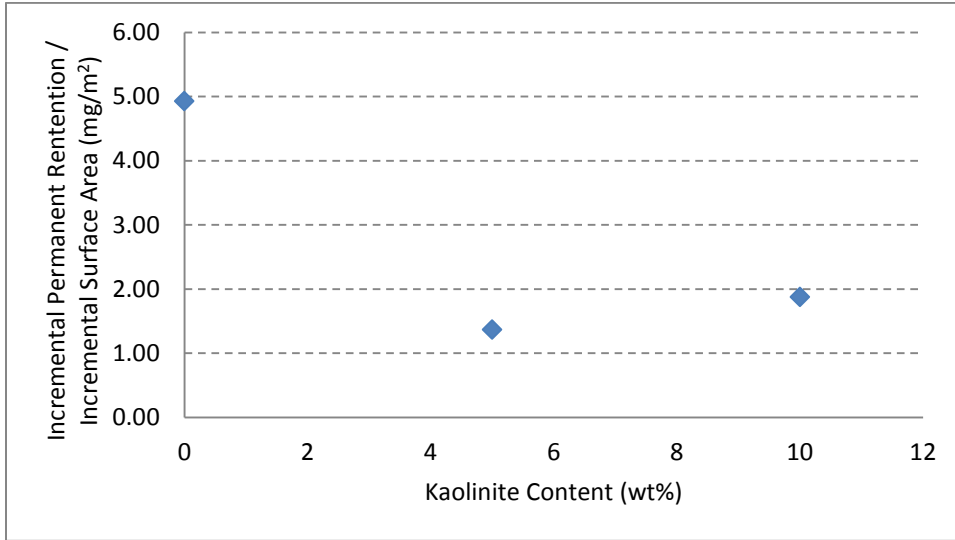


Figure 3.8: Incremental Nanoparticle Retention Concentration (mg/m^2) vs. Kaolinite Content for (Salt Tolerant 3M Nanoparticles Injected at 5 wt%)

3.3.2 The Effect of Kaolinite Content on Retention Concentration of Nexsil DP Particles

Experiments 73, 78 and 72 were run in 1 foot long sandpacks injecting Nexsil DP dispersion with a flow rate of 1 mL/min. Kaolinite content inside the sandpack was varied from 0 wt% to 5 wt% to 10 wt% in experiments 73, 78 and 72 respectively. The specific surface area for each column was extrapolated from BET measurements as described in section A.1.5. The resulting nanoparticle retention concentrations for these runs are plotted in Figure 3.9 below and the specific experimental parameters for this sensitivity are listed in Table 3.8.

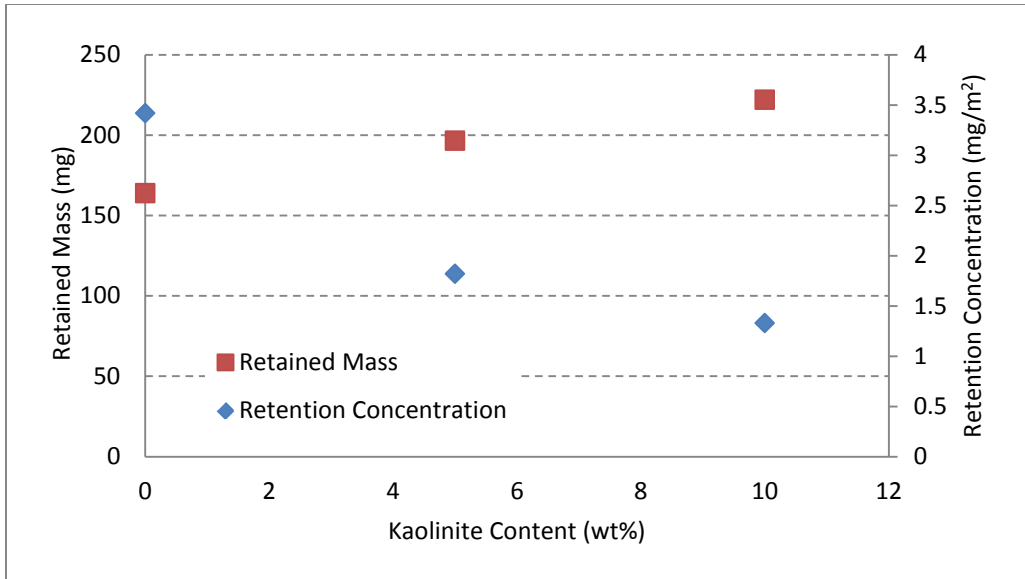


Figure 3.9: Retention Concentration vs. Kaolinite Content (Nexsil DP)

Exp	V_p (cc)	Sand Type	S_A (m ²)	R_M (mg)	R_{Conc} (mg/m ²)	$S_{A(Inc)}$ (m ²)	$R_{M(Inc)}$ (mg)	$R_{Conc(Inc)}$ (mg/m ²)
73	14.888	Boise	47.9	164	3.42	47.9	164	3.42
68	13.888	Boise + 5wt% kaolinite	108	197	1.82	60.1	32.7	0.545
72	13.388	Boise + 10 wt% kaolinite	167	222	1.33	59	25.6	0.433

Table 3.8: Data for Kaolinite Content Sensitivity (Nexsil DP)

As in the previous section, retained mass and surface area values of experiment 73 are subtracted from retained mass and surface area values of experiment 68 to estimate the increment in retention concentration and surface area due to the addition of 5 wt% kaolinite to the sandpack. Values from experiment 68 are subtracted from experiment 72

in a similar fashion to determine the incremental values for a 10 wt% kaolinite sandpack. Equation 2.9 gives the incremental retention concentration for the sandpack as shown in Figure 3.10. Boise sandstone appears to have a higher retention concentration than kaolinite per unit surface area for the Nexsil DP just as for the Salt Tolerant 3M. The incremental retention capacities for the 5 wt% and 10 wt% kaolinite cases, plotted in Figure 3.10, are very similar suggesting the retention concentration per unit surface area is constant. While the retained mass (mg) will increase linearly with increasing clay content the retention concentration (mg/m^2) will decrease in a non-linear fashion as it approaches the incremental retention concentration calculated in experiments 68 and 72 (approximately $0.6 \text{ mg}/\text{m}^2$).

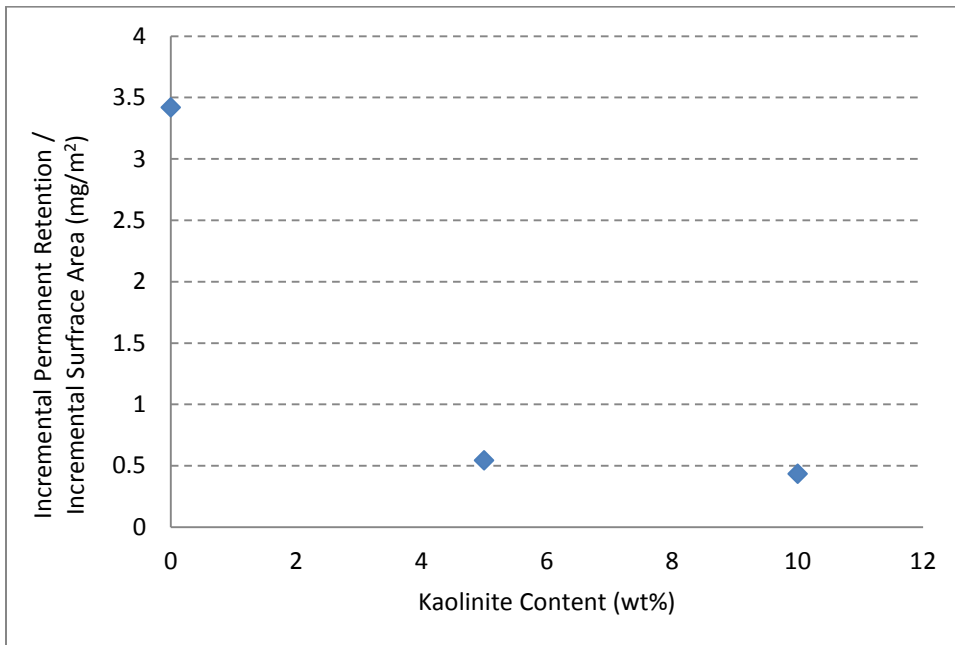


Figure 3.10: Incremental Nanoparticle Retention Concentration vs. Kaolinite Content (Nexsil DP)

Both Nexsil DP and Salt Tolerant 3M dispersions show similar trends with significantly lower retention concentration on kaolinite clay than on Boise sandstone. Retention concentration is approximately three times larger on Boise sandstone than kaolinite for Salt Tolerant 3M nanoparticles and approximately six times greater for Nexsil DP. The zeta potentials for the two particles are similar suggesting that relative difference in the retention measurements for the two particle types is not an electrostatic effect. Dynamic light scattering measurements show that the mean radius of the Salt Tolerant 3M particle is 10 nm and the mean radius of the Nexsil DP particle is 27 nm. The larger size of the Nexsil DP particles subjected it to relatively larger hydrodynamic forces. It's possible that a greater number of Nexsil DP particles attached to kaolinite grains during injection ultimately desorb during postflush due these larger hydrodynamic forces.

The retention concentration of kaolinite appears to be significantly lower than Boise sandstone for both Salt Tolerant 3M and Nexsil DP particles. DLVO theory would predict larger retention concentration on kaolinite and lower retention concentration on Boise sandstone. This suggests electrostatic effects are not a dominant interaction that controls retention in these experiments. Note these experiments were all carried out at 3 wt% NaCl. The large salt concentration results in significant screening suppressing the electrostatic interaction. It is likely DLVO effects play a larger role in the retention concentration of a porous medium when salt concentration is lower.

3.4 THE EFFECT OF CONSTANT FLOW RATE ON RETENTION CONCENTRATION

Table 3.9 lists a subset of experiments run at fixed flow rate. A high and low flow rate experiment is performed for each nanoparticle type tested. Figure 3.11, Figure 3.12 and Figure 3.13 show the nanoparticle concentration histories for Iron Oxide, Salt Tolerant 3M and Nexsil DP fixed flow rate sensitivities respectively.

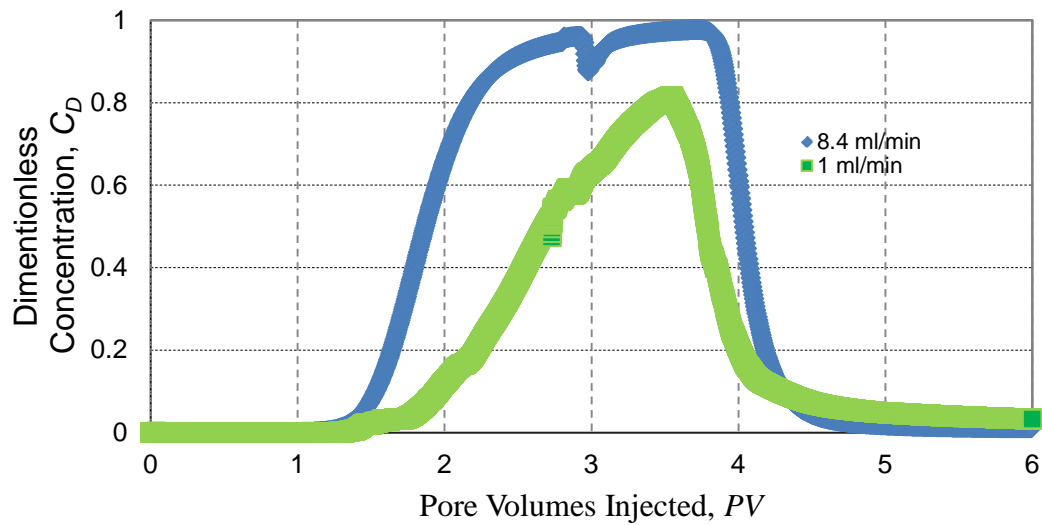


Figure 3.11: Sensitivity of Effluent Concentration History to Constant Flow Rate (Iron Oxide) [Experiments 91 and 92]

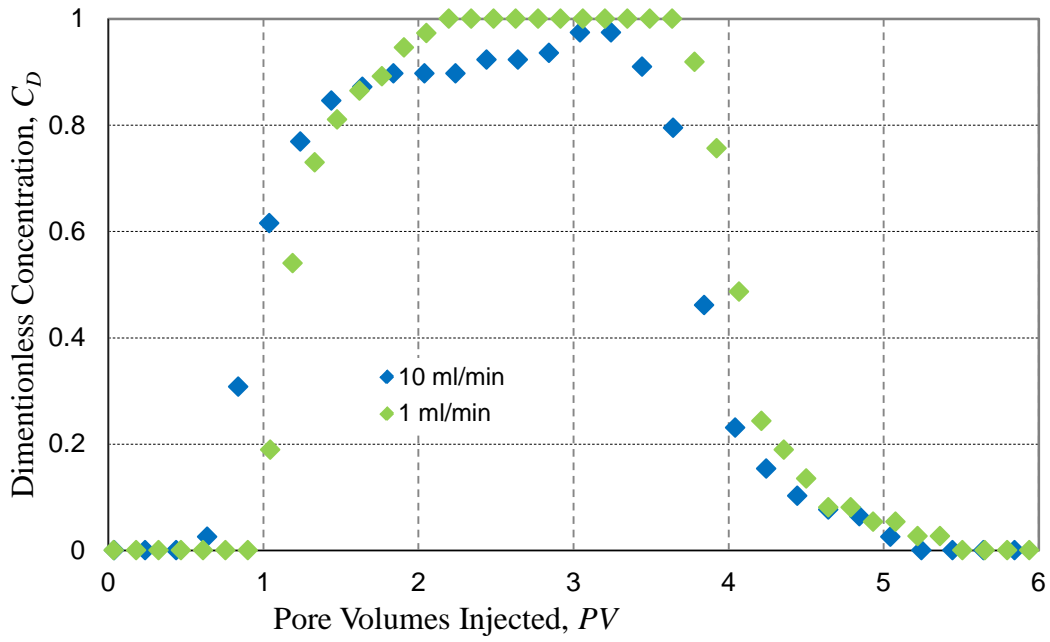


Figure 3.12 Sensitivity of Effluent Concentration History to Constant Flow Rate (Nexsil DP) [Experiments 68 and 80]

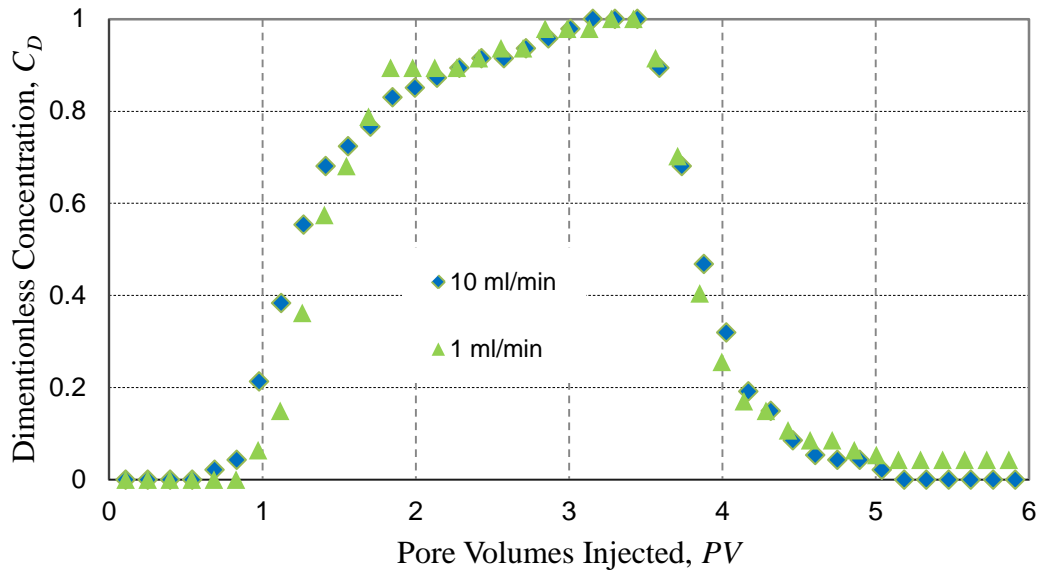


Figure 3.13: Sensitivity of Effluent Concentration History to Constant Flow Rate (Salt Tolerant 3M) [Experiments 66 and 67]

Exp	Sand Type	S_A (m ²)	q (cc/min)	v (ft/day)	C_I (wt%)	Nanoparticle	R_{NP} (%)	R_{Conc} (mg/m ²)	$R_{Monolayer}$ (%)	PVI (PVs)
66	Boise + 5 wt% kaolinite	109	10	1060	5.00	Salt Tolerant 3M	84.4	2.93	19.32	3.00
67	Boise + 5 wt% kaolinite	109	1.0	105.2	5.00	Salt Tolerant 3M	82.6	3.32	21.89	3.00
68	Boise + 5 wt% kaolinite	108	1.0	105.2	5.00	Nexsil DP	94.7	1.85	6.74	3.17
80	Boise + 5 wt% kaolinite	108	9.6	988	5.00	Nexsil DP	95.0	0.66	2.40	2.84
91	Boise	49.9	1.0	108.7	0.1	IO (Coating 1)	46.9	0.446	0.19	2.89
92	Boise	49.0	8.4	888	0.1	IO (Coating 1)	78.9	0.198	0.08	3.11

Table 3.9: Data for Constant Flow Rate Sensitivity

In all cases except experiment 91, the nanoparticle effluent concentration reached or almost reached the injection concentration, suggesting a finite retention capacity exists for nanoparticle deposition. Classical filtration theory does not predict this kind of behavior except at very small Damkohler number (e.g. slow deposition rates). (Experiment 94 (parts 1 and 2) described below confirms that the retention capacity is finite). These effluent histories are consistent with the Langmuir isotherm presumption of an retention capacity related to intrinsic number of sites per unit area of the substrate.

The third to last column in Table 3.9 shows the nanoparticle retention concentration for the runs. Findings in Section 3.3 of Chapter 3 suggest retention concentration [mg/m²] should decrease with increasing kaolinite content but the Salt Tolerant 3M runs (experiments 66 and 67) and the Nexsil DP runs (experiments 68 and

80) show significantly larger retention concentration than the Iron Oxide runs (experiments 91 and 92). Iron oxide nanoparticles are not monodisperse and aggregation leads to iron oxide clusters one order of magnitude larger than silica nanoparticles. The coatings are also chemically different leading to different surface properties. The measured zeta potential of iron oxide nanoparticles is higher than that of silica nanoparticles, which means the repulsion between iron oxide particles and sand surface is stronger than that between silica particles and sand surface. The silica nanoparticles were also injected at a higher concentration which, as section 3.2 of chapter 3 observed, tends to lead to higher retention concentration. Therefore, iron oxide particles yielded a lower retention concentration than silica particles. Senger *et al.* (1992) pointed out that a jamming limit coverage (54.6% of a monolayer) exists for irreversible retention of hard spheres onto a planar surface. The limit encountered in practice when ionic strength decreased in the dispersion or hydrodynamic forces and surface heterogeneity involved in the system is always lower than the jamming limit (Liu *et al.*, 1995; Johnson *et al.*, 1995). The experiments with silica nanoparticles are consistent with this expectation. Iron oxide clusters with larger sizes are also subject to stronger hydrodynamic forces than silica particles, which helps result in a lower retention concentration coverage in flow experiments with iron oxide nanoparticles.

A flow rate effect is evident in the effluent histories in Figure 3.11, Figure 3.12, and Figure 3.13: the larger velocity experiment in each pair shows earlier arrival. This is predicted by Equation 2.5 which suggests larger retention leads to a later arrival. Thus the earlier arrivals at larger flow rates in each pair of experiments imply smaller retention

capacity assuming the experimental conditions satisfy the assumption of large Damkohler number. This is consistent with the retention concentrations measured from a mass balance in Table 3.9: the larger flow rate experiment in each pair shows a smaller retention concentration. If none of the nanoparticles retained during injection are detached during the postflush, then the measured retention concentration is equal to the retention capacity. The differences in arrival are most pronounced in Figure 3.11 where the injected concentration is 0.1 wt%. This is to be expected, because the smaller injected concentration makes the second term on the right hand side of Equation 2.5 more sensitive to changes in the numerator (α or A_c).

Under flow conditions, we hypothesize that hydrodynamic forces also influence the nanoparticle/substrate interaction. The shear stress exerted on nanoparticles near the surface of a sand grain decreases the retention concentration observed in column floods. Within similar porous media, higher flow rate induces stronger shear stress. Therefore, the smaller retention concentrations measured at higher flow rates is consistent with this simple model. Burdick et al. (2001) has observed a critical Reynolds number (dimensionless quantity proportional to flow rate) for hydrodynamic removal of particles from surfaces and less particles left on the surface with a higher Reynolds number.

These experiments indicate that the capacity of a substrate for nanoparticle retention depends on flow rate. This is not anticipated by filtration theory or by Langmuir-type retention. A possible explanation outlined above is that larger hydrodynamic forces prevent nanoparticles from adsorbing at some surface sites. Another possible explanation invokes a competition between attractive forces and a tendency of particles to leave the

grain surface. Larger flow rates could increase the latter tendency by entraining adsorbed nanoparticles back into the flowing fluid more rapidly. The observed apparent retention capacity would then be a function not just of a concentration of nominal retention sites on the surface (the Langmuir capacity) but also of flow rate.

3.5 THE EFFECT OF STEP CHANGE FLOW RATE ON RETENTION CONCENTRATION

Having arrived at the notion of a dynamic (flow velocity dependent) retention capacity from the fixed-velocity experiments in the preceding section, column floods were conducted in which the velocity was changed in a discrete, essentially instantaneous step during the experiment. Figure 3.14 and Figure 3.15 demonstrate the effect of flow rate change during nanoparticle injection. In experiment 93 (Figure 3.14), 2.7 pore volumes of IO (with Coating 2 surface coating) nanoparticles were injected at 9.3 mL/min. The flow rate was instantaneously reduced to 1.07 mL/min and an additional 1.3 pore volumes of the same dispersion were injected. The postflush was conducted at 1 mL/min. In part 1 of experiment 94 (Figure 3.15), 4.2 pore volumes of IO (with Coating 3 surface coating) nanoparticle dispersion were injected at 0.87 mL/min into sandpack. Then the flow rate was increased to 10 mL/min with the same nanoparticle concentration until 8.1 pore volumes when the postflush began, also at a rate of 10 mL/min. The conditions of experiment 93 and experiment 94 are summarized in Table 3.10.

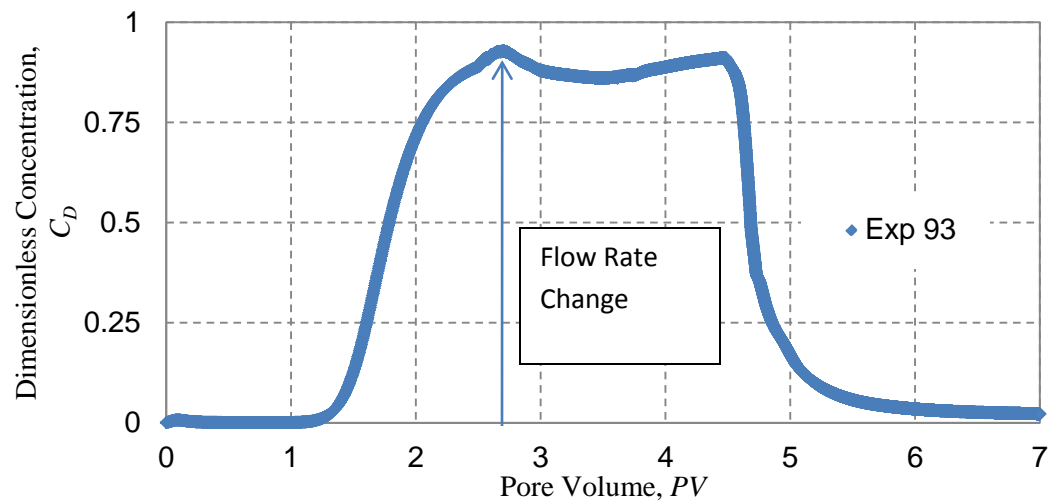


Figure 3.14: Step Change Flow Rate Effluent History ($q = 9.3$ mL/min for $t_p < 2.7$ PV, $q = 1.07$ mL/min for $t_p > 2.7$ PV)

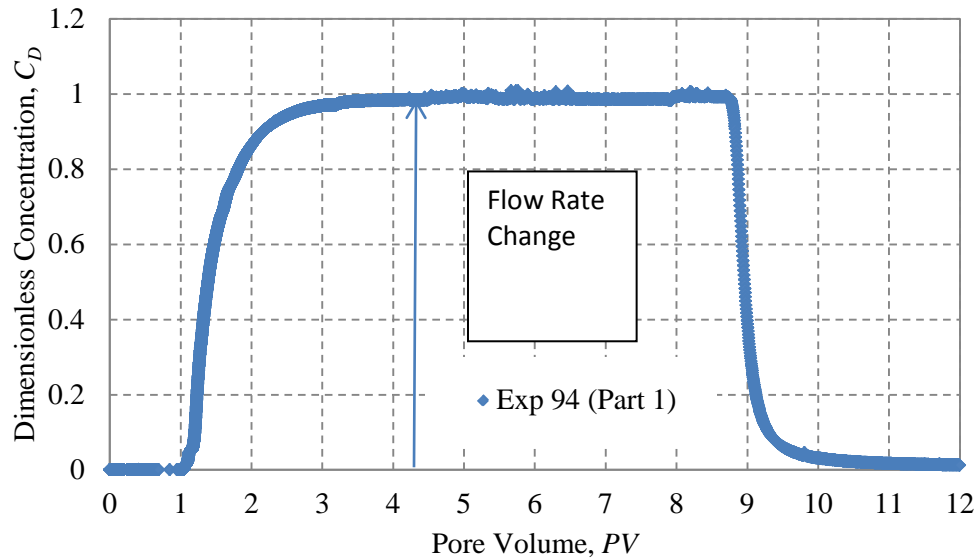


Figure 3.15: Step Change Flow Rate Effluent History ($q = 0.87$ mL/min for $t_p < 4.4$ PV, $q = 10$ mL/min for $t_p > 4.4$ PV)

Exp	S_A (m ²)	q (cc/min)	v (ft/day)	C_I (wt%)	Nanoparticle	R_{NP}	R_{Conc} (mg/m ²)	$R_{Monolayer}$ (%)	PVI (PVs)
93	46.5	9.3 then 1.07	937 then 108	0.10	IO (Coating 2)	72.49%	0.349	0.15	3.80
94 (Part 1)	47.6	0.87 then 10	80 then 919	0.10	IO (Coating 3)	92.45%	0.207	0.09	8.12

Table 3.10: Data for Step Change Flow Rate Experiments

In Figure 3.14, after injecting 2.7 pore volumes of dispersion, nanoparticle concentration in the effluent reached 95% of the injected concentration. Combined with the delay of about 0.8 *PV* in nanoparticle breakthrough, this indicates that most of the nanoparticle retention capacity has been filled. But when the flow rate was decreased at 2.7 *PV*, the corresponding decrease in effluent nanoparticle concentration shows that substantially more nanoparticles were adsorbed by the available sites. Had the dispersion injection continued at 10 mL/min, as in the experiments in Figure 3.11 to Figure 3.13, a rapid asymptotic increase in the effluent concentration toward the injected concentration would very likely have occurred. But decreasing the injection flow rate 10 times showed instead a reversal of the constant-flow-rate trend: a remarkable decline in the effluent concentration. Clearly a large increase in nanoparticle retention rate occurred when the flow rate decreased, either because the number of sites available for nanoparticle retention increased, or because the nanoparticle attachment rate increased. For Langmuir

type of retention, the Damkohler number is inversely proportional to flow rate. With a lower flow rate, Damkohler number is larger, which can result in faster retention and a decline in effluent concentration. On the other hand, if the nanoparticles are undergoing filtration, the steady-state concentration of nanoparticles in the effluent will decline to a lower value when flow rate decreases, and then keep constant until postflush begins. But the effluent concentration declined with the decrease in flow rate reaching a local minima with a dimensionless concentration of 86% and then rose to a dimensionless concentration of 86.3% before the postflush had begun. This implies that decreasing the flow rate increased the retention concentration of the sand pack by a fixed amount. It means neither the colloid filtration model nor the Langmuir isotherm can fully describe nanoparticle depositional properties during transport.

In Figure 3.15, the dimensionless concentration of nanoparticles in the effluent has reached unity when the flow rate was increased to 10 mL/min. In the fixed-rate experiments of Table 3.9 and Figure 3.11-Figure 3.13, larger flow rates always corresponded to smaller retention capacity. For experiments 91 and 92 the retention concentration dropped over 50% with an order of magnitude increase in velocity. If this correspondence held in experiment 94 Part 1, and the retention concentration dropped 50%, the nanoparticles adsorbed during the low flow rate part of the experiment would have exceeded the retention capacity of the column at the high flow rate by a factor as large as 2. If the nanoparticles obey a Langmuir-type reversible retention isotherm, then the effluent concentration should have increased significantly. If the expected 50% of the retained particles were to desorb when the velocity was increased, the dispersion

concentration would have increased 30%. This follows from a mass balance and the pore volume of the column, shown in Equation 3.5. As this dispersion was displaced from the column the dimensionless effluent concentration in experiment 94 (Part 1) would also have increased 30%. Instead, there is essentially no change in the effluent concentration. This suggests that nanoparticle adsorbed up to the time of increasing the flow rate were irreversibly bound to the grains. This behavior is consistent with a filtration model, not a Langmuir-type retention model.

$$\Delta C_D = \frac{\Delta R_{conc} * S_A}{\rho_{disp} * V_p * C_I} \quad \text{Equation 3.5}$$

where ΔR_{conc} [mg/m²] is the change in retention concentration, S_A [m²] is the surface area of the sandpack, V_p [cm³] is the pore volume of the sandpack, C_I [wt%] is the nanoparticle concentration of the injected dispersion, and ρ_{disp} [g/mL] is the density of the dispersion phase, approximately 1 g/mL.

3.6 THE EFFECT OF DISPERSION REINJECTION AND SECONDARY SLUG INJECTIONS ON RETENTION CONCENTRATION

3.6.1 Injection of Fresh Dispersion Into Postflushed Sandpack

In experiment 94 (Part 2), 14 pore volumes of 3 wt% NaCl brine were continuously injected as a postflush at 10 mL/min into the same column used for part 1 of experiment 94. To test whether the postflush created new retention capacity, or equivalently, whether any of the nanoparticles attached to grain surfaces during injection were reversibly removed during the postflush, an additional 3.4 pore volumes of the same type of iron oxide (with Coating 3 surface coating) nanoparticles were injected into the

same sandpack at the same flow rate, followed by postflush. Flow conditions for experiment 94 (Part 2) are shown in shown Table 3.11. Figure 3.16 shows effluent concentration history for experiment 94 (Part 2), compared with the tracer test.

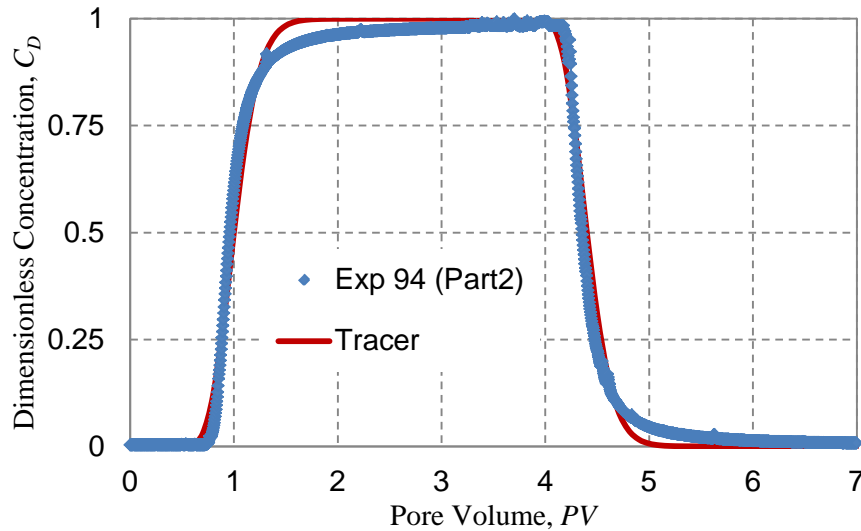


Figure 3.16: Effluent History of Second Nanoparticle Slug Injection for Experiment 94

The measured nanoparticle recovery for this second part of the experiment was over 99%, which means that essentially no new sites capable of nanoparticle retention were present in the column after the long postflush of the first part of the experiment. The arrival time of the nanoparticle slug, when ($C_D = 0.5$), also closely follows arrival predicted by the tracer experiment suggesting little to no retention occurred to retard nanoparticle arrival in the effluent. This is consistent with the fact that effluent concentration reached and remained at injected concentration during part 1 of this experiment, Figure 3.15: evidently the injected nanoparticles filled the retention capacity during part 1. This confirms a finite retention capacity exists in a porous medium for

nanoparticle deposition. Moreover almost all those sites are occupied by nanoparticles irreversibly adsorbed during injection of the dispersion. The postflush displaced a very small fraction of the nanoparticles attached during part 1. The small shoulder in the effluent history (deviation from the tracer concentration history between 1.5 *PV* and 2.5 *PV* in Figure 3.16) indicates some of the injected nanoparticles are nevertheless interacting with the porous medium, even though there are no sites available for irreversible attachment. The longer tail of the nanoparticle history (exceeds the tracer concentration from about 4.7 *PV* until about 5.5 *PV*) corresponds to these interacting nanoparticles being released from the substrate during the postflush. This indicates the presence of reversible retention sites, of the type expected in the classical Langmuir isotherm but not in the classical filtration theory.

3.6.2 Injection of Fresh Dispersion at Lower Flow Rate After Postflush

In experiment 96, 3.5 pore volumes of 3M[®] fluorescent silica nanoparticles were injected in a fresh sandpack at 1 mL/min, followed by postflush. In experiment 99 (Part1), the same kind of nanoparticles with the same concentration as in experiment 96 was injected into a fresh sandpack at 10 mL/min for 7.4 pore volumes. Then a postflush was conducted until no more nanoparticles were detected in the effluent. After that, 6 pore volumes of the same nanoparticle dispersion were injected into the same sandpack but at a smaller flow rate of 1 mL/min, which was then flushed by brine at 10 mL/min (experiment 99 Part 2). The flow conditions are listed in Table 3.11 with the nanoparticle retention concentration.

From the table, a retention concentration of 0.72 mg/m^2 was measured in experiment 96 at a fixed flow rate of 1 mL/min . In experiment 99 (Part 1 and Part 2), the cumulative retention concentration is 0.7 mg/m^2 ; this equals to 0.53 mg/m^2 occupied by nanoparticles at large injection rate in Part 1 plus 0.17 mg/m^2 occupied during flow at 1 mL/min in Part 2. This result suggests that the effect of lower velocity on retention concentration in a column is additive. The final retention concentration is determined by the lowest velocity of nanoparticle dispersion in the transport process. This is consistent with the flow rate step change experiments in Table 3.11, wherein a decrease in flow rate during an experiment led to increased retention concentration, but an increase in flow rate caused no change in retention concentration.

3.6.3 Injection of Effluent Dispersion from One Sandpack Into Fresh Sandpack

Two sets of experiments were performed to test whether nanoparticles that were not adsorbed during injection could nevertheless be adsorbed. In Experiment 96 and 97, the porous medium was a standard sandpack. In experiments 69 and 70 the porous medium was a packing of mesoporous silica.

In experiment 97, 3.4 pore volumes of effluent collected from experiment 96 was injected in a fresh sandpack at 1 mL/min , followed by a postflush. The flow conditions are listed in Table 3.11. The collected effluent from experiment 96 was diluted, due to mixing with the brine originally saturating the sandpack, and had a concentration of 0.6 wt% (recall that the injected concentration was 1 wt%). The effluent histories for experiments 96 and 97 are plotted in Figure 3.17. Experiment 96 reached a slightly higher

effluent concentration than experiment 97 due to the relatively larger injected concentration; this led to a slightly larger calculated retention. The calculated retention concentration for experiments 96 and 97 are 0.72 mg/m^2 and 0.70 mg/m^2 , respectively. These results suggest retention capacities for experiments 96 and 97 are very similar. The fact that a nanoparticle has migrated through a column without being retained does not appear to change the probability that it can be retained. In other words, the nanoparticles in dispersion that are retained in a column are no different from the particles that are not retained. It is possible for every particle to be retained in a porous medium of sufficient surface area. This is also reflected in experiment 91 where the large delay between nanoparticle injection and nanoparticle arrival downstream suggests 100% retention of nanoparticles for the first pore volume of dispersion injected.

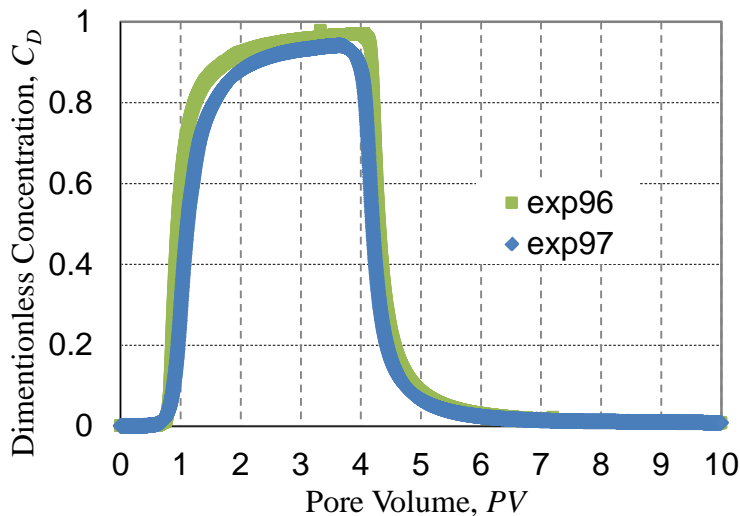


Figure 3.17: Sensitivity of Transport of Fluorescent 3M Nanoparticles to Nanoparticle History; Effluent Nanoparticles from Experiment 96 Were Injected Into New Sandpack in Experiment 97

Exp	S_A (m^2)	q (cc/min)	v (ft/day)	C_I (wt%)	Nanoparticle	R_{NP} (%)	R_{Conc} (mg/m^2)	$R_{Monolayer}$ (%)	PVI (PVs)
94 (Part 1)	47.6	1 then 10	92 then 919	0.10	IO (Coating 3)	92.45	0.207	0.09	8.12
94 (Part 2)	47.6	10	919	0.10	IO (Coating 3)	99.78	0.003	0.00	3.40
96	48.2	1	92.9	1.00	3M Fluorescent	93.94	0.722	7.22	3.54
97	48.6	1	93.6	0.60	3M Fluorescent*	89.92	0.708	7.00	3.41
99 (Part 1)	48.9	10	940	0.10	3M Fluorescent	77.48	0.532	5.26	7.40
99 (Part 2)	48.9	1	940	0.10	3M Fluorescent	91.13	0.170	1.68	6.00

* Effluent collected from experiment 96

Table 3.11: Data For Reinjection Experiments (100% Boise Sandstone Packs)

In experiment 69 3.03 pore volumes of 5 wt% Salt Tolerant 3M nanoparticle dispersion was injected into a slim-tube pack filled with mesoporous silica. Mesoporous silica was chosen for its well characterized surface area and uniform consistency and composition. It was possible to pack two very similar packs of known surface area for a more accurate estimation of retention capacity from the delay in nanoparticle arrival in the effluent. Effluent from experiment 69 was collected and injected into a new slim-tube of fresh mesoporous silica. The effluent histories for these experiments can be found in Figure 3.18 and a list of the pertinent experimental parameters for experiments 69 and 70 can be found in Table 3.12. Results indicate the retention concentration for experiment 70

is significantly less than the retention concentration for experiment 69. In light of experiments 73, 75, 76, 78-80, 68, 86, 96, 103, and 104 which showed, the dependence of retention concentration on injected nanoparticle dispersion concentration the smaller retention concentration in experiment 70 is to be expected. Experiments 73, 75, 76, 78-80, 68, and 86 showed that some nanoparticles exhibit a non-linear relationship between injected concentration and retention concentration at high nanoparticle concentrations. The significantly lower concentration of the injected nanoparticle dispersion in experiment 70 relative to experiment 69 led to a commensurate decrease in retention concentration. It is also interesting to note that the effluent concentration for experiments 69 and 70 reached 115% of the injected concentration for a short interval following nanoparticle breakthrough. The mechanism behind this unusual phenomenon is not known but has only appeared in these two experiments. These two runs are also the only experiments to use mesoporous silica suggesting the unusual spike in the effluent history might be linked to the type of porous medium used in experiments 69 and 70.

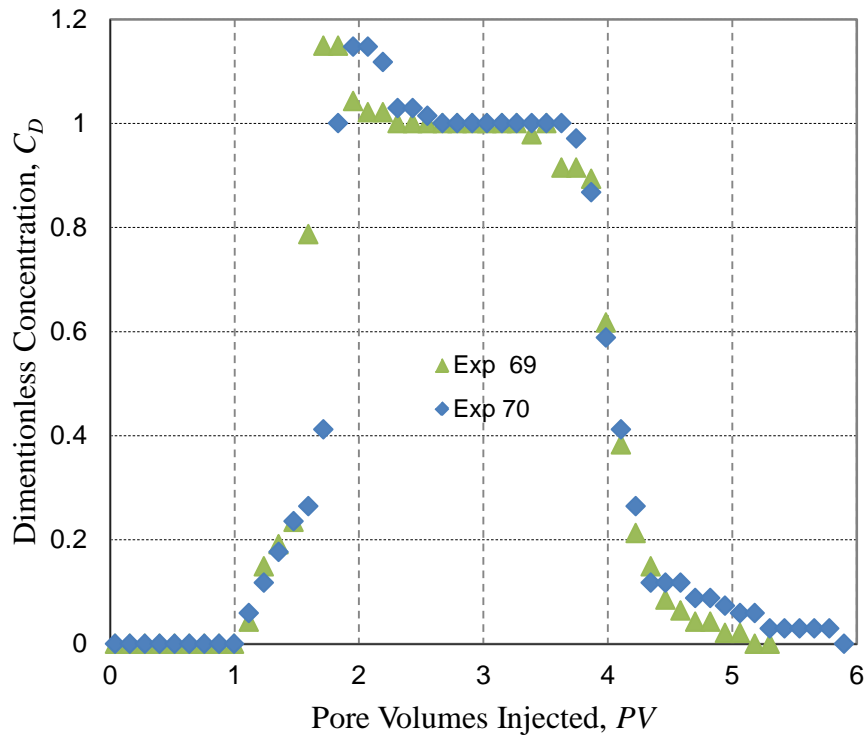


Figure 3.18: Effluent Reinjection Sensitivity Study (Salt Tolerant Silica)

Exp	Sand Type	S_A (m^2)	PVI (PVs)	R_{NP}	R_{Conc} (mg/m^2)	$R_{Monolayer}$ (%)	C_I (wt%)
69	Mesoporous	636	3	87%	0.757	4.99	5.00%
70*	Mesoporous	642	3	87%	0.535	3.53	3.40%

* Effluent from experiment 69

Table 3.12: Data for Effluent Reinjection Sensitivity Study (Salt Tolerant Silica Injected at 1 cc/min)

3.7 THE EFFECT OF TEMPORARY FLOW CESSATION ON NANOPARTICLE TRANSPORT

As discussed above, nanoparticle retention concentration depends on flow rate. The proposed explanation is that hydrodynamic forces alter the extent of irreversible attachment of nanoparticles. A test of this hypothesis is that a period of zero flow rate establishes conditions similar to a batch retention measurement, which is known to show a Langmuir-type concentration dependence for retention Shahavi et al. (2011). Moreover, because the retention concentration increases as flow rate decreases, it is not obvious what the upper bound on retention concentration might be. Thus it is of great interest to conduct experiments at the smallest practical flow rate.

Experiments 98, 99, and 100 injected the same kind of nanoparticle (3M[®] fluorescent silica) with the same injection concentration. The fixed flow rate in these three experiments was 1.02 mL/min, 10 mL/min and 0.206 mL/min respectively. The pump was stopped for 10 minutes in all three experiments after injecting 5 pore volumes of nanoparticle dispersion. Then an additional 2 pore volumes of nanoparticle dispersion were injected at the same flow rate as that before pump stop, followed by postflush until no more nanoparticles were detected in the effluent. Table 3.13 lists the flow conditions for those three experiments with their final concentration of retained nanoparticles. Figure 3.19 compares nanoparticle concentration histories in the effluent from experiments 98, 99 and 100.

Exp	V_p (cc)	ϕ_{brine} (%)	S_A (m ²)	q (cc/min)	PVI (PVs)	C_I (wt%)	R_{Conc} (mg/m ²)	$R_{Monolayer}$ (%)	v (ft/day)
98	15.7	53.18	49.4	1.02	7.10	0.10	0.664	6.56	97
99 Part 1	15.6	53.66	48.9	10.0	7.40	0.10	0.532	5.26	940
100	15.2	54.73	49.9	0.206	7.24	0.10	0.683	6.76	18.4
101	15.2	53.54	51.2	10.5	3.06	1.00	0.560	5.34	989

Table 3.13: Data for Pump Stop Experiments (3M Fluorescent Nanoparticles Injected into Boise Sandstone Packs)

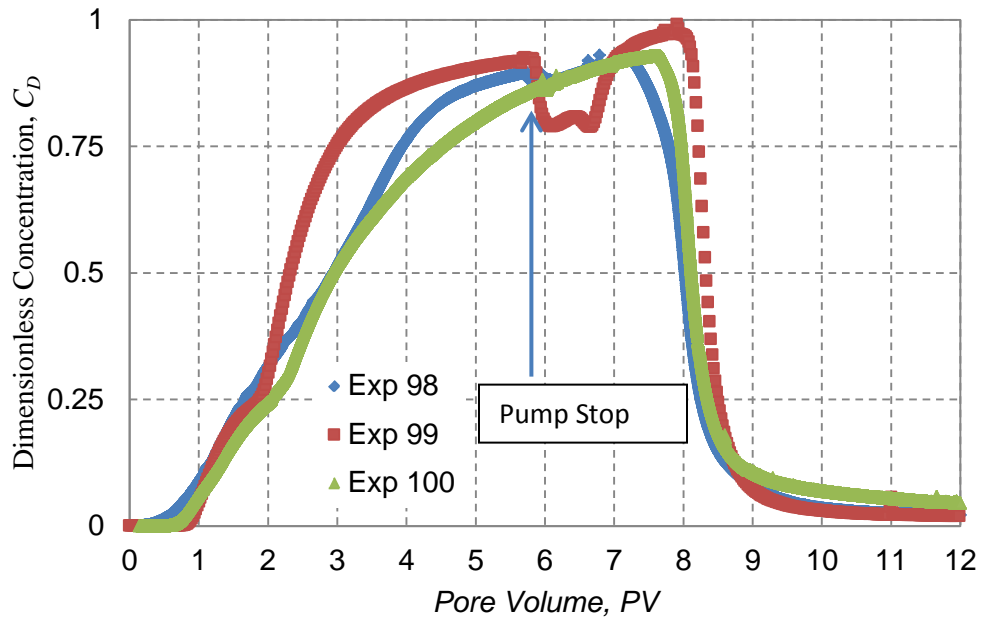


Figure 3.19: Pump Stop Sensitivity Study Effluent Histories

Due to the pump stops, experiments 98 and 99 exhibited notable decline in the effluent concentration history when dispersion injection resumed. With the highest flow

rate, experiment 99 shows the most obvious decrease. Increase in nanoparticle retention concentration due to the pump stop in every experiment was calculated as a difference between the expected effluent curve if the pump had not been stopped and the measured curve. As the dimensionless concentration in the effluent has not reached unity when the postflush started, we also extrapolated the effluent history to unity to calculate the expected retention capacity in those three experiments. The extrapolation was performed using a logarithmic trend line fit of the last 0.5 *PV* effluent history before postflush and can be found of Equations 2.10 and 2.11 of Chapter 2. The trend was extrapolated forward until the effluent concentration reached the injected concentration. The extrapolated data for experiments 98 and 100 with measured data are shown in Figure 3.20. The measured retention concentration, increased retention concentration due to pump stop, and the extrapolated retention capacity for experiments 98, 99 and 100 are plotted as a function of interstitial velocity in Figure 3.21.

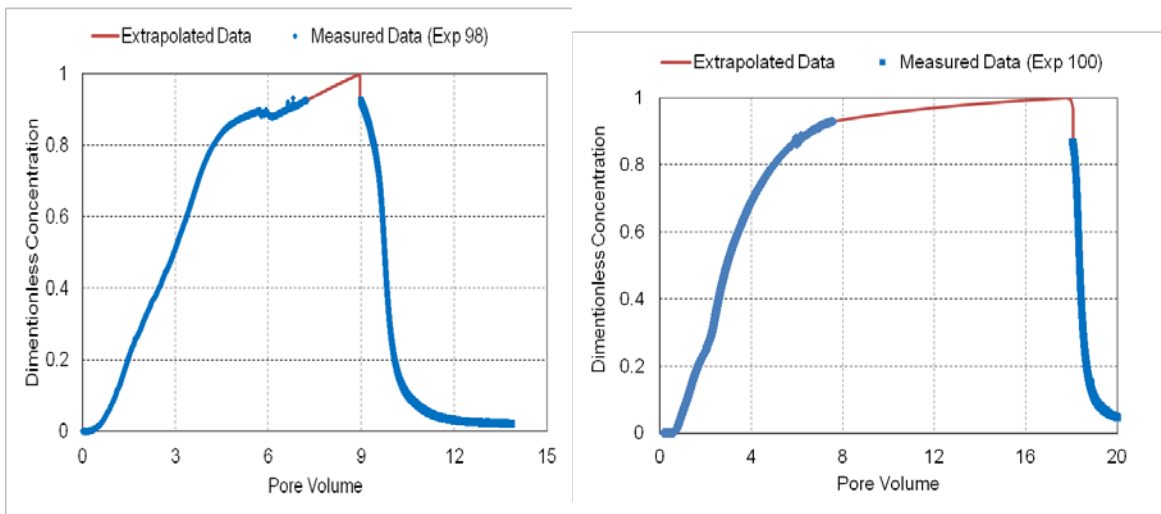


Figure 3.20: Extrapolated Effluent Histories for Pump Stop Experiments

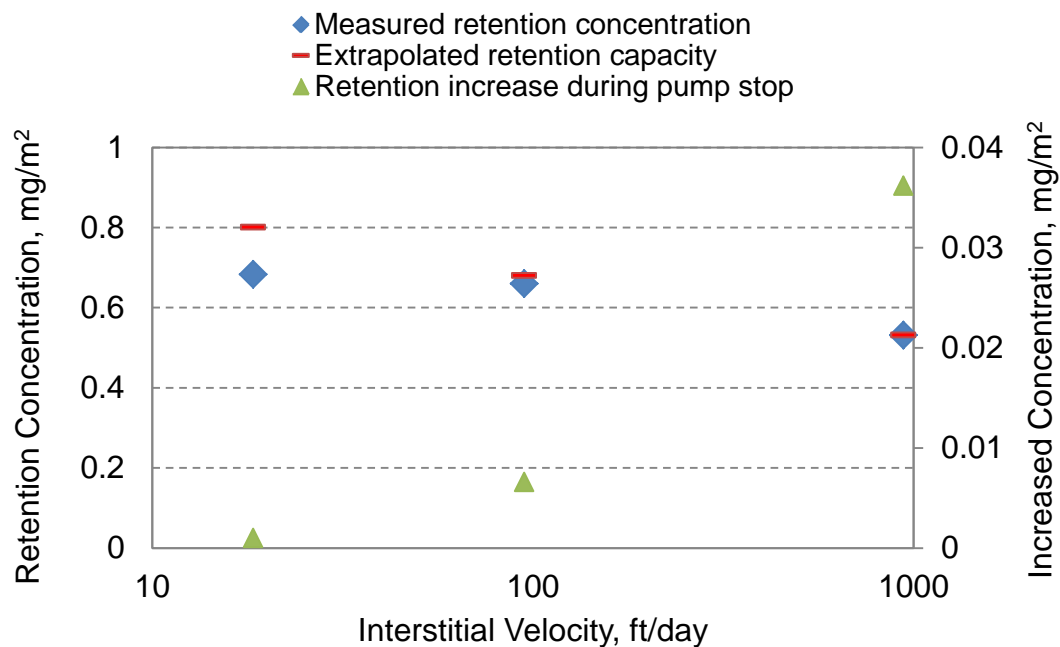


Figure 3.21: Summarized Results from Pump Stop Sensitivity

In experiment 101, 3 pore volume of 1 wt% Fluorescently Tagged 3M[®] nanoparticle dispersion were injected at 10 mL/min continuously. The calculated retention concentration for experiment 101 is similar to the calculated retention concentration for experiment 99 (Part1) for which 0.1 wt% 3M fluorescent silica nanoparticle dispersion was used. Previous results (experiments 96, 103, 104, 86, 68, 78, 79, 80, 73, 75, and 76) suggest retention concentration should increase with increasing injected concentration. If the retention concentration that occurred during the pump stop in experiment 99 (Part1) was reversible the injection concentration trend would suggest total retention concentration for experiment 99 part 1 would be lower than the retention concentration of experiment 101. The fact that the retention concentration is larger for experiment 101 than experiment 99 part 1 suggests nanoparticle attachment during the

no-flow period may have contributed to the retention concentration in experiment 99 part 1.

Data in Figure 3.21 illustrate that the final retention concentration increased with decreasing flow rate in the pump stop experiments, just as in the step change and fixed rate experiments. The extrapolated retention capacity increased faster than the measured retention concentration after postflush with decreasing velocity. Additional nanoparticles have been irreversibly adsorbed during pump stop. And the amount of nanoparticle adsorbed during 10-minute pump stop is larger when the interstitial velocity is higher before and after pump stop. This suggests a Langmuir-type attraction, rather than a filtration-type deposition, is necessary for nanoparticles to adhere to the substrate when there is no flow. The retention capacity in the Langmuir isotherm during this period will be the retention capacity measured in batch experiment minus the retention concentration during flow before pump stop. Therefore, this value will be larger in the experiment with higher flow rate, and more nanoparticles were adsorbed in high flow rate experiment during pump stop.

Interestingly, the pump stop has almost no effect on the 0.2 mL/min run (experiment 100) as the effluent history continues on the same trend before and after the 10-minute stop. At the same time the effluent concentration had only reached 89% of the injected concentration, which means some sites remain available for nanoparticle retention within the sandpack. But stopping the pump to allow for Langmuir-type retention induced no change in the effluent concentration and caused no significant increase in the retention concentration. This suggests that an intrinsic maximum in

retention capacity does exist, and that at sufficiently small flow rates the hydrodynamic forces no longer influence the nanoparticles interaction with the substrate.

3.8 THE EFFECT OF INJECTED SLUG SIZE ON RETENTION CONCENTRATION

A previous experiment, [Experiment 53 by Caldelas, (2010)] indicated injecting a small slug of nanoparticles might generate a significantly different effluent history from results seen with 3 *PV* slug experiments. Specifically, if the mass of nanoparticles injected is much smaller than the mass of nanoparticles needed to fill the retention capacity (presumed to be characteristic of the porous medium), then the effluent could show little or no nanoparticles. Experiments 65 and 66 were run to explore this possibility. Both experiments were run with similar experimental parameters, as shown in Table 3.14 below, but experiment 65 injected 1.5 pore volume of nanoparticle dispersion while experiment 66 injected 3 pore volume. The resulting effluent histories have been plotted in Figure 3.22 below.

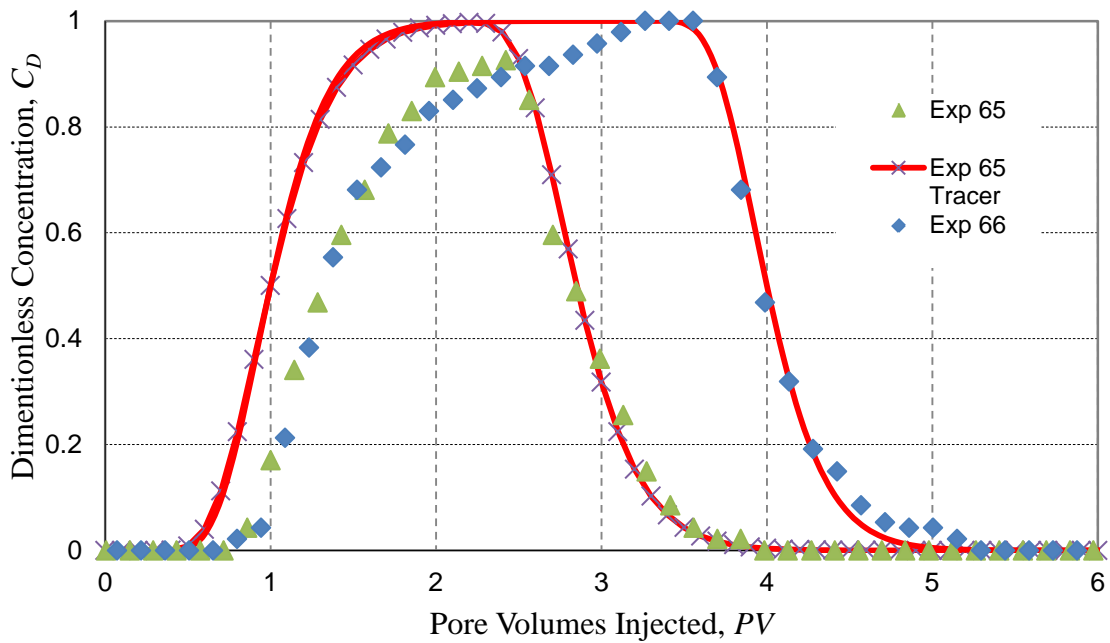


Figure 3.22: Injected Slug Size Sensitivity Study

Exp	Sand Type	S_A (m ²)	q (cc/min)	PVI (PVs)	R_{NP}	R_{Conc} (mg/m ²)	$R_{Monolayer}$ (%)	C_I (wt%)
65	Boise + 5 wt% kaolinite	108	10	1.85	77.95%	2.41	15.82	5.00
66	Boise + 5 wt% kaolinite	109	10	3.00	84.40%	2.93	19.32	5.00
65 Extrapolated	Boise + 5 wt% kaolinite	108	10	3.13	87%	2.69	17.74	5.00

Table 3.14: Data for Injected Slug Size Sensitivity Study (Salt Tolerant 3M Nanoparticles)

Results show exactly what previous experiments have led us to expect. Both experiments having very similar initial experimental parameters experienced nearly identical breakthroughs. The concentration for experiment 65 begins to fall first due to the smaller injected volume. Despite the significantly smaller injected volume the mass of nanoparticles retained is similar for the two experiments. This agrees with our theory that a porous medium has a fixed retention capacity. The effluent concentration for experiment 65 only reached a dimensionless concentration of 91% indicating the sandpack may not have reached its maximum retention capacity while experiment 66 reached a dimensionless concentration of 100% indicating all available sites for nanoparticle retention had been filled. Because all of the sites were filled in experiment 66 and some sites remained unfilled in experiment 65 the retention concentration for experiment 66 should be and is larger. Extrapolating the data from experiment 65 using Equation 2.12 we find the retention concentration increases to 2.69 mg/m^2 . The extrapolated effluent history is plotted alongside data from experiments 65 and 66 in Figure 3.23. While the extrapolated retention concentration for experiment 65 is larger than the retention concentration for the original experiment 65 data (2.41 mg/m^2) it is significantly smaller than the retention concentration of experiment 66 (2.93 mg/m^2). This difference is likely due to experimental error and inaccuracies associated with the extrapolation approximation of Equation 2.12.

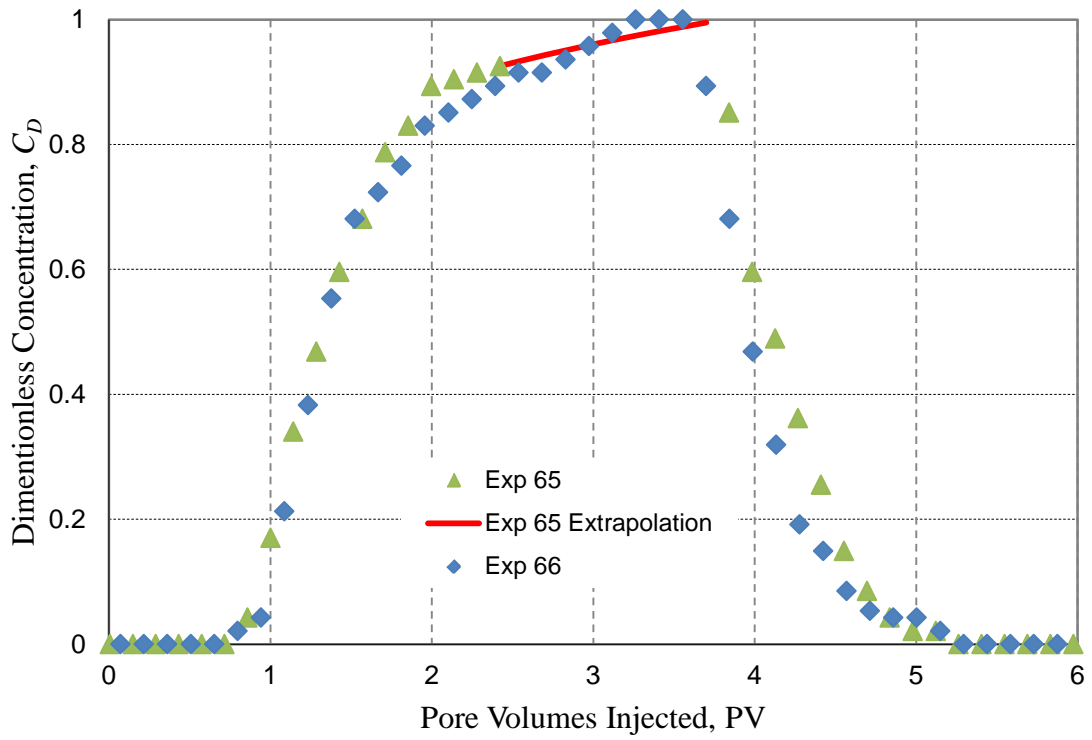


Figure 3.23: Experiment 65 Data Extrapolated to $C_D=1$

Chapter: 4 Conclusions

This chapter details the findings from the experiments discussed in chapter 3 of this thesis. Emphasis is placed on how experimental variables effect nanoparticle retention concentration and ultimately transport of nanoparticles through the unconsolidated porous medium. A list of recommendation for future work is also provided.

4.1 EXPERIMENTAL FINDINGS

- Injected concentration affects nanoparticle retention concentration with larger injected concentrations leading to larger retention concentrations. This trend has been shown for 3 different nanoparticle types.
- Nanoparticle retention concentration appears to be significantly lower on kaolinite than on crushed Boise sandstone. The high salinity environment under which experiments illustrating this effect were performed precludes electrostatic repulsion as being responsible for this phenomenon. The effects appear to be independent of substrate composition and dispersion velocity.
- Velocity of nanoparticle dispersion transit through porous medium appears to influence retention concentration. Higher flow rates generally led to lower permanent nanoparticle retention concentration for a variety of nanoparticle types tested.
- Velocity-based retention concentration appears to be additive with the lowest dispersion velocity observed dictating ultimate retention concentration for the sandpack. Switching from low velocity to high velocity injection does not

cause additional nanoparticle desorption suggesting nanoparticle retention concentration is permanent and order of magnitude shifts in velocity do not generate enough hydrodynamic force to trigger significant desorption.

- For experiments with fixed injected concentration and flow rate the dimensionless concentration of the effluent eventually reaches unity. This suggests the sandpack porous medium used has a fixed retention capacity. After this capacity is filled, subsequently injected nanoparticle dispersion is transported through the porous medium without significant retention on the grain substrate.
- Re-injecting nanoparticle dispersion from the effluent of one sandpack into another does not appear to affect nanoparticle retention concentration beyond what injection concentration trends would predict. This suggests each nanoparticle in the dispersion is equally likely to be adsorbed and given a large enough capacity a porous medium could retain all the nanoparticles from an injection slug.

4.2 FUTURE WORK

The results reported in this Thesis raise a number of further questions regarding the mechanisms of nanoparticle retention in porous media. This section lists a set of recommended experiments and the questions or hypotheses each is designed to test.

- Injecting nanoparticle dispersion at quite low concentrations, $C_I < 0.1$ wt%, and checking the effluent for significant particle concentration could serve to test

whether retention concentration trends match a Langmuir isotherm or more closely agree with filtration theory. Given the need for high sensitivity to detect very low nanoparticle concentrations use of 3M Fluorescently Tagged 3M nanoparticles and the Ultimate 3000 UVD will produce the most accurate results.

- Characterizing the nanoparticle retention concentration distribution in the column after postflush could confirm the hypothesis that nanoparticles retain uniformly across the sandpack. A qualitative estimate may be possible for fluorescently tagged nanoparticles by exposing sand samples extruded from the slim tube to a black light and observing the distribution of nanoparticles.
- Results from Section 3.3 indicate the retention capacity for kaolinite clay and Boise sandstone is significantly different. By running a pair of experiments at very low salinity, one with clay and one without, an analysis of how DLVO effects in the absence of significant electrostatic screening affect this relationship could be performed. Significant fines migration is likely to occur with low salinity injection. The UV detector cannot tolerate fines migration. It will be necessary to use the refractometer to measure nanoparticle concentration.
- Effluent tails were observed for virtually every experiment run for this thesis. These effluent tails suggest nanoparticles are desorbing from the grain substrate during the postflush. The shape of the effluent tail often closely mirrors the shoulder in the leading edge of the nanoparticle slug in the effluent history for $C_D > 0.80$. This leads to the hypothesis that the majority of reversible adsorption

occurs after the effluent concentration exceeds $C_D = 0.80$. This theory can be tested by halting nanoparticle injection before C_D exceeds 0.80 and observing the effect on the effluent tail.

- The reinjection experiments of Section 3.6 and the slug size experiments of Section 3.8 suggest residence time does not influence nanoparticle retention concentration. Running an experiment with a significantly longer sandpack to extend residence time could test the hypothesis that residence time does not affect nanoparticle retention concentration.
- The vast majority of reversible retention is conjectured to occur after the effluent concentration exceeds $C_D = 0.50$. Re-running the flow cessation experiments of Section 3.7 with the pump stops performed before C_D reaches 0.50 could confirm the hypothesis that irreversible nanoparticle retention is possible in a no-flow environment.
- In-situ flow velocities in the field are often much lower than those tested in this thesis. A low flow rate experiment ($q < 0.2$ cc/min) could be performed to extend the flow rate sensitivity to reservoir velocities. A shorter column with a wider internal diameter should be employed decrease experimental run time to practical levels.
- It is believed that the size and shape of the injected nanoparticles leads to hydrodynamic forces influencing retention concentration. By injecting short-chain PEG polymer and observing how polymer suspension retention compares to PEG

coated nanoparticle transport experiments, the effect of hydrodynamic forces on nanoparticle retention can be quantified.

- The experiments of Section 3.3 illustrate retention concentration is related to the concentration of the injected nanoparticle dispersion. It is likely additional nanoparticle retention that results from increasing the injected concentration is additive and that the retention concentration will depend on the highest injected concentration observed. By injecting a slug of nanoparticle dispersion at low concentration, postflushing, and then injecting a slug of high concentration nanoparticle dispersion the incremental increase in retention concentration could be characterized. If a second experiment is run in which a single high concentration nanoparticle slug is injected into a fresh sandpack the hypothesis that nanoparticle retention from increasingly concentrated slugs is additive can be tested.
- Experiments with small injected concentration have not been run to the point that the effluent concentration reached the injected concentration. The retention capacity for experiments with small injected concentrations in this thesis was estimated using the extrapolation method detailed in Section 2.2.3. Results from this approximation could be confirmed by running a low injected concentration experiment in which the effluent concentration reaches $C_D = 1.00$.
- The large pore throats of the unconsolidated sandpacks used for experiments in this thesis make significant nanoparticle straining unlikely. By reversing flow direction and checking for spikes in effluent concentration is possible to test for

nanoparticle staining. It would be necessary to alter the experimental apparatus so that flow direction could be reversed without significantly agitating the sandpack.

- The experiments of this thesis made use of unconsolidated sandpacks to characterize nanoparticle retention concentration in a porous medium. It would be instructive to run a suite of experiments using sandstone core to observe how the consolidated nature of the porous medium affects retention.

A Appendix

A.1 EXPERIMENTAL

A.1.1 Nanoparticle Dispersion Dilution

Nanoparticle dispersions arrived in high concentration batches and were diluted before use. The dispersion were diluted with deionized water (Nanopure) and mixed with sodium chloride (Fisher Scientific) to generate 3 wt% NaCl dispersions with a variety of nanoparticle concentrations. Example values for the mixing of 100 g of each dispersion type and concentration discussed in this thesis can be found in Table A.1-Table A.9 below.

Material	Weight	Weight %	Water % wt	Salt % wt	Nano % wt
Nanoparticle Dispersion	24.863	24.86%	79.9%	0.0%	20.11%
DI	72.137	72.14%	100.0%	0.0%	0.0%
NaCl	3.000	3.00%	0.0%	100.0%	0.0%
Mixture	100.000	100.0%	92.00%	3.0%	5.0%

Table A.1: Diluting 20.11 wt% Salt Tolerant 3M to 5 wt% Salt Tolerant 3M with 3 wt% NaCl

Material	Weight	weight%	Water %wt	Salt %wt	Nano %wt
Nanoparticle Dispersion	16.6	16.67%	70.0%	0.0%	30.0%
DI	80.3	80.3%	100.0%	0.0%	0.0%
NaCl	3.000	3.00%	0.0%	100.0%	0.0%
Mixture	100.0	100.0%	92.00%	3.0%	5.0%

Table A.2: Diluting 5 wt% Nexsil DP to 5 wt% Nexsil DP with 3 wt% NaCl

Material	Weight	weight%	Water %wt	Salt %wt	Nano %wt
Nanoparticle Dispersion	11.6	11.6%	70.0%	0.0%	30.0%
DI	85.3	85.33%	100.0%	0.0%	0.0%
NaCl	3.0	3.00%	0.0%	100.0%	0.0%
Mixture	100.0	100.00%	93.5%	3.0%	3.5%

Table A.3: Diluting 30 wt% Nexsil DP to 3.5 wt% Nexsil DP with 3 wt% NaCl

Material	Weight	weight%	Water %wt	Salt %wt	Nano %wt
Nanoparticle Dispersion	8.667	8.67%	70.0%	0.0%	30.0%
DI	88.3	88.3%	100.0%	0.0%	0.0%
NaCl	3.000	3.00%	0.0%	100.0%	0.0%
Mixture	100.0	100.00%	94.40%	3.0%	2.6%

Table A.4: Diluting 30 wt% Nexsil DP to 2.6 wt% Nexsil DP with 3 wt% NaCl

Material	Weight	weight%	Water %wt	Salt %wt	Nano %wt
Nanoparticle Dispersion	5.000	5.00%	70.0%	0.0%	30.0%
DI	92.000	92.0%	100.0%	0.0%	0.0%
NaCl	3.000	3.00%	0.0%	100.0%	0.0%
Mixture	100.0	100.0%	95.50%	3.0%	1.5%

Table A.5: Diluting 30 wt% Nexsil DP to 1.5 wt% Nexsil DP with 3 wt% NaCl

Material	Weight	weight%	Water %wt	Salt %wt	Nano %wt
Nanoparticle Dispersion	4.667	4.67%	70.0%	0.0%	30.0%
DI	92.333	92.3%	100.0%	0.0%	0.0%
NaCl	3.000	3.00%	0.0%	100.0%	0.0%
Mixture	100.000	100.0%	95.60%	3.0%	1.40%

Table A.6: Diluting 30 wt% Nexsil DP to 1.4 wt% Nexsil DP with 3 wt% NaCl

Material	Weight	weight%	Water %wt	Salt %wt	Nano %wt
Nanoparticle Dispersion	24.272	24.27%	79.4%	0.0%	20.6%
DI	72.728	72.73%	100.0%	0.0%	0.0%
NaCl	3.000	3.00%	0.0%	100.0%	0.0%
Mixture	100.0	100.0%	92.00%	3.0000%	5.0%

Table A.7: Diluting 20.6 wt% Fluorescent PEG 3M to 5 wt% Fluorescent PEG 3M with 3wt% NaCl

Material	Weight	weight%	Water %wt	Salt %wt	Nano %wt
Nanoparticle Dispersion	4.854	4.85%	79.4%	0.0%	20.6%
DI	92.146	92.15%	100.0%	0.0%	0.0%
NaCl	3.000	3.00%	0.0%	100.0%	0.0%
Mixture	100.0	100.0%	96.0%	3.0%	1.0%

Table A.8: Diluting 20.6 wt% Fluorescent PEG 3M to 1 wt% Fluorescent PEG 3M with 3 wt% NaCl

Material	Weight	weight%	Water %wt	Salt %wt	Nano %wt
Nanoparticle Dispersion	0.485	0.49%	79.4%	0.0%	20.6%
DI	96.515	96.51%	100.0%	0.0%	0.0%
NaCl	3.000	3.00%	0.0%	100.0%	0.0%
Mixture	100.0	100.0%	96.9%	3.0%	0.1%

Table A.9: Diluting 20.6 wt% Fluorescent PEG 3M to 0.1 wt% Fluorescent PEG 3M with 3 wt% NaCl

A.1.2 Sand Acquisition and Washing

The sand packs were filled with crushed Boise sandstone taken from a large block, see Figure A.1. Pieces of the block that could not be drilled to create cores were broken off with a hammer. The pieces were partially crushed using a mortar and pestle, see Figure A.2. The sand samples were then run through a Cuisinart blender to further crush the material, see Figure A.3. The resulting crushed sand was sorted using a series of meshed sieves (Sargent-Welch Scientific or Fisher Scientific; ranging from 40 mesh to 250 mesh) agitated in a Ro-Tap testing sieve shaker, see Figure A.4. The incremental changes in mesh size defined the range of grain sizes in the separated batches. These ranges were: 63-75 μm , 75-90 μm , 90-105 μm , 105-125 μm , 125-149 μm , 149-177 μm , 177-210 μm , 210-250 μm , 250-297 μm , 297-420 μm , and 420-590 μm . Grains larger than 590 μm were further crushed in the Cuisinart blender.



Figure A.1: Boise Sandstone Source Block (1 Foot Tape Measure for Scale)



Figure A.2: Mortar and Pestle



Figure A.3: Cuisinart Blender



Figure A.4: Mesh Sieves loaded into Ro-Tap Sieve Shaker

Finally to minimize fines migration the collected sand samples were placed in a small mesh size sieve and repeatedly rinsed with deionized water. The rinsed samples are then heated to 105 C for 45 minutes in a Blue M series oven, see Figure A.5, ensuring the samples are completely dried before packing.



Figure A.5: Blue M Series Oven

A.1.3 Sandpack Preparation and Packing

Sand was packed into 1 foot long Swagelok stainless steel slim tubes (inner diameter= 0.43 inches), see Figure A.6. The ends of the column were capped with Swagelok half-inch to eight-inch reducing unions with several layers of wire mesh epoxied onto them to ensure no sand was transported outside of the column. During packing one of these end caps was fitted to the column and a funnel was fit to the other end to facilitate loading of the crushed sand into the column. A small wrench was used to agitate the column and encourage closer packing of the sand grains. This packing process was undertaken methodically in order to produce similar grain packing for each column. A complete description of the packing process can be found in the experimental procedure section A.2.

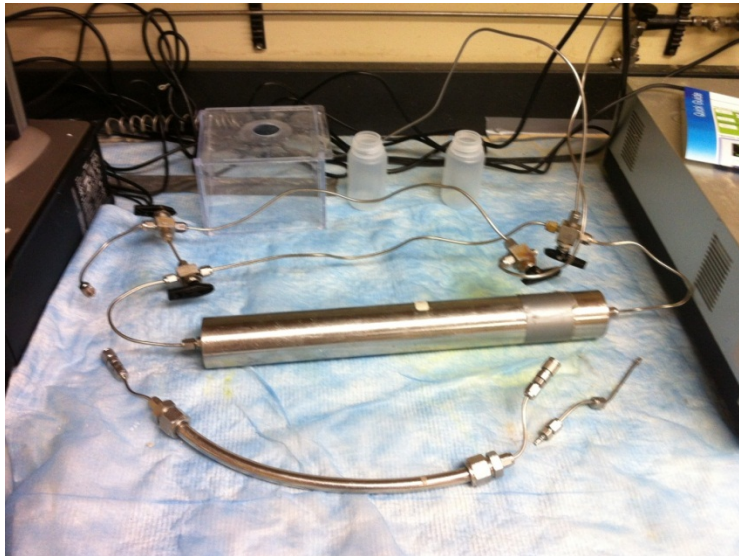


Figure A.6: 1 ft Slim-Tube Column

A.1.4 Sandpack Vacuum Saturation

The packed column was attached to the vacuum saturation apparatus via Swagelok quick connects. The vacuum pump, Figure A.7, was run for 30 minutes and then stopped for an hour. If pressure in the sandpack remains constant over this hour the pressure seals was deemed intact and the vacuum pump was run for another 3 hours to ensure all air has been removed from the column. Connection to the vacuum pump was then shut with a 2-way valve and a downstream valve connecting the column to a brine source was opened allowing the evacuated column to fill.



Figure A.7: Vacuum Pump

A.1.5 Sandpack Characterization

All sandpacks used in experiments for this thesis were run with 1 foot long Swagelok stainless steel tubing with known internal volumes. By weighing the slim tubes when empty, when filled with sand and when saturated with 3 wt% brine it was possible to characterize the porosity and pore volume of the sandpack. Using the known internal volume (V_{Bulk}), the density of the brine, the dry weight of the slim tube filled with sand, and the weight of the slim tube saturated the porosity of the sandpack can be calculated with Equation A.1.

$$\phi_{Grain} = \frac{\left[\frac{W_{Dry} - W_{Sat}}{\rho_{Brine}} \right]}{V_{Bulk}}$$

Equation A.1

Surface area for the sandpacks was calculated from the masses of crushed sand and kaolinite loaded into the slim tube using interpolations between BET measurements. BET measurements were taken by Ki Youl Yoon (The University of Texas at Austin) on a sample of 63-75 μm Boise sandstone and a sample of 297-420 μm Boise sandstone. Interpolation between these values was used relate the inverse of the mean grain radius to surface area per mass of sand. The specific surface area for each pack was calculated as a function of the mean radius of the grain size using Equation A.2. The product of Equation A.2 and the weight of Boise sandstone loaded into the slim tube could then be used to determine the bulk surface area of the pack. BET measurements were also taken for sand samples with varying amounts kaolinite. The BET isotherm tests were performed with a Quantichrome Instruments Nova 2000 series surface area analyzer using nitrogen as the adsorbent gas. The measurements were performed by Ki Youl Yoon of the University of Texas Chemical Engineering department and included 7 data points that fit the Brunauer-

Emmett-Teller equation with a 0.99 correlation coefficient. The results for all BET measurements used can be found in Table A.10 below.

$$A_{BET} = \left[\frac{49.223}{r} + 0.959 \right] \frac{m^2}{g}$$

Equation A.2

where, r is the average sand grain size in μm

Sample		A_{BET} (m^2/g)
Grain size / type	Added Clay	
63 – 75 μm Boise	-	1.6724
297 – 420 μm Boise	-	1.0963
297 – 420 μm Texas Cream	-	0.7453
250 – 297 μm Boise	5 wt% Kaolinite	2.6649
250 – 297 μm Boise	10 wt% Kaolinite	3.9062
250 – 297 μm Boise	25 wt% Kaolinite	9.1352
250 – 297 μm Boise	40 wt% Kaolinite	13.2060
250 – 297 μm Boise	10 wt% Illite	2.8942

Table A.10: BET Measurements

A.1.6 Zeta Potential

Zeta potential measurements were measured by Ki Youl Yoon and Andrew Worthen of the Chemical Engineering department of the University of Texas at Austin. The measurements were taken using a ZetaPlus dynamic light scattering apparatus at a 90° scattering angle and temperature of 25°C . The complete list of zeta potential results can be found in Table A.11 below.

Sample	Zeta Potential (mV)
Boise sandstone	-22.12 ± 5.58
Kaolinite clay	-17.77 ± 4.09
NexSil 20	-50.51 ± 2.62
Salt Tolerant 3M	-3.22 ± 3.05
Nexsil DP	-3.91 ± 2.01

Table A.11: Zeta Potential Measurements

A.1.7 Tracer Test

Characterization of the dispersivity of the sandpacks was essential for modeling purposes. To this end a brine tracer test was performed prior to nanoparticle dispersion injection for each experiment. The process involved saturating the column with 3 wt% NaCl brine and injecting 3 pore volumes of a higher concentration NaCl brine. 3 mL samples were collected in borosilicate glass test tubes. The conductivity was measured using an Orion 3 Star conductivity probe, see Figure A.8.



Figure A.8: Orion 3Star Conductivity Probe

The conductivity of each sample was a direct function of its salinity. The relationship between conductivity and salinity was found to be linear for concentrations used. Dimensionless brine concentration where ($C_D= 0\%$) is the saturation concentration and ($C_D= 100\%$) is the injected concentration was calculated using Equation A.3 below. The calculated dimensionless concentration history was fit to the dimensionless convection-dispersion equation by solving for the Peclet number, see Equation A.4 below.

$$C_D = \frac{C_{measured} - C_{saturated}}{C_{injected} - C_{saturated}} \quad \text{Equation A.3}$$

$$C_D = \frac{1}{2} \left[1 - \operatorname{erf} \left(\frac{x_D - t_D}{2\sqrt{\frac{t_D}{N_{Pe}}}} \right) \right] = \frac{1}{2} \operatorname{erfc} \left(\frac{x_D - t_D}{2\sqrt{\frac{t_D}{N_{Pe}}}} \right)$$

$$\text{where } N_{Pe} = \frac{uL}{\phi K_l}$$

Equation A.4

A.1.8 Effluent Concentration Using Refractometer

Experiments making use of experimental apparatus (setup 1) measured nanoparticle concentration in the effluent with a Leica Mark II Plus Refractometer. The relationship between concentration and refractive index was found to be linear for all particle types and concentrations tested. Example calibration curves for Nexsil DP and Salt Tolerant 3M can be found in Figure A.9 and Figure A.10 below.

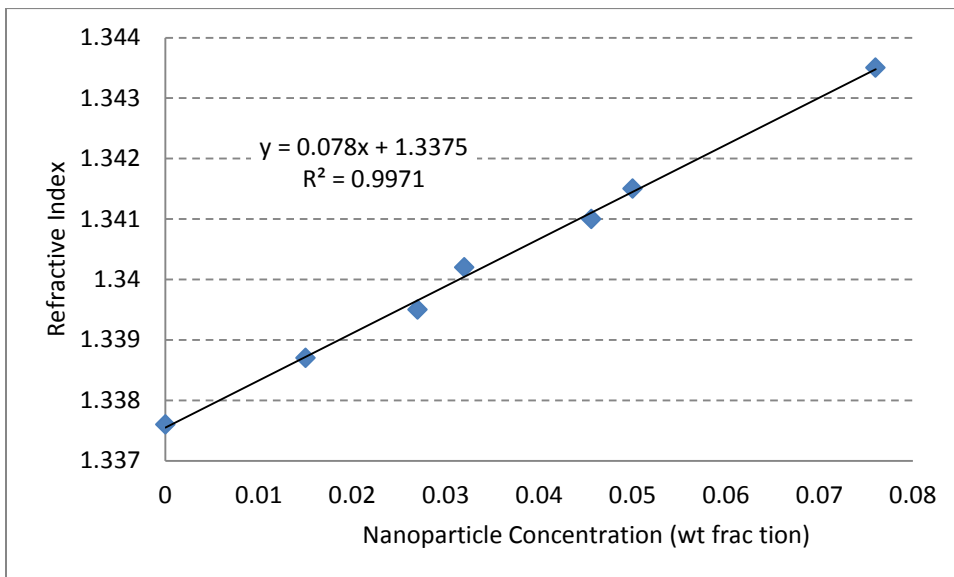


Figure A.9: Nexsil DP Refractive Index Calibration Curve

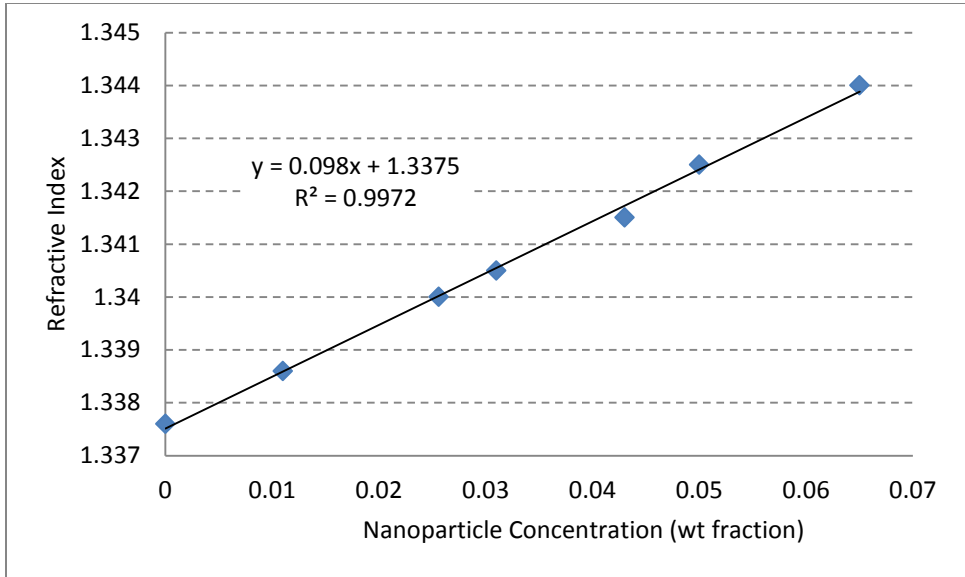


Figure A.10: Salt Tolerant 3M Refractive Index Calibration Curve

For all experiments using experimental apparatus (setup 1) the refractive index of the injected brine and the nanoparticle dispersion to be injected were taken using a Leica Mark II Plus Refractometer, see Figure A.11. A linear interpolation between these numbers was used to determine dimensionless effluent nanoparticle concentration in the i th sample as described in Equation A.5.



Figure A.11: Leica Mark II Plus Refractometer

$$C_{Di} = \frac{RI_i - RI_{\min}}{RI_{\max} - RI_{\min}} \quad \text{Equation A.5}$$

A.1.9 Effluent Concentration Using UV Detector

Experiments making use of experimental apparatus (setup 2 and setup 3) measured nanoparticle concentration in the effluent with an Ultimate 3000 UV detector, see Figure A.13. Experiments involving fluorescently tagged silica particles made use of the UV lamp and absorbance was measured at wavelengths between 400 nm and 500 nm depending on injected concentration. Experiments involving iron oxide made use of the Vis lamp and absorbance was measured at wavelengths between 600 nm and 700 nm depending on injected concentration. The relationship between concentration and refractive index was found to be linear for all particle types and concentrations tested. An example calibration curve for Fluorescently Tagged 3M particles can be found in Figure

A.12 below. Note that there is an inverse relationship between absorbance readings and velocity of the injected fluid for fluorescently tagged particles. The effect of velocity on absorbance of iron oxide particles, due to its measurement using the visible light spectrum lamp, is effectively negligible for the resolution of the Ultimate 3000. A detailed description of the preparation of the detector prior to each experiment and how the data is modified to enhance the accuracy of the results can be found in the procedure, section A.2, of this thesis.

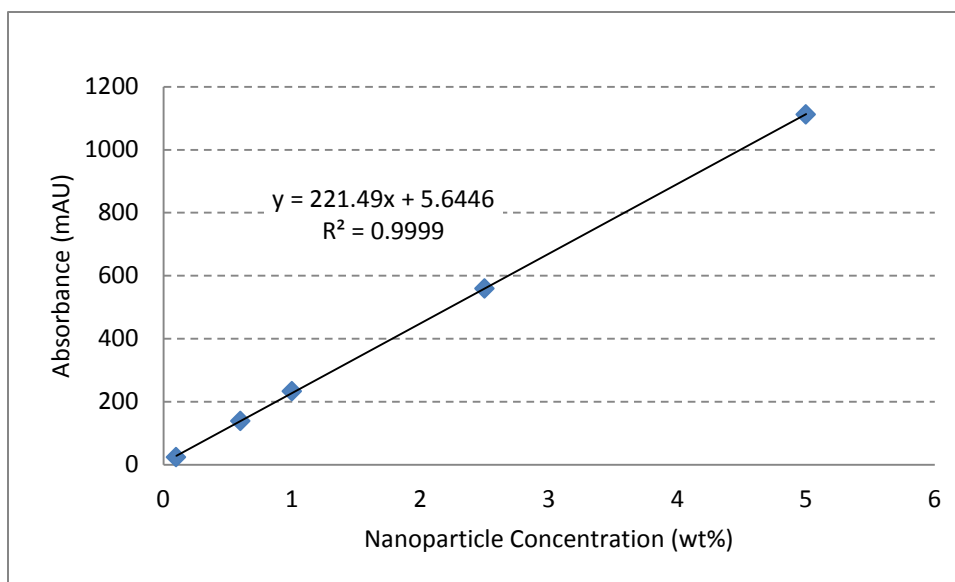


Figure A.12: Fluorescent 3M PEG UV Calibration Curve



Figure A.13: Ultimate 3000 UV-Vis detector

A.2 PROCEDURE

The following is a list detailing the procedure for the experimental process undertaken for the experiments of this thesis. “Sand acquisition” describes the process for repeated generating crushed Boise sandstone properties. “Sand packing and saturation” describes how the sandpack is loaded to ensure similar grain packing and saturation characteristics between experiments. The “experimental apparatus” subsection describes the setup and use of the purpose built apparatus and detailing necessary steps to minimize experimental error.

A.2.1 Sand Acquisition

- Use hammer to break off Boise sandstone from sample block
- Grind sandstone with mortar and pestle
- Further grind with blender
- Assemble sieves in order of decreasing mesh size, fill top sieve with no more than 100 g of crushed sandstone, and agitate in Ro-Tap for 20 minutes

- Collect sand samples into labeled bins
- Load sand samples into sieve smaller than bin size and rinse repeatedly with deionized water (500 mL of deionized water for every 100 g of ground sand)
- Load sieve with rinsed sand into oven and heat to 105 C for 45 minutes

A.2.2 Sand Packing and Saturation

- Weigh empty column and end pieces; record measurement
- Affix downstream end piece to column (note it is important to consistently orient the same end downstream, if one end is set downstream for the vacuum saturation and the other end is set downstream for the experiment sand will flow from the column into the end pieces at both ends altering the packing, porosity and effective length)
- Fill the column with 5 g of sand and agitate with the wrench (10 equally spaced strikes across the length of the column repeated 5 times)
- Repeat the filling and agitation cycle until column is filled and tightly packed
- Weigh packed column, record measurement
- Check vacuum saturation apparatus (empty and refill graduated cylinder with freshly mixed 3 wt% NaCl)
- Attach packed column to vacuum saturation apparatus (pay attention to downstream orientation)
- Run vacuum pump for one hour and then turn the pump off, note pressure gauge reading
- If the pressure gauge reading does not change over the course of an hour restart vacuum pump and run for an additional 3 hours

- Shut upstream valve cutting off connection to vacuum pump and open downstream connection to brine filled graduated cylinder
- Once the water level in the graduated cylinder has stopped falling remove the column from the vacuum saturation apparatus
- Weigh saturated column, record measurement

A.2.3 Experimental Apparatus Setup (for Setup 1, 2 and 3)

- Load freshly mixed brine into pump source beaker
- Prime Pump
- Run at 1 mL/min for 10 minutes collecting fluid in graduated cylinder to validate pump is fully purged
- Flush upstream portions of experimental apparatus with brine from pump
- Load upstream end of accumulator with fresh DI
- Load downstream end of accumulator with low salinity brine for tracer experiment
- Attach accumulator to experimental apparatus
- Direct pump flow to accumulator and push 5 mL of low salinity brine through the upstream tubing (this flushes out fluids from previous experiments and pressurizes accumulator)
- Close valves connecting accumulator to pump and upstream tubing
- Flush upstream tubing with 100 mL of brine
- Attach packed column to experimental apparatus
- Flush with 5 *PV* of brine
- Run pump at experimental flow rate and measure volume of effluent produced to validate flow rate

A.2.4 Brine Tracer Experiment

- Measure conductivity of 3 wt% brine and low salinity brine, record measurements
- Load fraction collector with 36 16×100mm borosilicate glass test tubes
- Set fraction collector to collect 3mL / tube (set timer based on flow rate [i.e. 3 min/tube at $q= 1 \text{ mL/min}$])
- Start pump (set to flow rate to be used in nanoparticle injection to follow), start fraction collector timer and open connections to accumulator
- Inject 3 *PV* of low salinity brine
- Shut connection to accumulator and inject an additional 4 *PV* of 3 wt% brine
- Take conductivity measurements as experiment proceeds (note evaporation will affect conductivity measurements, it is important that each measurement be taken immediately after the test tube is filled)
- Analyze results and ensure that tracer results are normal before proceeding to nanoparticle injection
- Disconnect accumulator and load downstream end with nanoparticle dispersion
- Reattach accumulator and detach sandpack column
- Direct pump flow to accumulator and push 5 mL of nanoparticle dispersion through the upstream tubing (this flushes out the low salinity brine from the tracer experiment and pressurizes accumulator)
- Flush upstream tubing with 100 mL of brine
- Reattach column

A.2.5 Nanoparticle Injection (For Experimental Apparatus Setup 1)

- Measure refractive index of nanoparticle dispersion to be injected, record measurement

- Load fraction collector with 12×100 mm borosilicate glass test tubes
- Start pump (set to flow rate to be used in nanoparticle injection to follow), start fraction collector timer and open connections to accumulator
- Close connection to accumulator after prescribed number of *PV* of NP dispersion has been injected
- Flush column with several *PV* of brine while continuing to collect effluent

A.2.6 Nanoparticle Injection (For Experimental Apparatus Setup 2 and 3)

- Remove column and bridge connection between upstream and downstream tubing
- Turn on UV spectrometer (activate UV lamp for fluorescently tagged particles and the Vis lamp for iron oxide particles) and launch Chameleon Software
- Turn on pump and run flow rate validation experiment
- Check upstream pressure at pump (if pressure exceeds 50 psi at $q = 4$ mL/min a flow obstruction exists in the UV detector flow cell and must be cleared)
- Run UV detector with 1 mL/min brine flow for one hour or until flow temperature reaches steady state
- Set baseline for UV detector absorbance readings
- Open connections to accumulator and inject nanoparticle dispersion until absorbance measurement reaches steady state (if this value is greater than 1500 mAu the wavelength of measure must be adjusted and the baseline reset)
- For fluorescently tagged nanoparticles it is necessary to run this calibration test at the same flow rate as the experiment to follow
- Create new data file for experiment
- Prepare graduated cylinder for effluent collection
- Start data acquisition and begin nanoparticle injection

- Take periodic measurements of the volume of effluent produced and recorded volume and time since data acquisition began
- After brine flush detach column and bridge downstream and upstream tubing
- Inject brine and record absorbance to establish drift (this is assumed to vary linearly over the course of the experiment, recorded data is adjusted to account for this phenomena)

A.3 RUNS

This section provides a detailed list of the experimental parameters for each run followed by figures depicting the dimensionless effluent concentration history for each experiment and the corresponding tracer curve. A short summary of defining experimental parameters and goals for each run is also provided.

A.3.1 Experimental Parameters

A full list of experimental parameters for each run is provided in Table A.12 below. This table includes many calculated parameters including the porosity, interstitial velocity, residence time, nanoparticle recovery, nanoparticle retention concentration, and nanoparticle percent monolayer coverage. Porosity is calculated using the method described in section A.1.5 of the Appendix and Equation A.1.

The interstitial velocity was calculated from the flow rate, cross sectional area and porosity using Equation A.6.

$$v = \frac{u}{\phi} = \frac{q}{\phi A} \quad \text{Equation A.6}$$

Residence time was calculated from the pore volume and velocity using Equation A.7.

$$t_{res} = \frac{V_p}{q} = \frac{AL\phi}{q} \quad \text{Equation A.7}$$

A.3.2 Results Summary

A complete list of measured and calculated experimental parameters for the experiments detailed in Chapter 3 of this thesis follows below.

Exp	60	61	62	63	64	65	66
V_p (cc)	14.3	10.9	13.9	16.4	15.17	14.1	13.8
ϕ_{brine} (%)	42.3	35.1	46.4	53.8	50.3	48.6	47.6
Sand Type	Boise + 10 wt% kaolinite	Boise + 10 wt% kaolinite	Boise	Boise	Boise	Boise + 5 wt% kaolinite	Boise + 5 wt% kaolinite
S_A (m ²)	165	159	59.4	50	41.9	108	109
q (cc/min)	1	1	1	1	10	10	10
v (ft/day)	119.2	143.5	108.7	93.78	1002	1037	1059
PVI (PVs)	3.0	3.3	3.177	3.03	3.0	1.9	3.0
C_I (wt%)	5.00	5.00	5.00	5.00	5.00	5.00	5.00
Nanoparticle	Salt Tolerant 3M	Salt Tolerant 3M	Salt Tolerant 3M	Nexsil 20	Salt Tolerant 3M	Salt Tolerant 3M	Salt Tolerant 3M
R_{NP} (%)	78.00	60.50	87.50	103	97.00	77.90	84.40
R_{Conc} (mg/m ²)	2.83	4.46	4.94	-0.855	1.42	2.41	2.93
$R_{Monolayer}$ (%)	18.68	29.41	32.57	-4.23	9.36	15.82	19.32
Experimental Apparatus	Setup 1	Setup 1	Setup 1	Setup 1	Setup 1	Setup 1	Setup 1
D_p (μm)	250-297	250-297	90-105	105-125	297-420	177-210	177-210
R_M (mg)	466.95	709.14	293.44	-42.75	29.49	260.28	319.37
$t_{arrival}$	1.41	2.18	1.47	0.98	1.06	1.32	1.33

Exp	67	68	69	70	71	72	73
V_p (cc)	13.9	13.9	25.1	25.0	14.7	13.4	14.9
ϕ_{brine} (%)	47.9	47.9	86.6	86.3	50.7	46.2	51.4
Sand Type	Boise + 5 wt% kaolinite	Boise + 5 wt% kaolinite	Mesoporous	Mesoporous	Boise	Boise + 10 wt% kaolinite	Boise
S_A (m ²)	109	108	636	642	47.5	167	47.9
q (cc/min)	1	1	1	1	1	1	1
v (ft/day)	105.2	105.2	58.22	58.46	99.45	109.1	98.12
PVI (PVs)	3	3.19	3.03	3	3	3	3
C_I (wt%)	5.00	5.00	5.00	3.40	5.00	5.00	5.00
Nanoparticle	Salt Tolerant 3M	Nexsil DP	Salt Tolerant 3M	Salt Tolerant 3M	Nexsil DP	Nexsil DP	Nexsil DP
R_{NP} (%)	82.60	94.80	87.30	86.60	91.30	88.90	92.70
R_{Conc} (mg/m ²)	3.32	1.84	0.757	0.535	4.03	1.3	3.42
$R_{Monolayer}$ (%)	21.89	6.74	4.99	3.53	14.76	4.76	12.53
Experimental Apparatus	Setup 1	Setup 1	Setup 1	Setup 1	Setup 1	Setup 1	Setup 1
D_p (μm)	177-210	177-210	-	-	150-177	150-177	177-210
R_M (mg)	361.88	198.72	481.45	343.47	191.43	217.1	163.81
$t_{arrival}$	1.46	1.17	1.53	1.73	1.17	1.1	1.06

Exp	74	75	76	77	78	79	80
V_p (cc)	14.4	14.6	14.6	13.5	14.1	14.0	14.2
ϕ_{brine} (%)	49.6	50.3	50.4	46.6	48.6	48.3	49
Sand Type	Boise	Boise	Boise	Boise + 10 wt% kaolinite	Boise + 5 wt% kaolinite	Boise + 5 wt% kaolinite	Boise + 5 wt% kaolinite
S_A (m ²)	48.7	447.8	48	52.6	108	109	107
q (cc/min)	1	1	0.88	9.8	10	10	9.6
v (ft/day)	101.5	100.1	88.12	1083	1037	1044	988.3
PVI (PVs)	3	3	2.64	2.9	3	3	2.84
C_I (wt%)	2.60	2.84	1.50	5.00	1.30	3.00	5.00
Nanoparticle	Nexsil DP	Nexsil DP	Nexsil DP	Nexsil DP	Nexsil DP	Nexsil DP	Nexsil DP
R_{NP} (%)	102	96.00	95.00	92.20	96.30	97.40	96.40
R_{Conc} (mg/m ²)	-0.414	1.25	0.964	2.93	0.192	0.309	0.656
$R_{Monolayer}$ (%)	-1.52	4.58	3.53	10.73	0.70	1.13	2.40
Experimental Apparatus	Setup 1	Setup 1	Setup 1	Setup 1	Setup 1	Setup 1	Setup 1
D_p (μm)	177- 210	177-210	177-210	177-211	177-212	177-213	177-214
R_M (mg)	-20.16	59.75	46.27	154.12	20.74	33.68	70.19
$t_{arrival}$	1.1	1.04	1.09	1.1	1.17	1.04	0.96

Exp	81	82	83	84	85	86	91
V_p (cc)	14.4	13.9	14.7	14.1	14.1	13.9	14.5
ϕ_{brine} (%)	49.7	47.9	50.7	48.6	48.6	47.9	46.4
Sand Type	Boise + 5 wt% kaolinite	Boise + 5 wt% kaolinite	Boise + 40 wt% kaolinite	Boise + 5 wt% kaolinite	Boise + 5 wt% kaolinite	Boise + 5 wt% kaolinite	Boise
S_A (m ²)	107	107	190	108	108	109	49.9
q (cc/min)	1	1	1	1	1	1	1
v (ft/day)	101.5	105.2	99.45	103.7	103.7	105.2	108.7
PVI (PVs)	3	3	N/A	3	3	3	2.9
C_I (wt%)	5.00	5.00	N/A	1.40	5.00	1.20	0.10
Nanoparticle	Nexsil DP (Centrifuge Depleted)	Nexsil DP	N/A	Nexsil DP (Freeze Depleted)	Nexsil DP (Centrifuge Depleted)	Nexsil DP	IO (Coating 1)
R_{NP} (%)	87.70	96.10	N/A	85.50	92.40	89.70	46.90
R_{Conc} (mg/m ²)	2.47	1.8	N/A	0.793	1.072	0.49	0.455
$R_{Monolayer}$ (%)	9.05	6.59	N/A	2.90	3.93	1.79	0.19
Experimental Apparatus	Setup 1	Setup 1	N/A	Setup 1	Setup 1	Setup 1	Setup 2
D_p (μm)	177-215	177-216	N/A	210-250	210-250	210-250	150-180
R_M (mg)	264.29	192.60	N/A	85.64	115.78	53.41	22.70
$t_{arrival}$	1.2	1.14	N/A	1.15	1.12	1.02	2.6

Exp	92	93	94 (Part 1)	94 (part 2)	96	97	98
V_p (cc)	14.8	15.5	16.1	16.1	16.2	16.1	15.7
ϕ_{brine} (%)	47.3	50	55	55	54	54	53
Sand Type	Boise						
S_A (m ²)	49	46.5	47.6	47.6	48.3	48.6	49.4
q (cc/min)	8.33	9.3 then 1.07	0.87 then 10	10	1	1	1.02
v (ft/day)	888	937 then 108	80 then 919	919.3	92.95	93.57	97
PVI (PVs)	3.108	3.8	8.12	3.4	3.55	3.41	7.104
C_I (wt%)	0.10	0.10	0.10	0.10	1.0	0.60	0.10
Nanoparticle	IO (Coating 1)	IO (Coating 2)	IO (Coating 3)	IO (Coating 3)	3M Fluorescent	3M Fluorescent	3M Fluorescent
R_{NP} (%)	78.90	72.50	92.50	99.80	93.90	89.90	70.60
R_{Conc} (mg/m ²)	0.198	0.348	0.207	0.0025	0.73	0.708	0.663
$R_{Monolayer}$ (%)	0.08	0.15	0.09	0.00	7.22	7.00	5.56
Experimental Apparatus	Setup 2						
D_p (μm)	150-181	150-177	150-177	150-177	150-177	150-177	150-177
R_M (mg)	9.70	16.18	9.85	0.12	35.26	34.41	32.75
$t_{arrival}$	1.86	1.85	1.4	1	0.98	1.1	2.94

Exp	99	99 part 2	100	98 Extrapolated	100 Extrapolated	101	102
V_p (cc)	15.6	15.6	15.2	15.7	15.2	15.2	15.5
ϕ_{brine} (%)	53.7	53.7	54.7	53.1	54.7	53.5	50.8
Sand Type	Boise	Boise	Boise	Boise	Boise	Boise	Boise
S_A (m ²)	48.9	48.9	49.9	49.4	49.9	51.2	51.4
q (cc/min)	10	1	0.206	1	0.2	10.5	1.02
v (ft/day)	939.8	939.8	19	94.83	18.43	989	96
PVI (PVs)	7.4	6	7.24	7.1	7.24	3.03	3.01
C_I (wt%)	0.10	0.10	0.10	0.10	0.10	1.00	0.50
Nanoparticle	3M Fluorescent	3M Fluorescent	3M Fluorescent	3M Fluorescent	3M Fluorescent	3M Fluorescent	3M Fluorescent
R_{NP} (%)	77.50	91.10	69.00	75.70	84.90	94.20	87.80
R_{Conc} (mg/m ²)	0.532	0.17	0.683	0.683	0.803	0.54	0.553
$R_{Monolayer}$ (%)	5.26	1.68	6.76	6.76	7.94	5.34	5.74
Experimental Apparatus	Setup 2	Setup 2	Setup 2	Setup 2	Setup 2	Setup 2	Setup 2
D_p (μm)	150-177	150-177	150-177	150-177	150-177	125-150	125-150
R_M (mg)	26.01	8.31	34.08	33.74	40.07	17.65	28.42
$t_{arrival}$	2.33	1.17	2.93	2.94	2.93	1.1	1

Exp	103	104
V_p (cc)	15.1	15.5
ϕ_{brine} (%)	48.7	48.5
Sand Type	Boise	Boise
S_A (m ²)	51.4	48.3
q (cc/min)	1	1
v (ft/day)	105.1	104
PVI (PVs)	3.1	3.01
C_I (wt%)	5.00	0.50
Nanoparticle	3M Fluorescent	3M Fluorescent
R_{NP} (%)	98.10	87.40
R_{Conc} (mg/m ²)	0.876	0.605
$R_{Monolayer}$ (%)	8.66	5.98
Experimental Apparatus	Setup 3	Setup 3
D_p (μm)	125-150	125-150
R_M (mg)	45.03	29.22
$t_{arrival}$	1.08	1.19

Table A.12: Results Summary

A.3.3 Effluent Histories

Figures illustrating the effluent concentration histories and accompanying descriptions of relevant experimental parameters and motivation for performing each run follow below.

A.3.3.1 Experiment 59*

*Flow rate is believed to be far lower than nominal value for experiment 59 resulting in early decrease in effluent concentration. The effluent PV was computed from elapsed time and the nominal injection rate, not from actual volume in the effluent collector See experiment 61.

For this experiment 3 PV of 5 wt% Salt Tolerant 3M dispersion was injected into a 1 foot column of 90 wt% 250-297 μm Boise sandstone mixed with 10 wt% kaolinite. This experiment was performed to compare with experiment 32, a similar experiment that used 5 wt% PEG 3M nanoparticle dispersion. There is significant air saturation in both experiments; neither result is used for systematic analysis of retention properties in the results section.

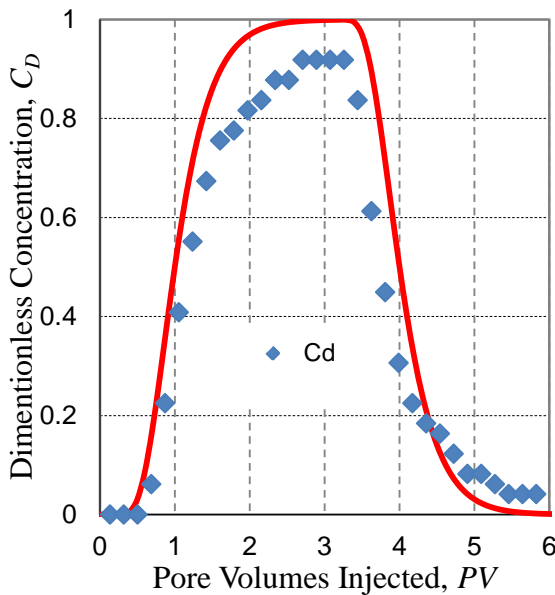


Figure A.15: Experiment 32 Effluent History

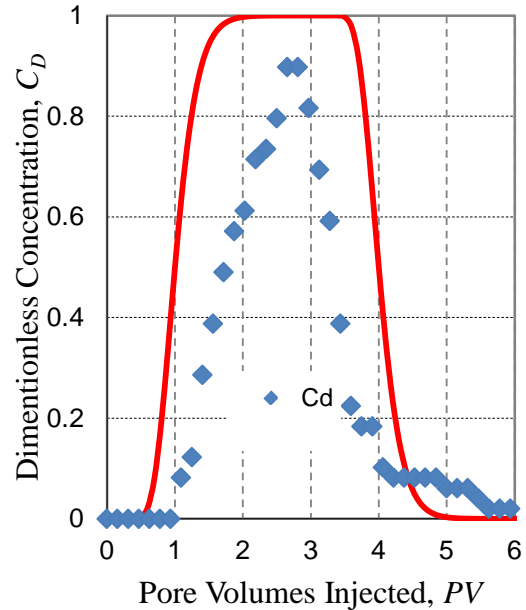


Figure A.14: Experiment 59 Effluent History

A.3.3.2 Experiment 60

In this experiment 3 PV of 5 wt% Salt Tolerant 3M dispersion were injected into a 1 foot column of 90 wt% 250-297 μm Boise sandstone mixed with 10 wt% kaolinite. This was the first experiment to use a vacuum pump to ensure no air remained in the sandpack, with the exception of experiment 61 all experiments after 60 were packed with a vacuum pump considered free of air. This experiment was also used as part of a kaolinite sensitivity study for Salt Tolerant 3M particles which included experiments 60, 62 and 70.

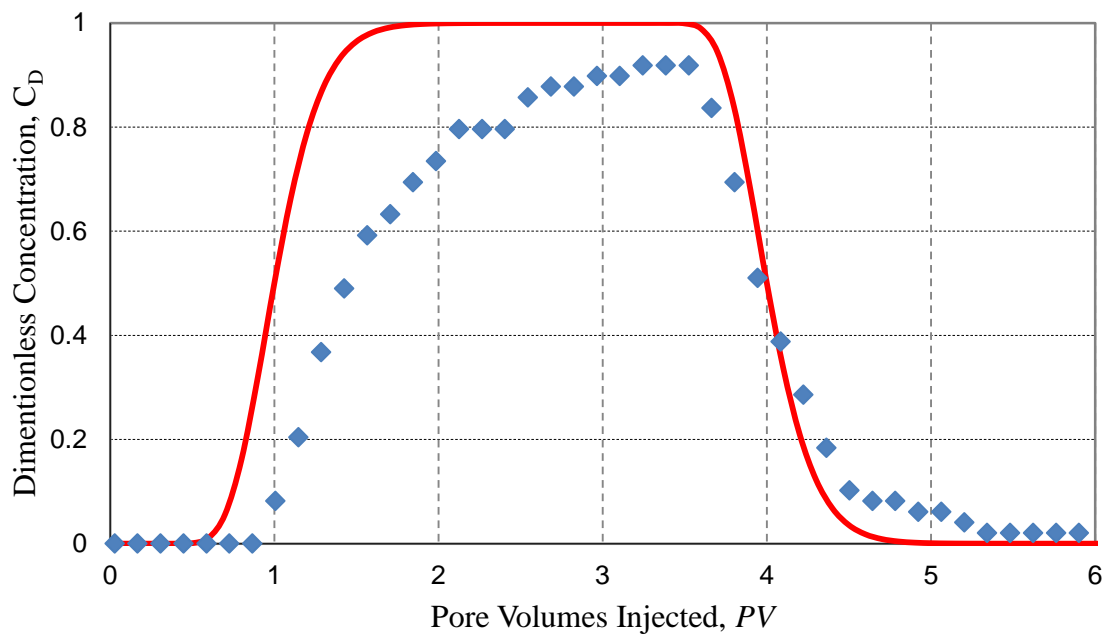


Figure A.16: Experiment 60 Effluent History

A.3.3.3 Experiment 61*

*This is a repeat of experiment 59 with special care taken to calculate the correct flow rate.

For this experiment 3 PV of 5 wt% Salt Tolerant 3M dispersion was injected into a 1 ft column of 90 wt% 250-297 μm Boise sandstone mixed with 10 wt% kaolinite. The Sandpack was saturated with a pump and had significant air filled porosity (11.4 %). This experiment was performed to compare with experiment 32, a similar experiment that used 5 wt% PEG 3M nanoparticle dispersion, and experiment 60 which used a vacuum pump. Comparison of experiments 60 and 61 indicate air saturation significantly impacts the effluent history by increasing retention capacity for the sandpack. The effluent concentration history is plotted ignoring the air saturation, that is, the volume of fluid injected is normalized by the entire pore volume of the sand pack.

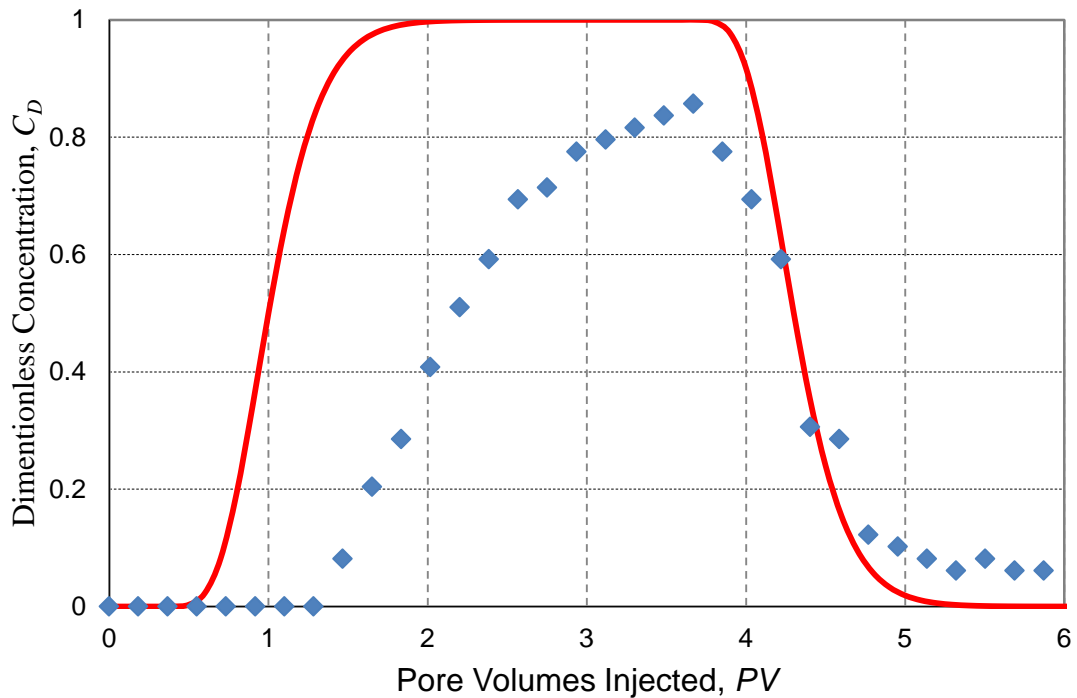


Figure A.17: Experiment 61 Effluent History

A.3.3.4 Experiment 62

In this experiment 3.178 PV of 5 wt% Salt Tolerant 3M dispersion was injected into a 1 foot column of 100 wt% Boise sandstone. This experiment was run as part of a kaolinite sensitivity study for Salt Tolerant 3M particles which included experiments 60, 62 and 70.

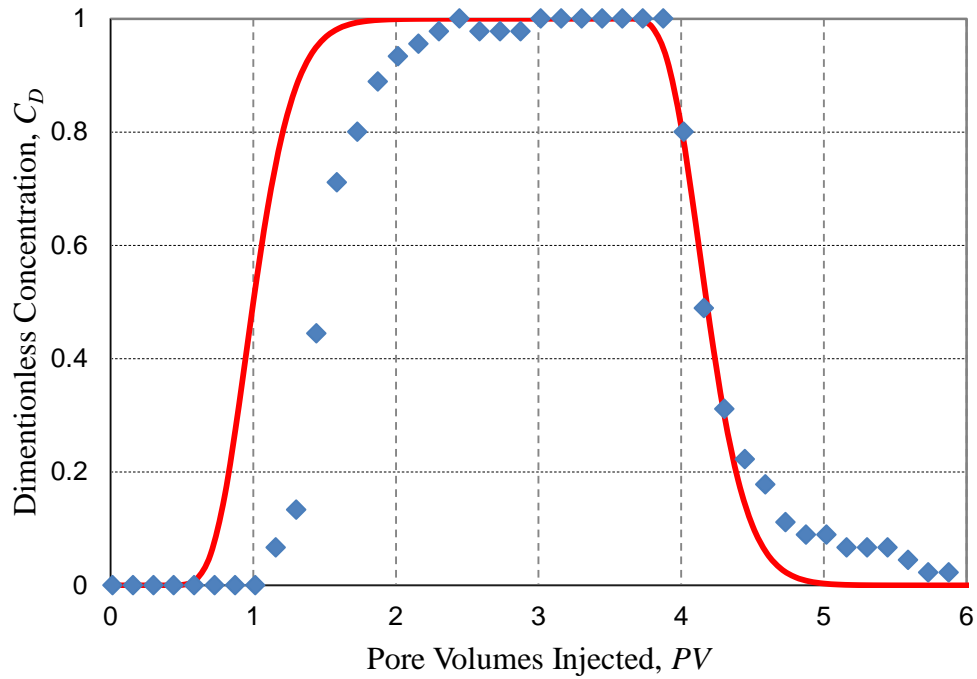


Figure A.18: Experiment 62 Effluent History

A.3.3.5 Experiment 63

In this experiment 3.178 PV of 5 wt% Nexsil 20 dispersion was injected into a 1 foot column of 100 wt% Boise sandstone. The experiment exhibited a recovery over 100 %. This is physically impossible and believed to be a result of experimental error. It is likely that the total volume of nanoparticles injected was underestimated.

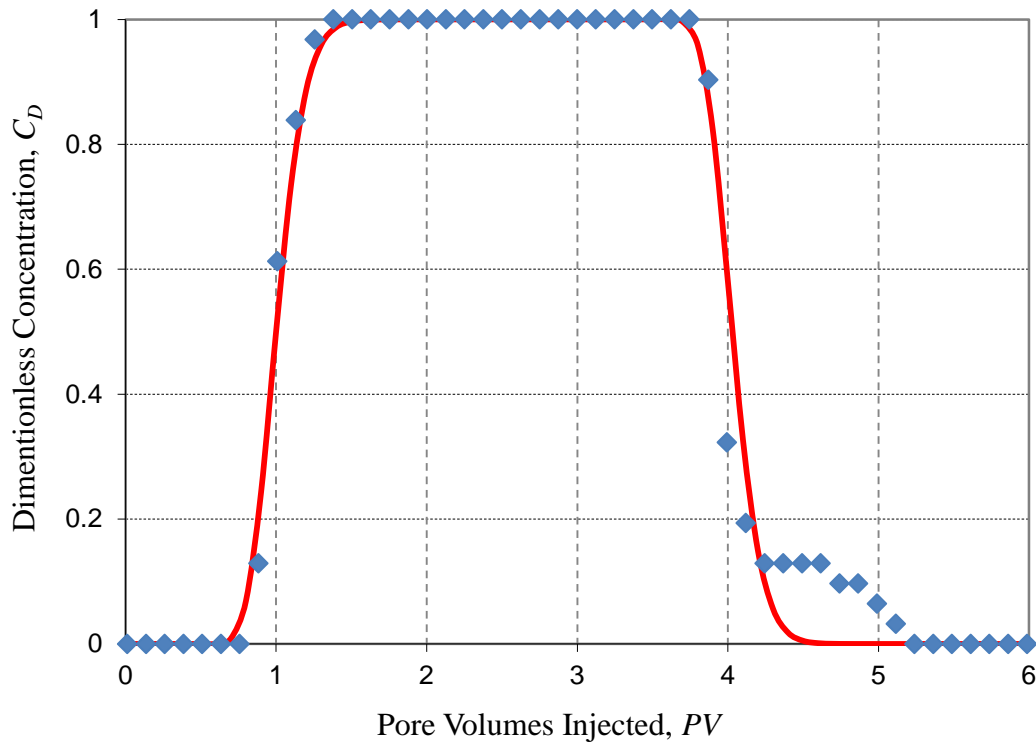


Figure A.19: Experiment 63 Effluent History

A.3.3.6 Experiment 64

In this experiment 3 PV of 5 wt% Salt Tolerant 3M dispersion was injected into a 1 foot column of 100 wt% Boise sandstone at 10 mL/min to test the effect of high flow rate on nanoparticle retention in a Sandpack. Results were compared with experiment 58 (run at 1 mL/min).

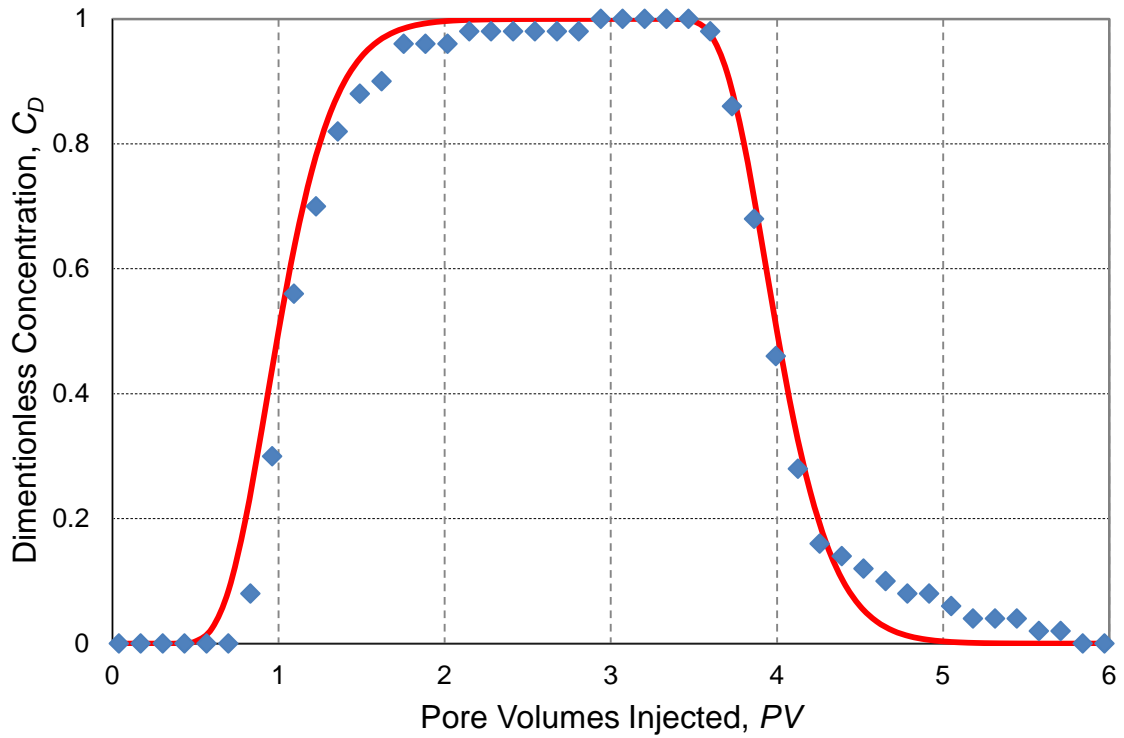


Figure A.20: Experiment 64 Effluent History

A.3.3.7 Experiment 65

For this experiment 1.9 PV of 5 wt% Salt Tolerant 3M dispersion was injected into a 1 ft column of 95 wt% 177-210 μm Boise sandstone mixed with 5 wt% kaolinite at 10 mL/min. Results were compared with experiment 66 to observe the effect of slug size on retention concentration

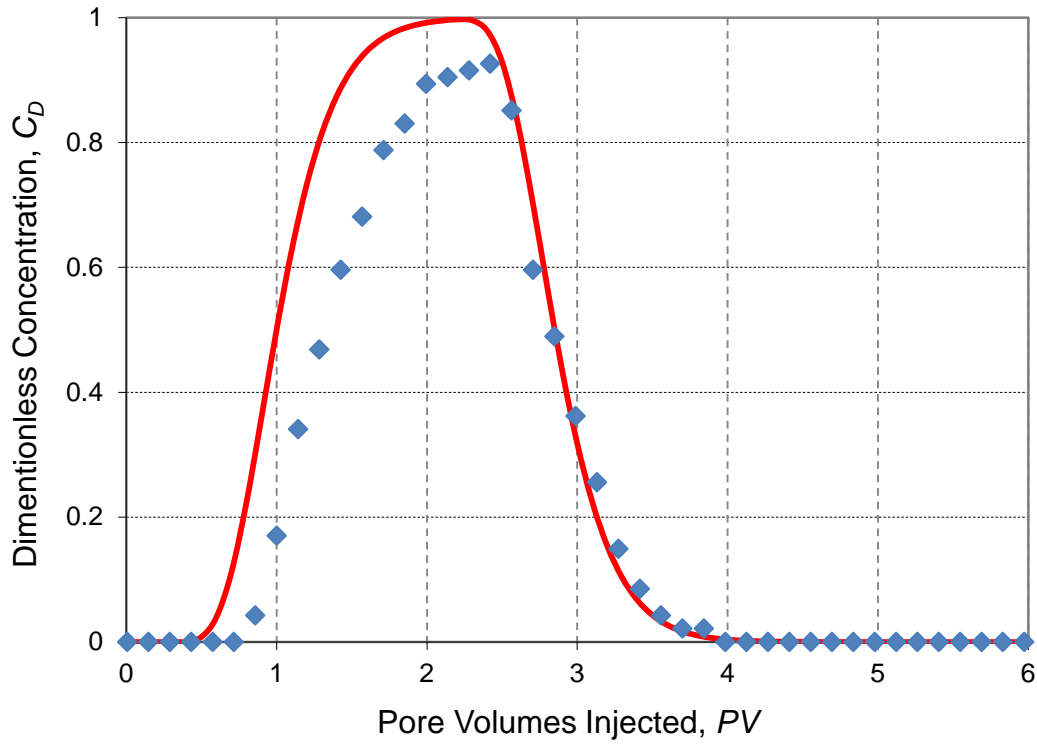


Figure A.21: Experiment 65 Effluent History

A.3.3.8 Experiment 66

For this experiment 3 PV of 5 wt% Salt Tolerant 3M dispersion was injected into a 1 ft column of 95 wt% 177-210 μm Boise sandstone mixed with 5 wt% kaolinite at 10 mL/min. Experiments 65 and 66 represent a slug size sensitivity. Experiment 66 also tests high flow rate nanoparticle retention in the presence of kaolinite.

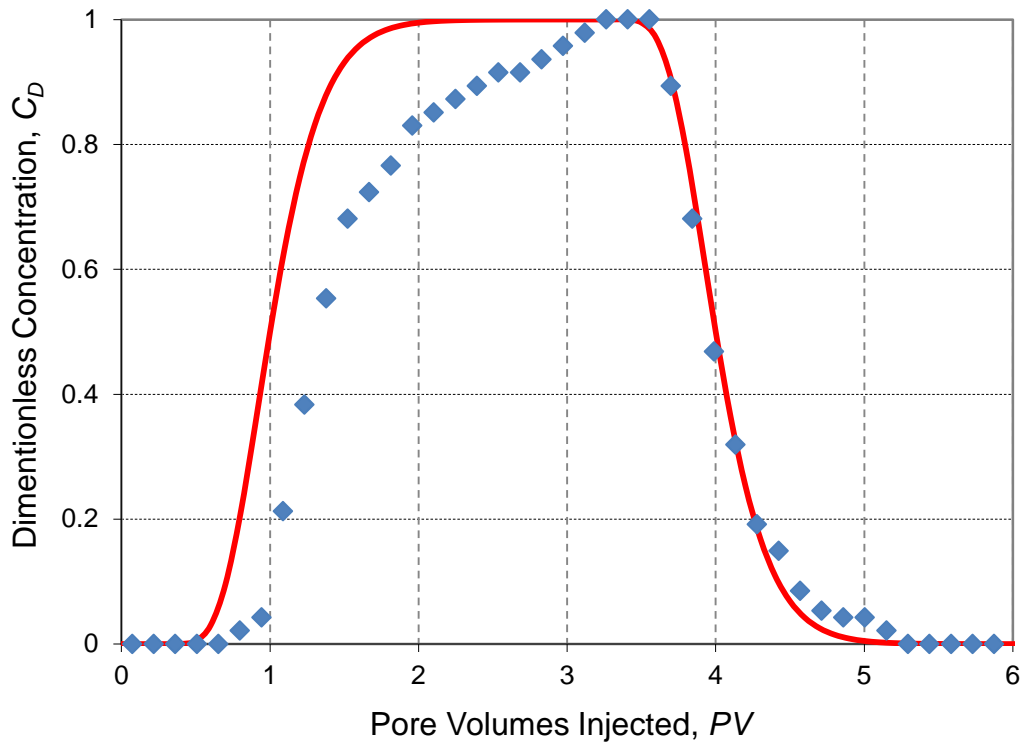


Figure A.22: : Experiment 66 Effluent History

A.3.3.9 Experiment 67

Experiment 67 was run with diluted 5 wt% Salt Tolerant 3M dispersion fluid injected at 1 mL/min using a sandpack that included 5 wt% kaolinite. 3 PV of nanoparticle dispersion was injected. Experiment 67 tests low flow rate nanoparticle retention in the presence of kaolinite. Experiments 66 and 67 represent a flow rate sensitivity for Salt Tolerant 3M nanoparticle retention in the presence of kaolinite.

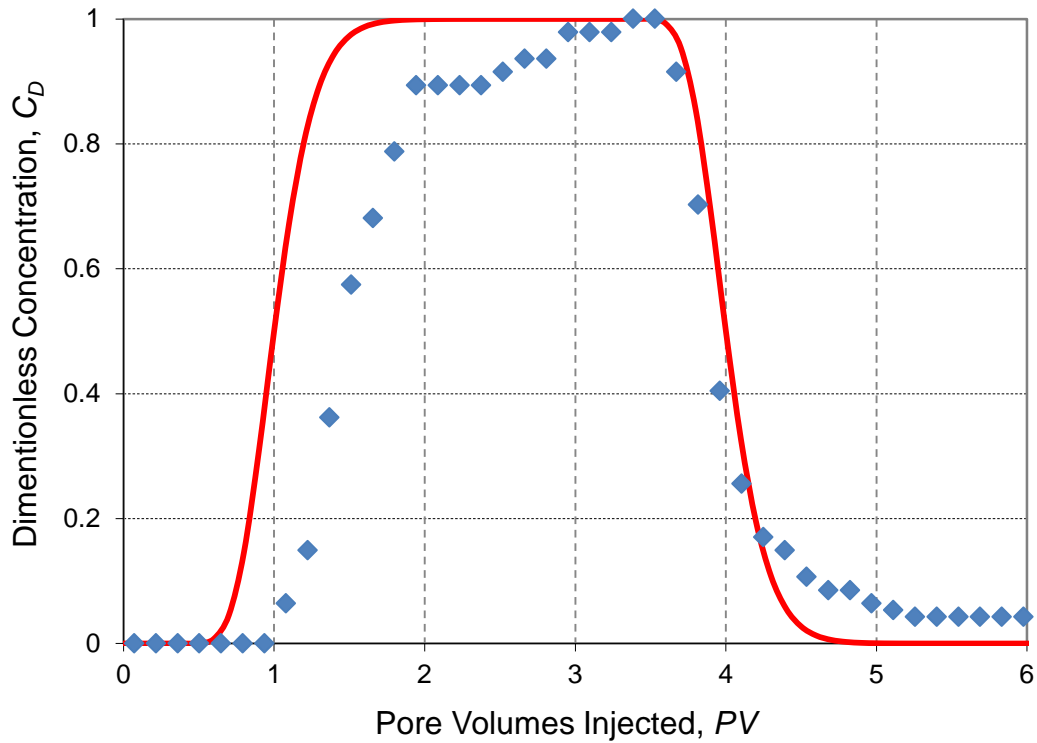


Figure A.23: Experiment 67 Effluent History

A.3.3.10 Experiment 68

For this experiment 3 PV of 5 wt% Nexsil DP dispersion was injected into a 1 ft column of 95 wt% 177-210 μm Boise sandstone and 5 wt% kaolinite injected at 1 mL/min. Experiments 68 and 80 represent a flow rate sensitivity for Nexsil DP nanoparticle retention in the presence of kaolinite. Experiments 68 and 86 were used as a sensitivity of the effect of injected concentration on nanoparticle retention with low injected dispersion velocity in the presence of kaolinite.

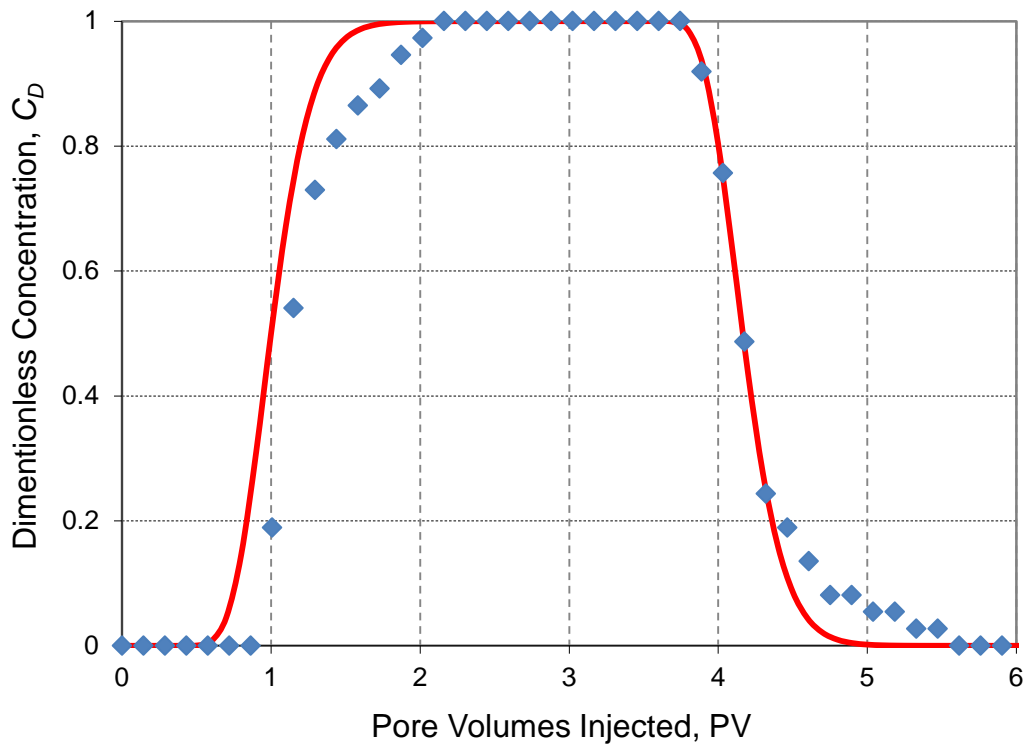


Figure A.24: Experiment 68 Effluent History

A.3.3.11 Experiment 69

Experiment 69 was run with diluted 5 wt% Salt Tolerant 3M dispersion injected at 1 mL/min using a slim tube filled with mesoporous silica. The effluent from experiment 69 was collected and injected into experiment 70 to test the effect of reinjection on nanoparticle retention.

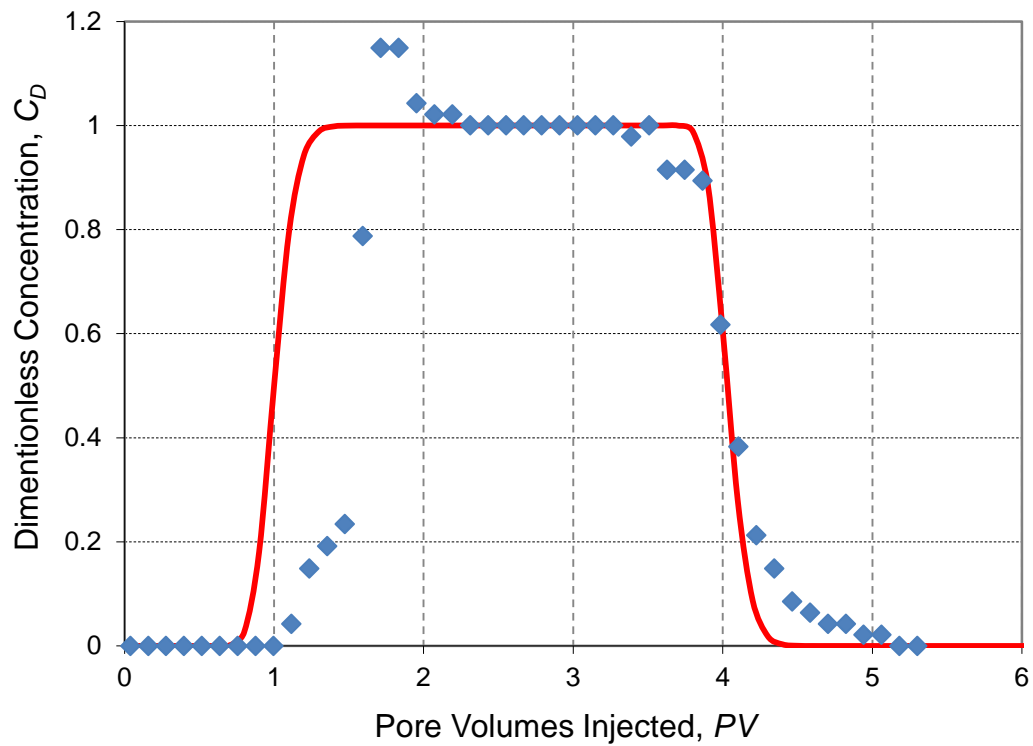


Figure A.25: Experiment 69 Effluent History

A.3.3.12 Experiment 70

Experiment 70 was run with the effluent from experiment 69 injected at at 1 mL/min using a sandpack filled with mesoporous silica. Experiment 70 shows a lower retention than experiment 69. This is believed to be an effect of injected concentration.

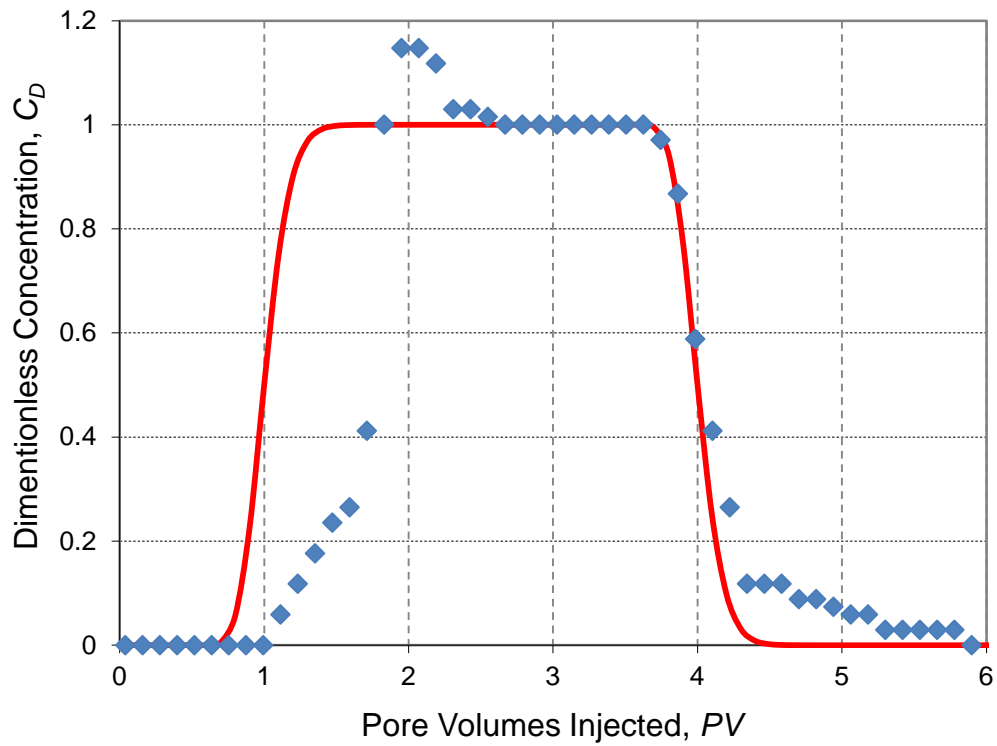


Figure A.26: Experiment 70 Effluent History

A.3.3.13 Experiment 71

Experiment 71 was run with diluted 5 wt% Nexsil DP dispersion fluid injected at 1 mL/min using a sandpack of 100% Boise sandstone.

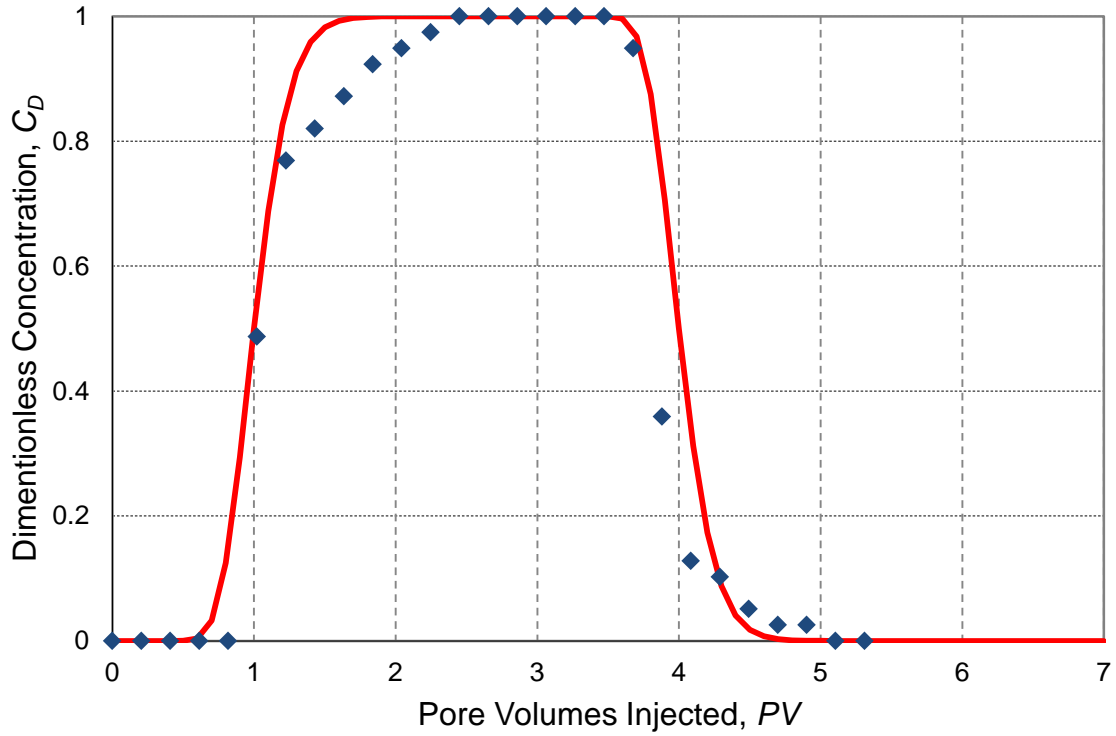


Figure A.27: Experiment 71 Effluent History

A.3.3.14 Experiment 72

Experiment 72 was run with diluted 5 wt% Nexsil DP dispersion fluid injected at 1 mL/min using a sandpack with 10 wt% kaolinite and 90 wt% Boise sandstone. Experiments 72 and 77 are a flow rate sensitivity for retention of Nexsil DP nanoparticles for sandpacks with 10% kaolinite. Concentration measurements were made using both a UV spectrometer and a refractometer. UV spectrometer measurements were made using a Cray 500 to confirm results with a UV spectrometer would agree with measurements taken with the refractometer confirming that an in-line UV spectrometer could be purchased for use in future experiments.

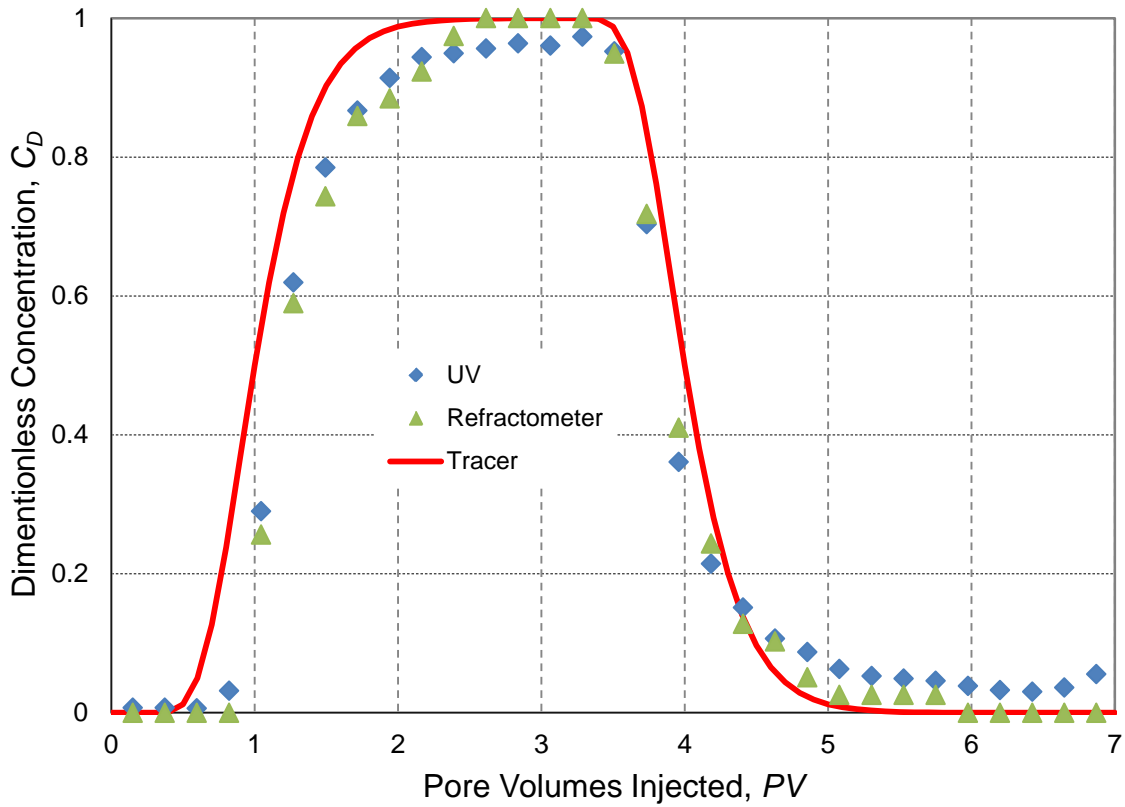


Figure A.28: Experiment 72 Effluent History

A.3.3.15 Experiment 73

Experiment 73 was run with diluted 5 wt% Nexsil DP dispersion fluid injected at 1 mL/min using a sandpack of 100% Boise sandstone. Experiments 73, 74, 75 and 76 are a sensitivity of injected concentration. Concentration measurements were made using both a UV spectrometer and a refractometer.

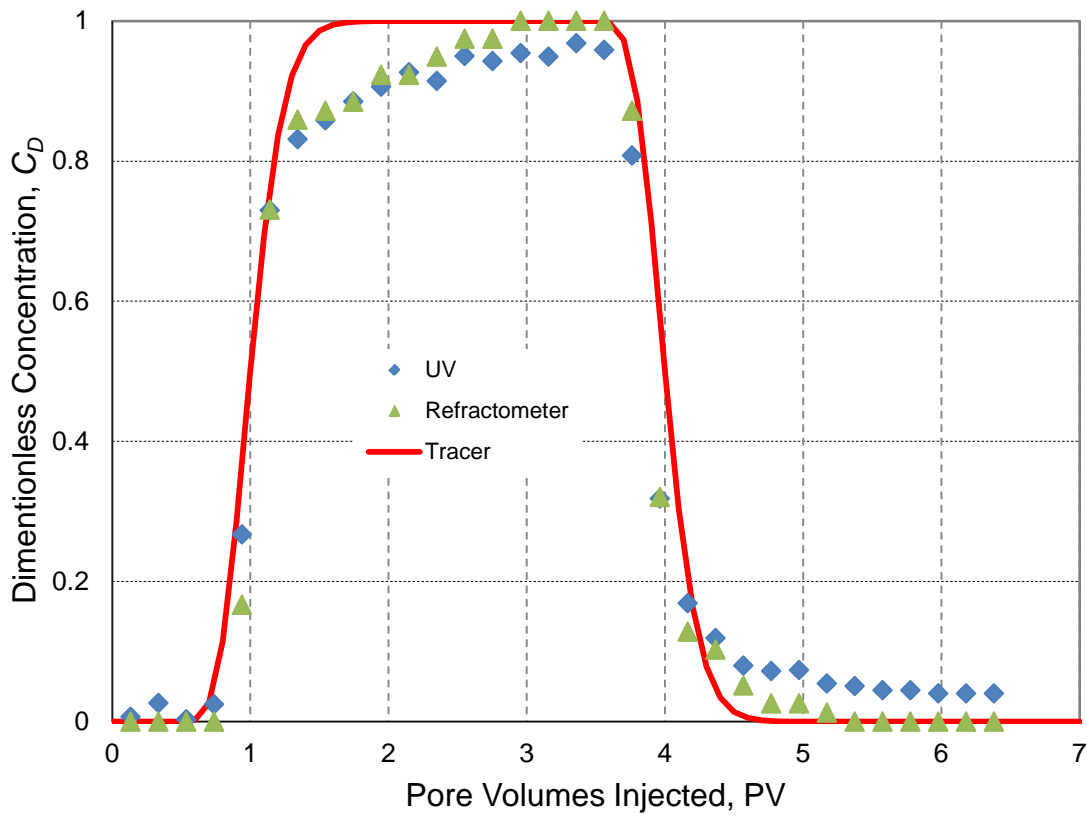


Figure A.29: Experiment 73 Effluent History

A.3.3.16 Experiment 74

Experiment 74 was run with diluted 2.6 wt% Nexsil DP dispersion fluid injected at 1 mL/min using a sandpack of 100% Boise sandstone. Experiments 73, 74, 75 and 76 are a sensitivity of injected concentration.

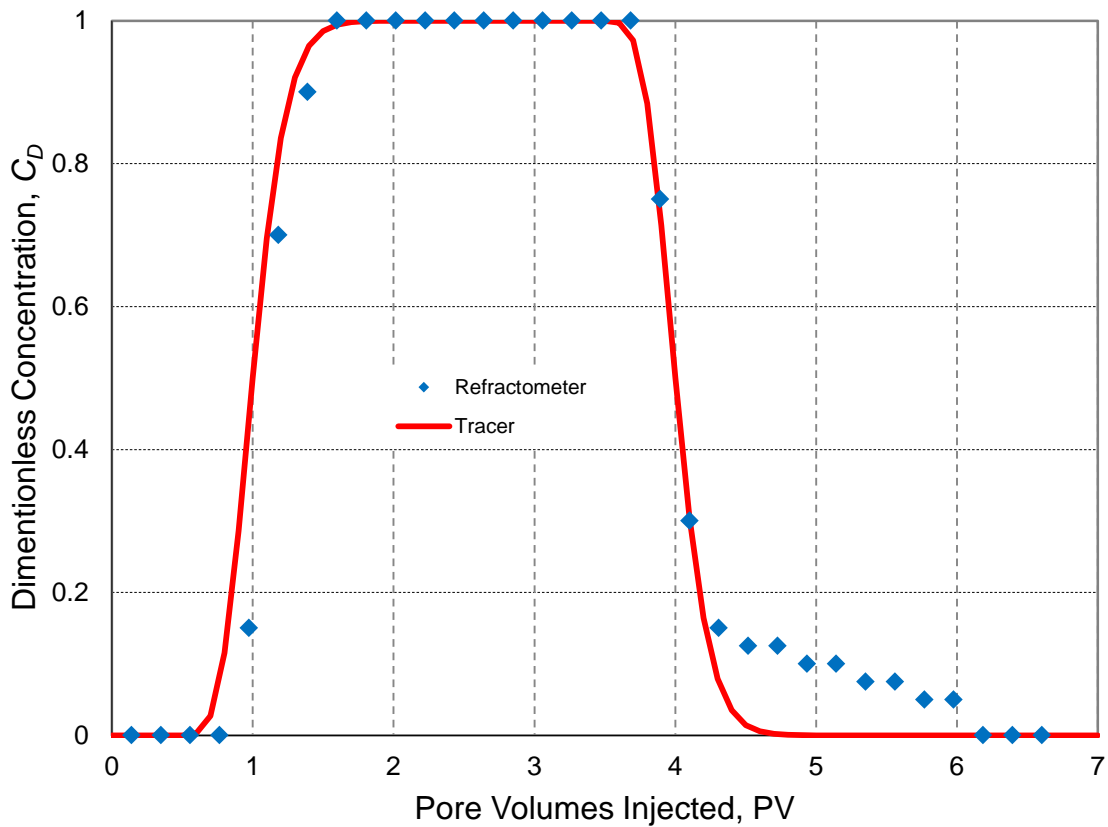


Figure A.30: Experiment 74 Effluent History

Recovery over 100% is impossible. This result contradicts the trend illustrated by experiments 73, 75 and 76. It is likely that error in the refractometer measurements at small nanoparticle concentrations is the cause of the mass balance discrepancy.

A.3.3.17 Experiment 75

Experiment 75 was run with diluted 3.5 wt% Nexsil DP dispersion fluid injected at 1 mL/min using a sandpack of 100 % Boise sandstone. Experiments 73, 74, 75 and 76 are a sensitivity of injected concentration.

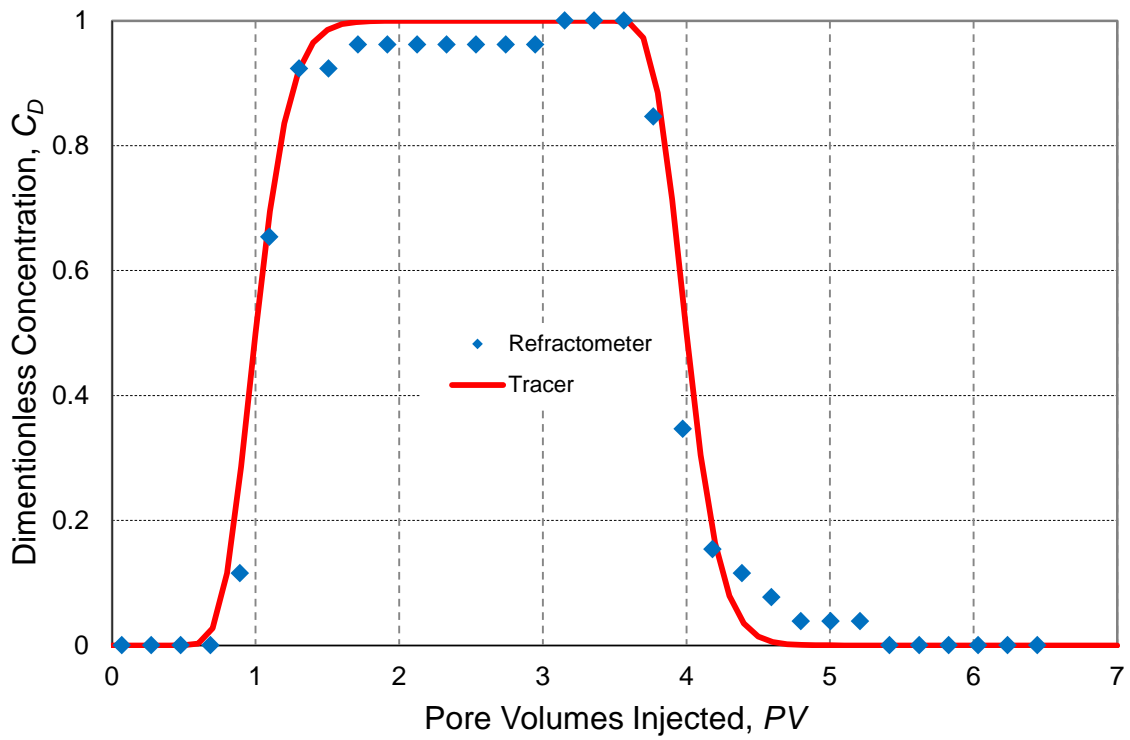


Figure A.31: Experiment 75 Effluent History

A.3.3.18 Experiment 76

Experiment 76 was run with diluted 1.5 wt% Nexsil DP dispersion fluid injected at 1 mL/min using a sandpack of 100% Boise sandstone. Experiments 73, 74, 75 and 76 are a sensitivity of injected concentration.

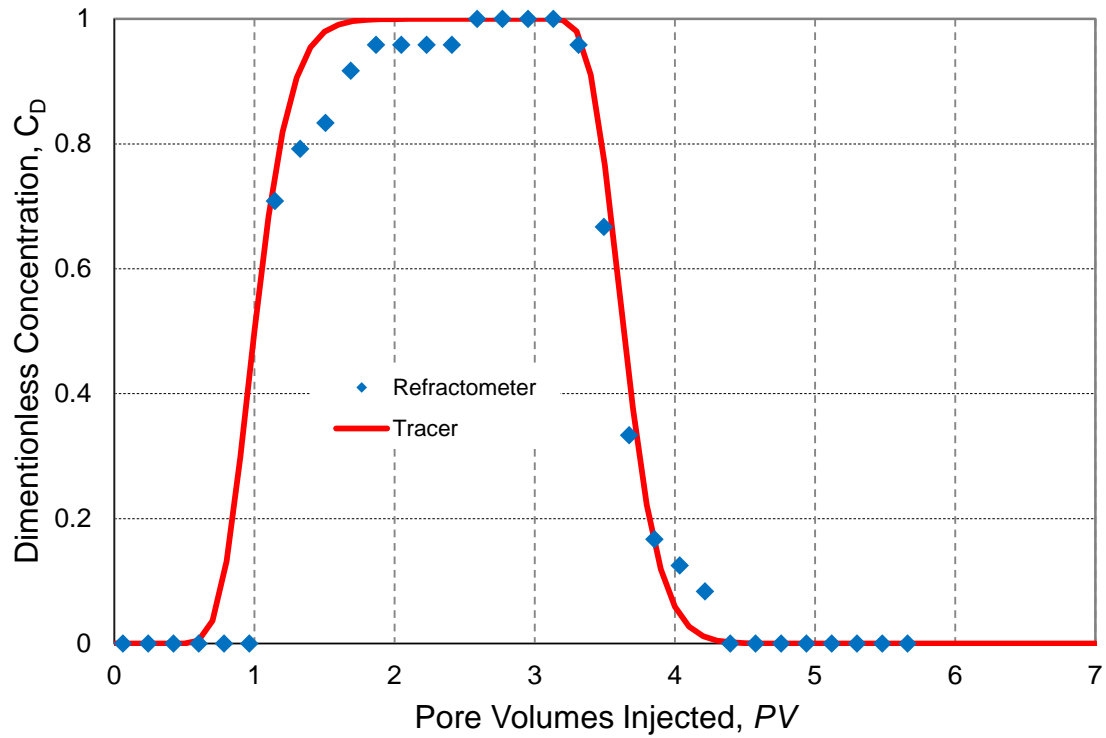


Figure A.32: Experiment 76 Effluent History

A.3.3.19 Experiment 77

Experiment 77 was run with diluted 5 wt% Nexsil DP dispersion fluid injected at 10 mL/min using a sandpack with 10 wt% kaolinite and 90 wt% Boise sandstone. Experiments 72 and 77 were run as a flow rate sensitivity for retention of Nexsil DP nanoparticles for sandpacks with 10% kaolinite.

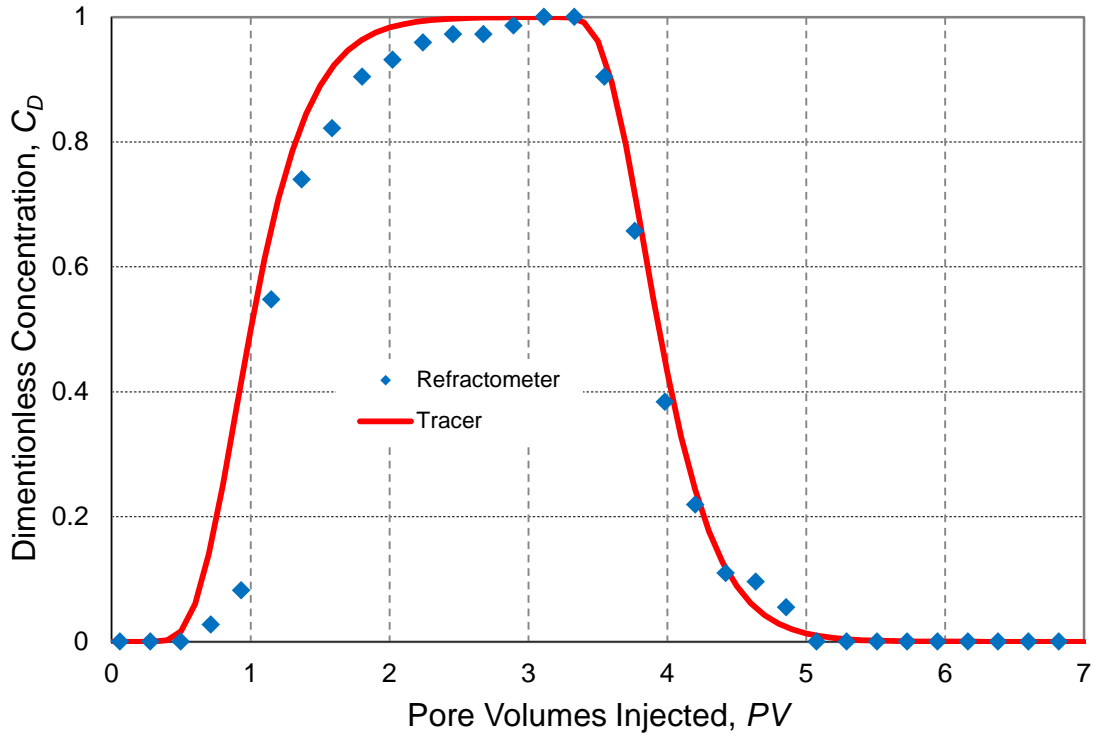


Figure A.33: Experiment 77 Effluent History

A.3.3.20 Experiment 78

Experiment 78 was run with diluted 1.5 wt% Nexsil DP dispersion fluid injected at 10 mL/min using a sandpack of 5 wt% kaolinite and 95 wt% Boise sandstone. Experiments 78, 79 and 80 were run as a sensitivity of injected concentration in the presence of kaolinite.

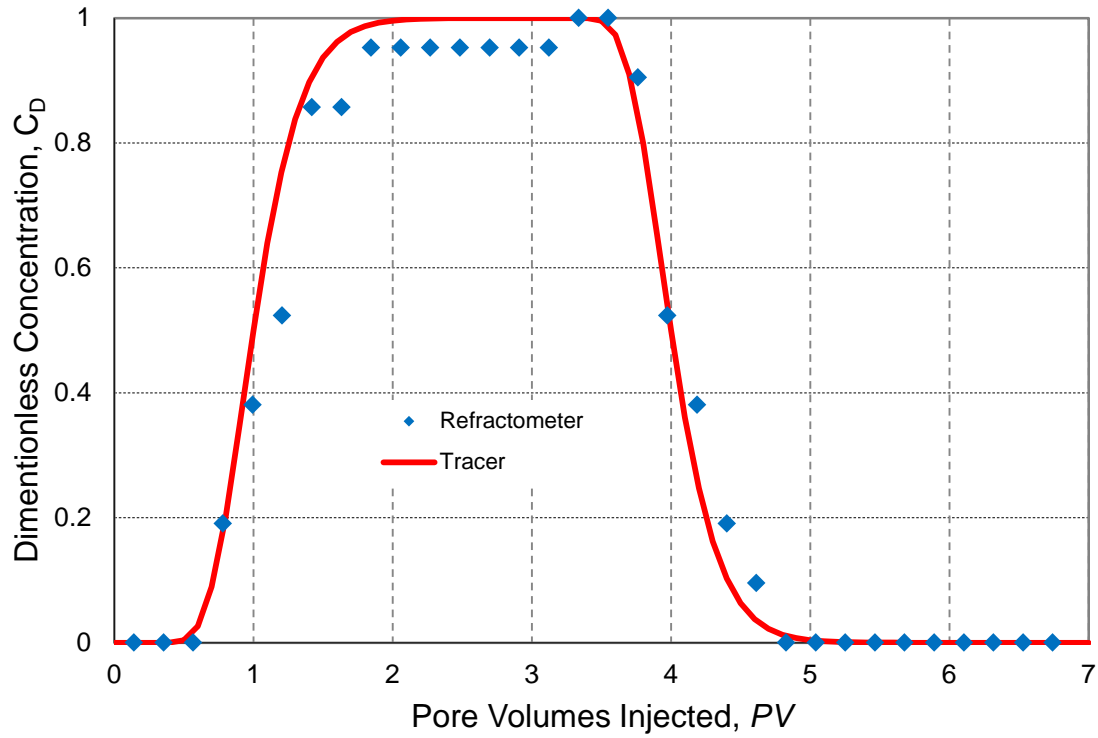


Figure A.34: Experiment 78 Effluent History

A.3.3.21 Experiment 79

Experiment 79 was run with diluted 3.5 wt% Nexsil DP dispersion fluid injected at 10 mL/min using a sandpack of 5 wt% kaolinite and 95 wt% Boise sandstone. Experiments 78, 79 and 80 were run as a sensitivity of injected concentration in the presence of kaolinite.

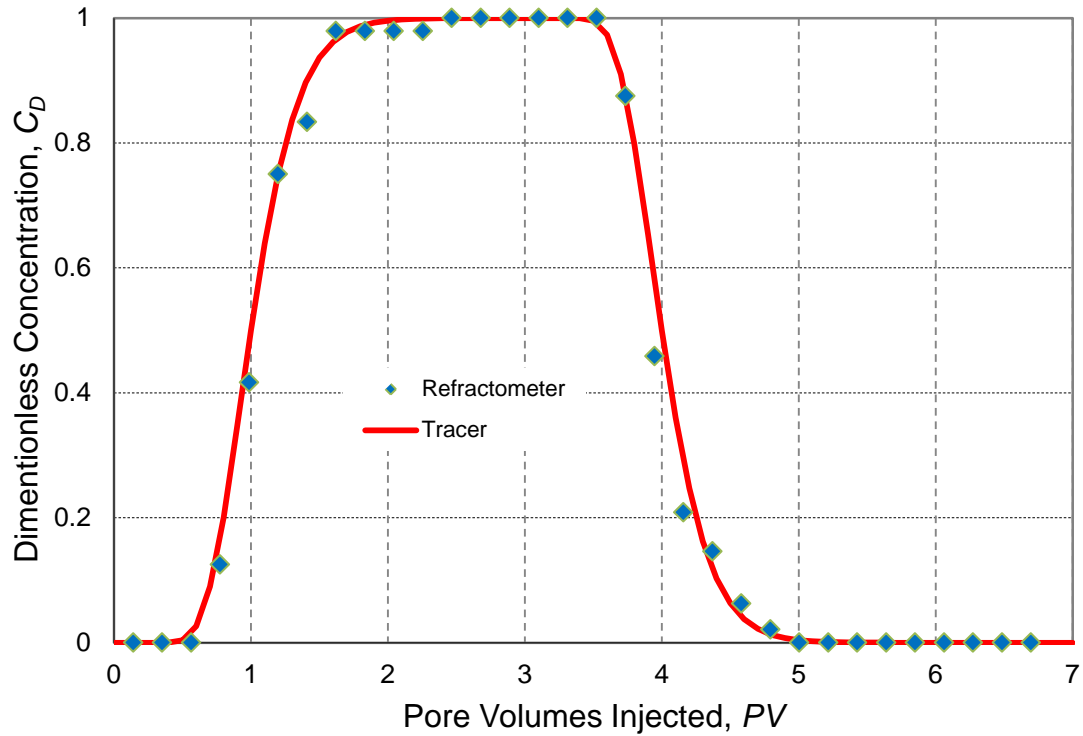


Figure A.35: Experiment 79 Effluent History

A.3.3.22 Experiment 80

Experiment 80 was run with diluted 5 wt% Nexsil DP dispersion fluid injected at 10 mL/min using a sandpack of 5 wt% kaolinite and 95 wt% Boise sandstone. Experiments 78, 79 and 80 were run as a sensitivity of injected concentration in the presence of kaolinite.

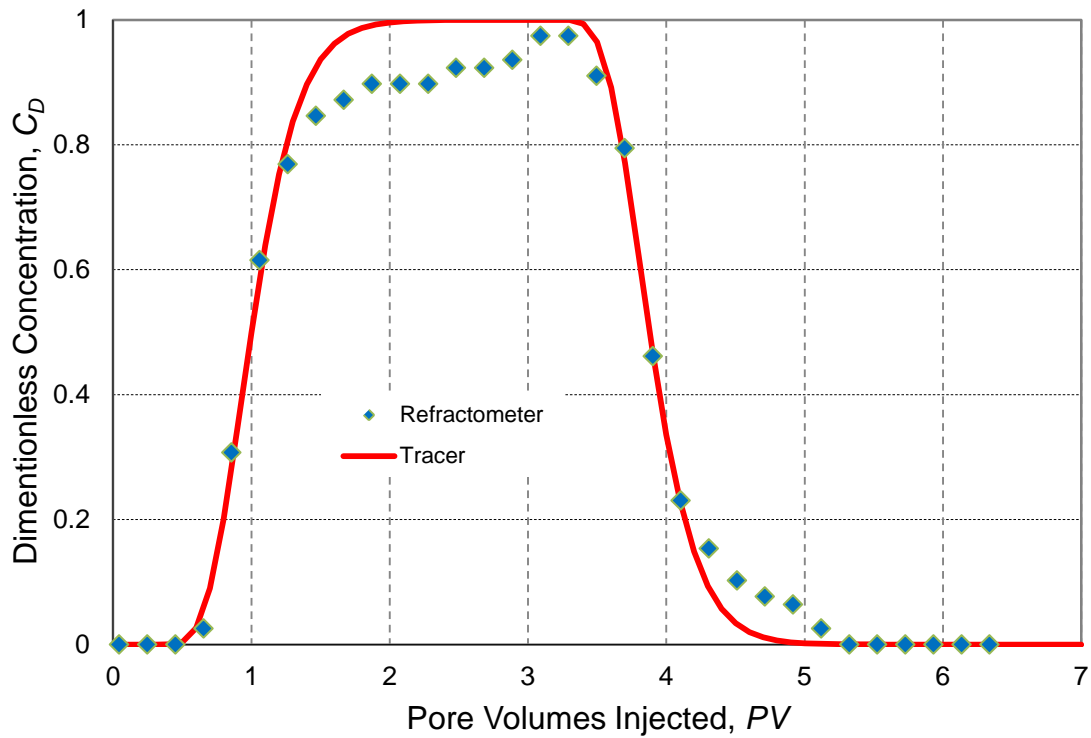


Figure A.36: Experiment 80 Effluent History

A.3.3.23 Experiment 81

For this experiment 3 PV of 5 wt% Nexsil DP dispersion was injected into a 1 ft column of 95 wt% 177-210 μm Boise sandstone and 5 wt% kaolinite injected at 1 mL/min. The 5 wt% Nexsil DP dispersion was centrifuged to remove nanoparticles from the dispersion. Measurement of the dispersion concentration after it had been rotated in the centrifuge suggested the new nanoparticle concentration was 4.4 wt%. The effluent history below is plotted with $C_D = 1$ at 5 wt% NexSil DP hence the plateau at $C_D = 0.87$.

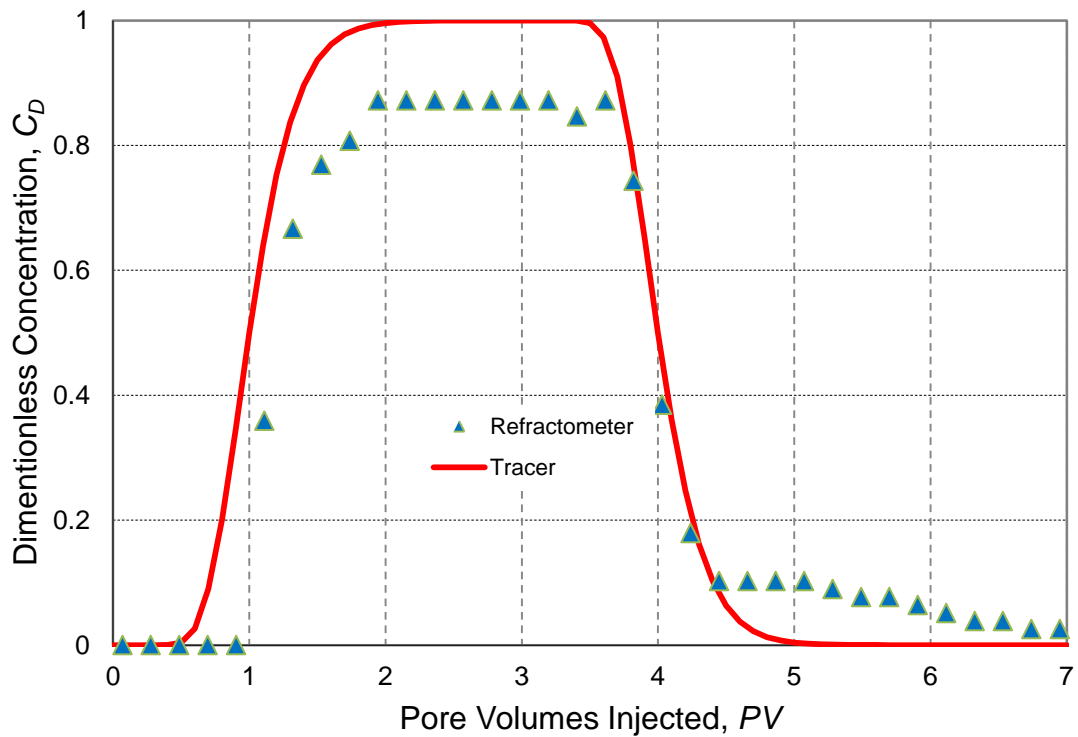


Figure A.37: Experiment 81 Effluent History

A.3.3.24 Experiment 82

For this experiment 3 PV of 5 wt% Nexsil DP dispersion was injected into a 1 ft column of 95 wt% 177-210 μm Boise sandstone and 5 wt% kaolinite at 1 mL/min. The experiment was run to test whether a UV spectrometer could be used to measure nanoparticle concentration from the effluent for sandpacks with kaolinite.

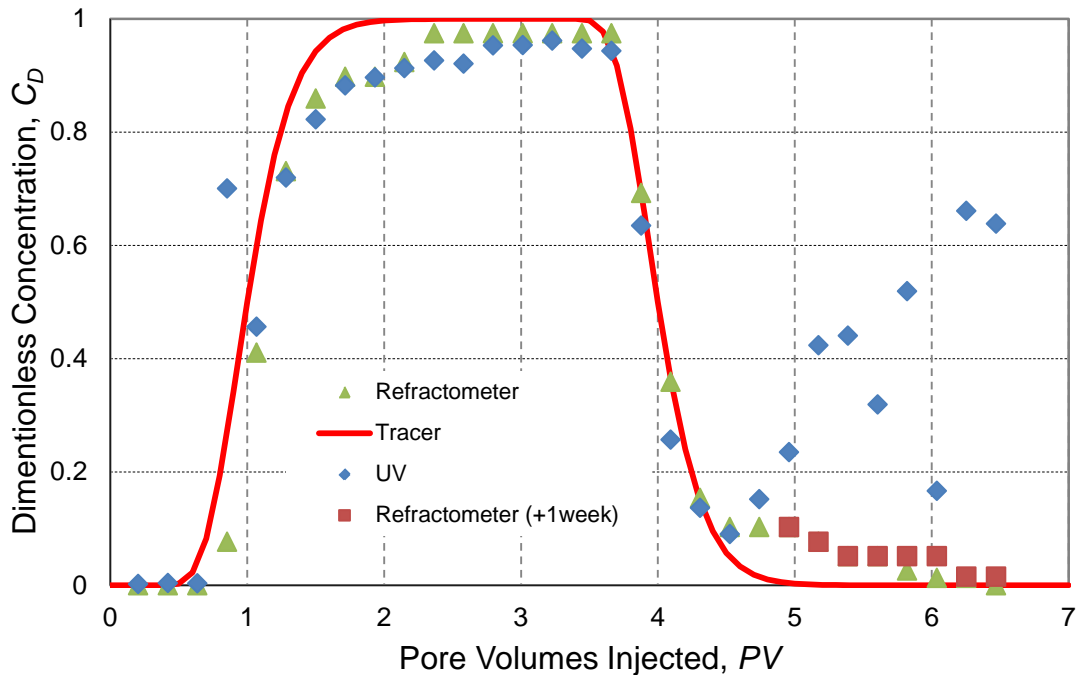


Figure A.38: Experiment 82 Effluent History

UV measurements were made using a Cray 500 and 3 mL effluent samples from a fraction collector. Initial refractometer measurements were made immediately after the brine flush ended. UV measurements were taken the following day. Effluent samples containing small concentrations of the injected nanoparticle dispersion (less than 15 %) developed visible solids which were floating in the sample. These visible solids affected UV readings (Blue Diamonds) resulting in large overestimations of nanoparticle concentration at the front and the tail of the effluent history. Re-measuring these same samples in the refractometer (Red Squares) shows these aggregations do not affect refractometer measurements which were very similar to the measurements taken immediately after the experiment ended.

A.3.3.25 *Experiment 83*

Experiment 83 included a sandpack with 40 wt% kaolinite. Complications due to wormhole effects through the kaolinite matrix would have prevented the vast majority of grain substrate from being contacted with nanoparticle dispersion. The experiment was aborted after the tracer test confirmed wormholes would be an issue.

A.3.3.26 Experiment 84

For this experiment 3 PV of 5 wt% Nexsil DP dispersion was injected into a 1 ft column of 95 wt% 210-250 μm Boise sandstone and 5 wt% kaolinite injected at 1 mL/min. The nanoparticle dispersion was frozen prior to injection and material from the dispersion (presumably nanoparticles) fell out of solution. RI measurements of the resulting dispersion suggest the nanoparticle concentration was reduced to 1.4 wt%. Concentration measurements for the effluent history were made using a refractometer and a Cray 500 UV spectrometer (calibrated with samples of nanoparticle dispersion that had not been frozen).

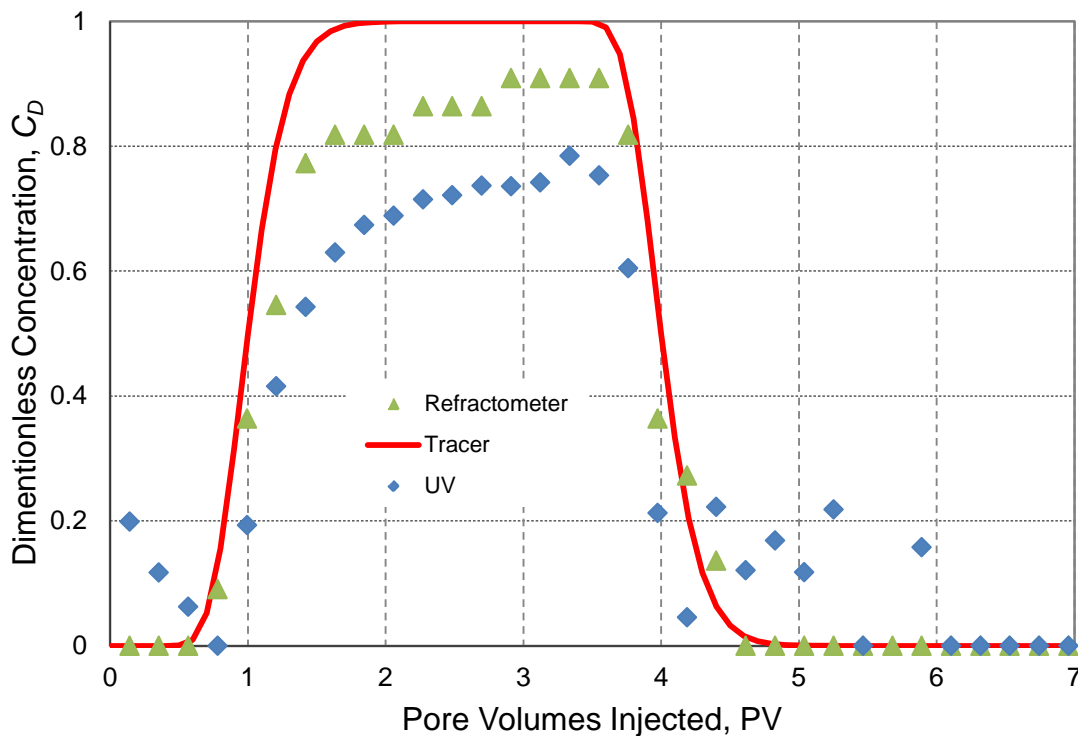


Figure A.39: Experiment 84 Effluent History

Results show the UV spectrometer and the refractometer generate different results for this unusual case. As described in the summary of experiment 82 above, low concentration effluent samples generate suspended solids within a day which affect UV spectrometer readings.

A.3.3.27 Experiment 85

For this experiment 3 PV of 5 wt% Nexsil DP dispersion was injected into a 1 ft column of 95 wt% 210-250 μm Boise sandstone and 5 wt% kaolinite injected at 1 mL/min. The diluted nanoparticle dispersion was centrifuged prior to injection, presumably reducing the nanoparticle concentration. Results from refractometer and UV spectrometer measurements agree reasonably well.

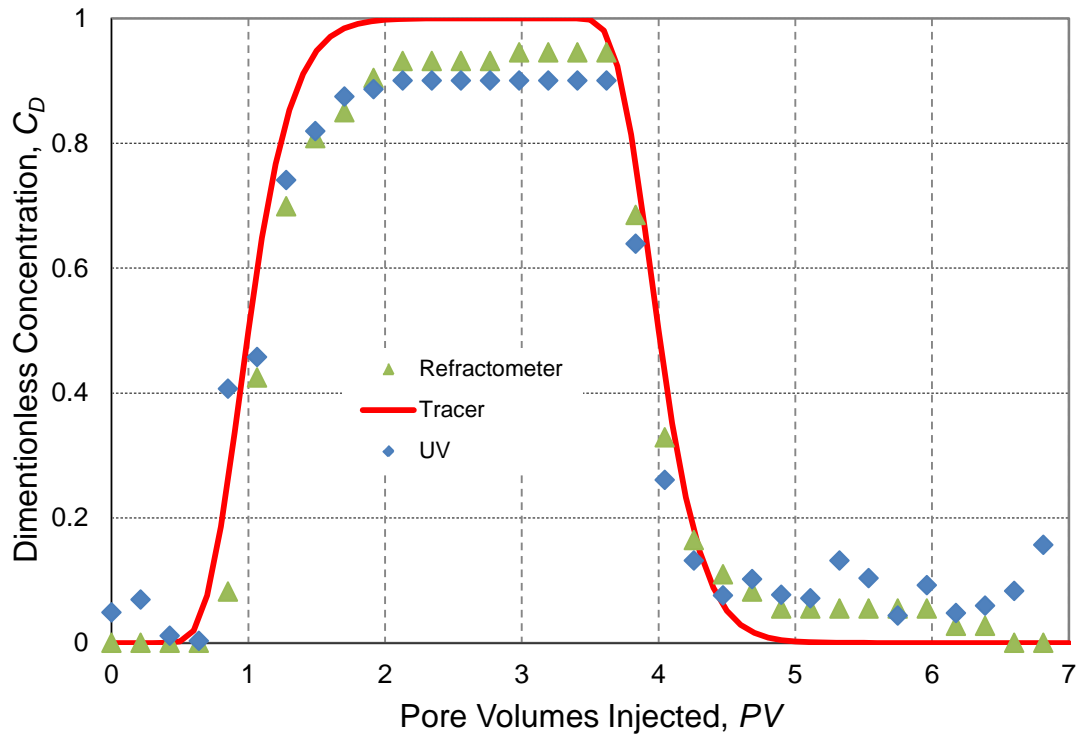


Figure A.40: Experiment 85 Effluent History

A.3.3.28 Experiment 86

For this experiment 3 PV of 1.2 wt% Nexsil DP dispersion was injected into a 1 ft column of 95 wt% 210-250 μm Boise sandstone and 5 wt% kaolinite injected at 1 mL/min. Experiments 68 and 86 were used as a sensitivity of the effect of injected concentration on nanoparticle retention with low injected dispersion velocity in the presence of kaolinite.

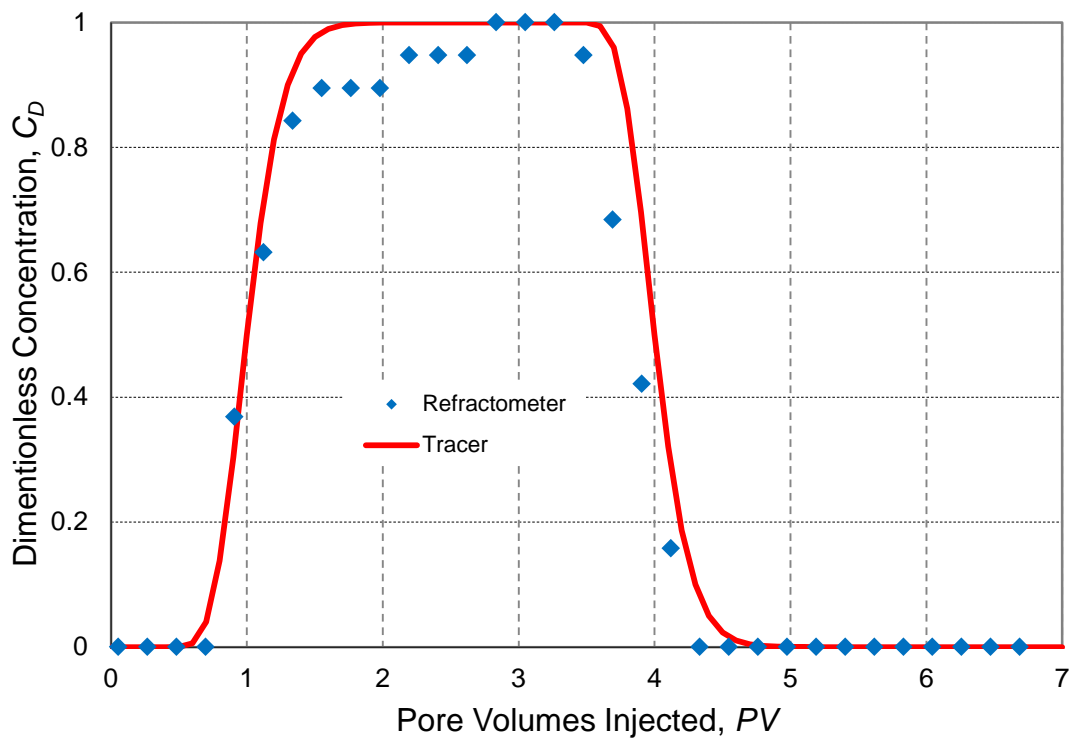


Figure A.41: Experiment 86 Effluent History

Experiments 87-90 were sandpacks used for initial testing of the Ultimate 3000 UVD. The naming convention of this thesis numbers every packed slim-tube for which dispersivity measurements were taken. No useful experimental results were generated. The packs were used to run tests for the new device and develop an experimental process for future runs. A summary of the next experiment to test and a hypothesis and generate usable results (experiment 91) is below.

A.3.3.29 Experiment 91

In experiment 91 2.9 PV of 0.1 wt% COATING 1 coated iron oxide nanoparticles were injected into a 100% Boise sandstone sandpack at 1 mL/min. This was the first experiment to use the new UV spectrometer setup. The experiment was used to observe iron oxide nanoparticle retention at low concentration and low flow rate. Experiments 91 and 92 were run as a flow rate sensitivity for COATING 1 coated iron oxide nanoparticles.

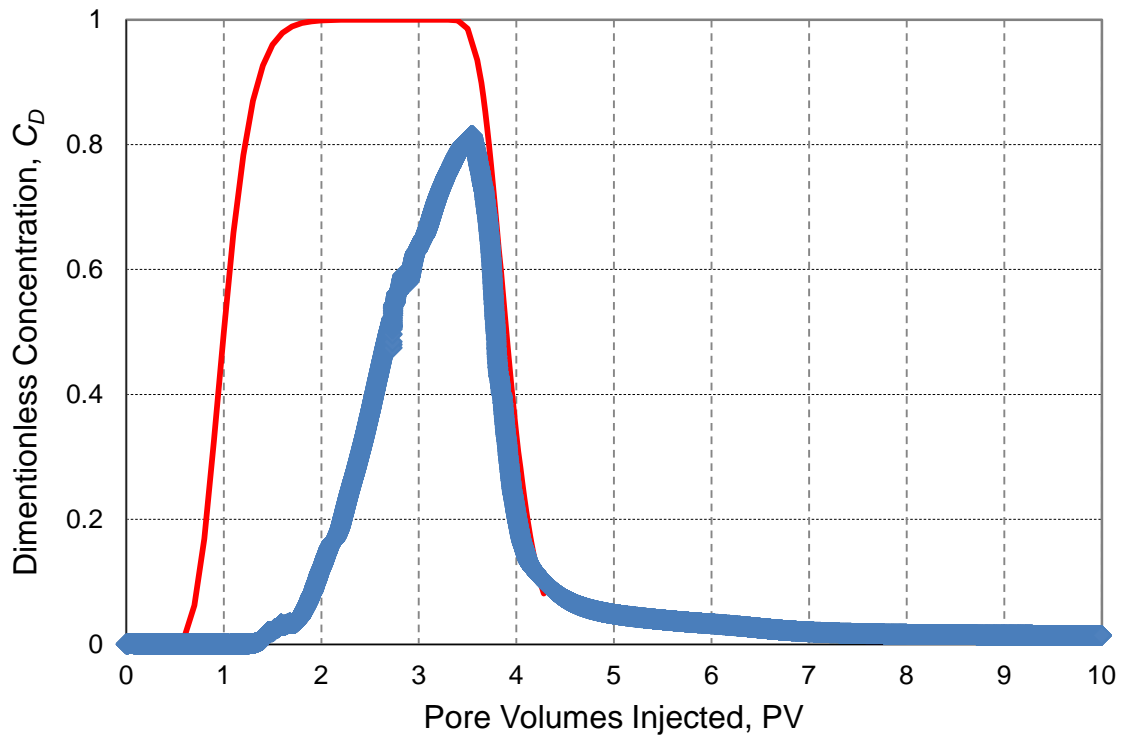


Figure A.42: Experiment 91 Effluent History

A.3.3.30 Experiment 92

In experiment 92 3.1 PV of 0.1 wt% COATING 1 coated iron oxide nanoparticles were injected into a 100 % Boise sandstone sandpack at 10 mL/min. The experiment was used to observe iron oxide nanoparticle retention at low concentration and high flow rate. Experiments 91 and 92 were run as a flow rate sensitivity for COATING 1 coated iron oxide nanoparticles.

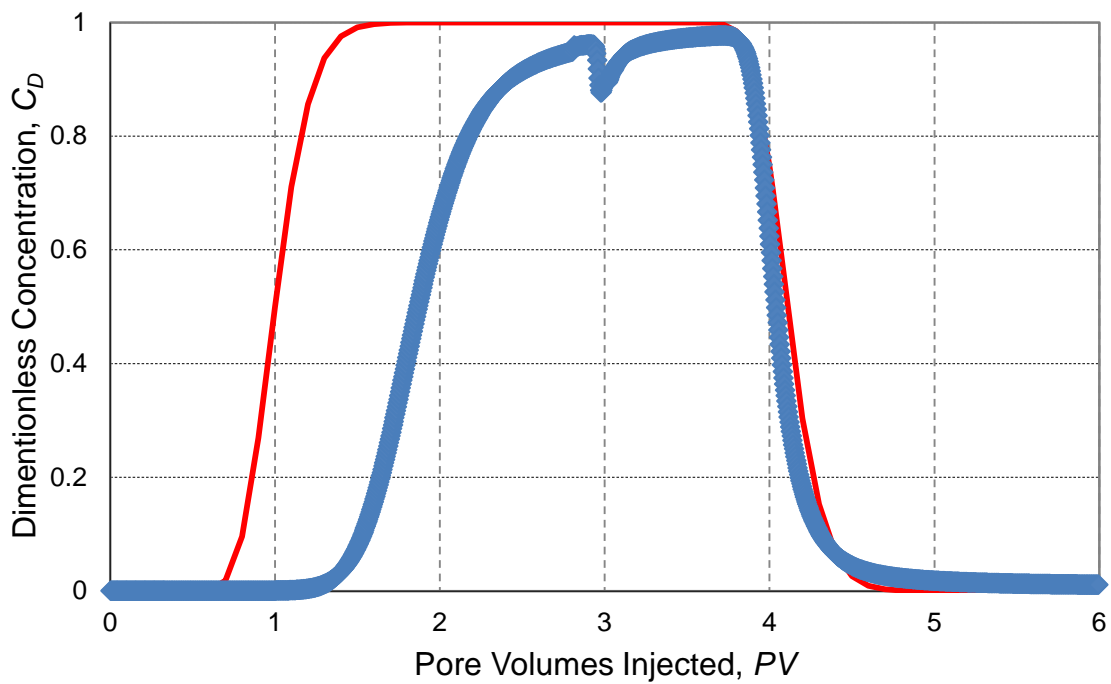


Figure A.43: Experiment 92 Effluent History

The sudden drop in dimensionless concentration at 2.8 *PVI* is due to a 10 second pump stop as the flow path is switched from nanoparticle injection to brine injection.

A.3.3.31 Experiment 93

In experiment 93 3.8 PV of 0.1 wt% Coating 2 coated iron oxide nanoparticles were injected into a 100% Boise sandstone sandpack. Initially the diluted nanoparticle dispersion was injected at 10 mL/min then at 2.5 PVI the flow rate was dropped to 1 mL/min. The experiment was used to observe the effect of decreasing flow rates on the effluent history.

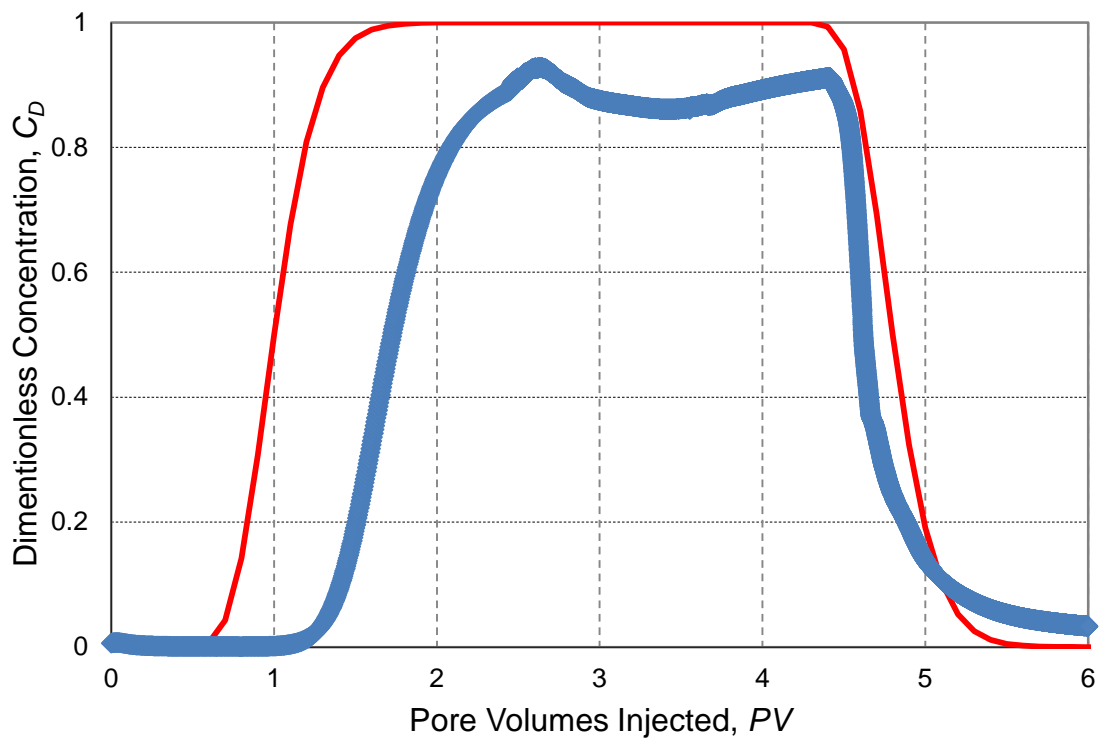


Figure A.44: Experiment 93 Effluent History

A.3.3.32 Experiment 94 (Part 1)

In experiment 94 8.12 PV of 0.1 wt% Coating 3 coated iron oxide nanoparticles were injected into a 100% Boise sandstone sandpack. Initially the diluted nanoparticle dispersion fluid was injected at 1 mL/min then at 4.18 PVI the flow rate was dropped to 1 mL/min. The experiment was used to observe the effect of increasing flow rates on the effluent history.

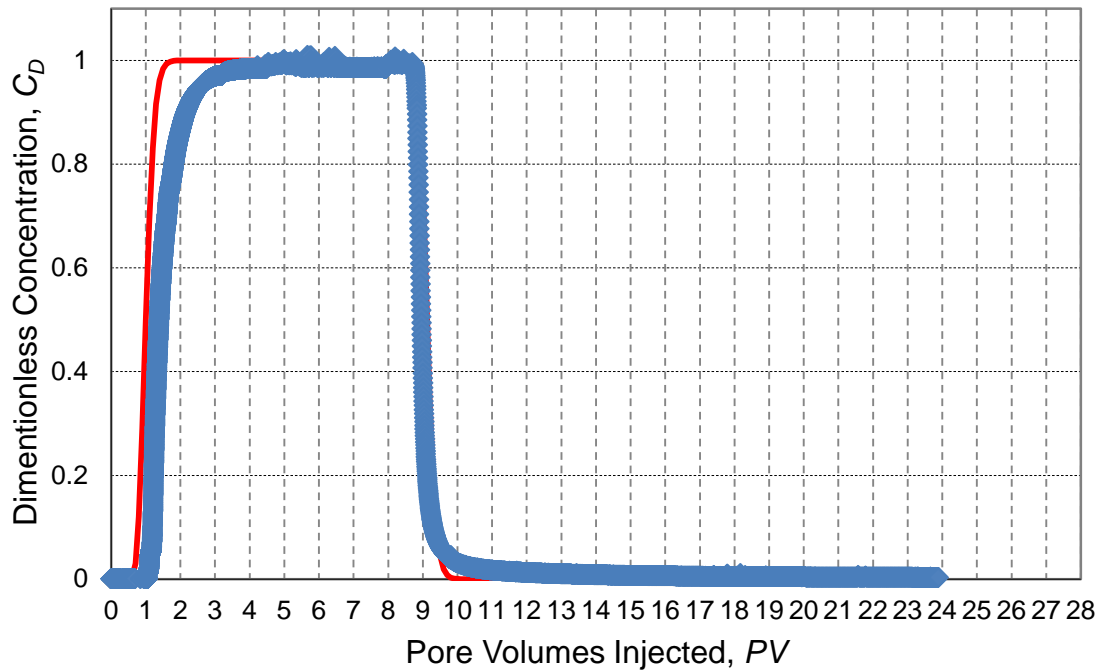


Figure A.45: Experiment 94 (Part 1) Effluent History

A.3.3.33 Experiment 94 (Part 2)

In experiment 94 (Part 2) 3.4 PV of 0.1 wt% Coating 3 coated iron oxide nanoparticles were injected at 10 mL/min into the Boise sandstone sandpack used in experiment 94. The experiment was used to test the theory that the sandpacks have an upper bound retention concentration beyond which no further nanoparticle retention would occur. This upper bound would correspond to the retention capacity of the sandpack at the experimental conditions.

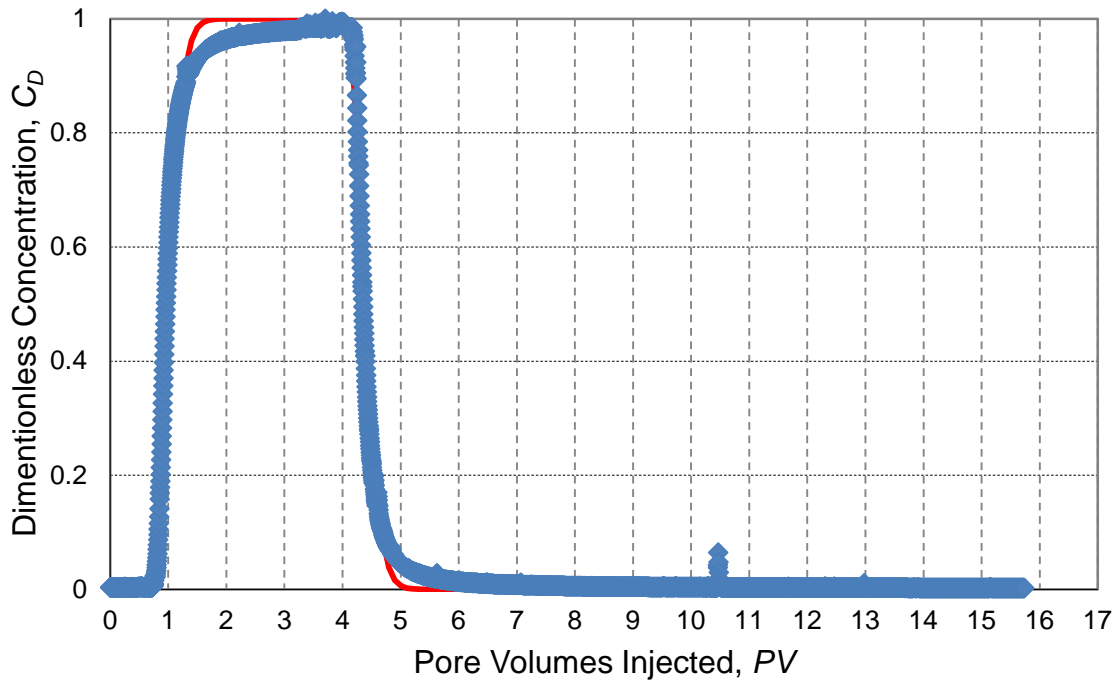


Figure A.46: Experiment 94 (Part 2) Effluent History

A.3.3.34 Experiment 95

Experiment 95 involved Iron oxide nanoparticles coated with a polymer that was not Salt Tolerant. The experiment failed to produce any nanoparticle dispersion in the effluent and was aborted.

A.3.3.35 Experiment 96

In experiment 96 3.5 PV of 1 wt% tagged Fluorescent 3M nanoparticle dispersion was injected at 1 mL/min into a 100% Boise sandstone sandpack. This experiment was the first half of an effluent reinjection experiment. The results can also be used as an injection concentration sensitivity.

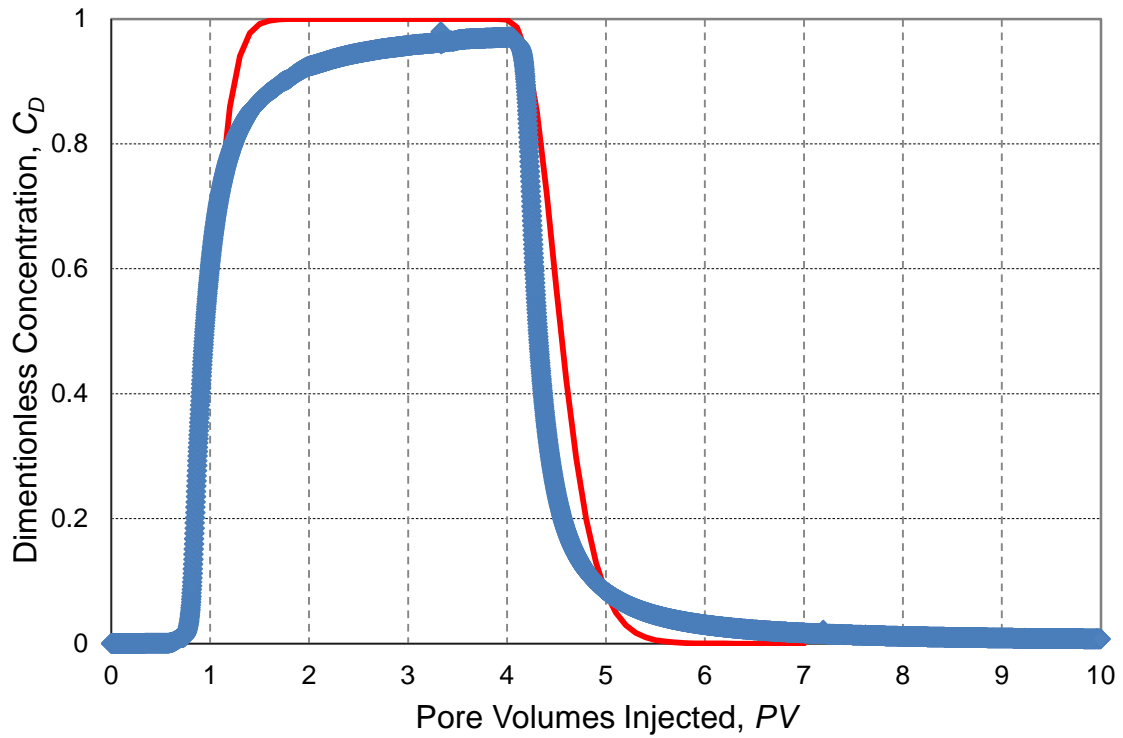


Figure A.47: Experiment 96 Effluent History

A.3.3.36 Experiment 97

In experiment 97 3.54 PV of effluent from experiment 96 (calculated to be 0.6 wt% tagged fluorescent 3M nanoparticles) was injected at 1 mL/min into a 100% Boise sandstone sandpack. This experiment was the second half of an effluent reinjection experiment. The results can also be used as an injection concentration sensitivity.

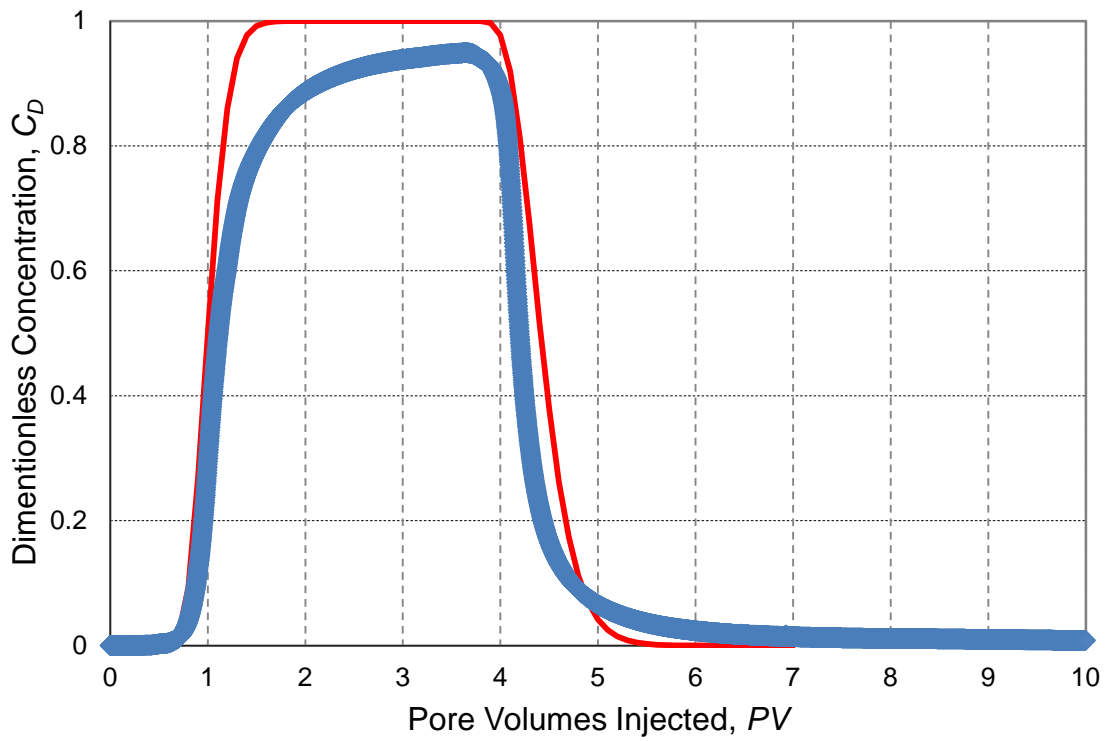


Figure A.48: Experiment 97 Effluent History

A.3.3.37 Experiment 98

In experiment 98 7.1 *PV* of 0.1 wt% tagged fluorescent 3M nanoparticle dispersion was injected into a 100% Boise sandstone sandpack at 1 mL/min. At 5.7 *PVI* the pump was halted for 10 minutes and the fluid within the sandpack left stationary. The pump was then restarted and an additional 1.4 *PV* of 0.1 wt% tagged fluorescent 3M nanoparticle dispersion was injected followed by a brine postflush. This experiment is part of a flow rate sensitivity that included a 10 minute pump stop.

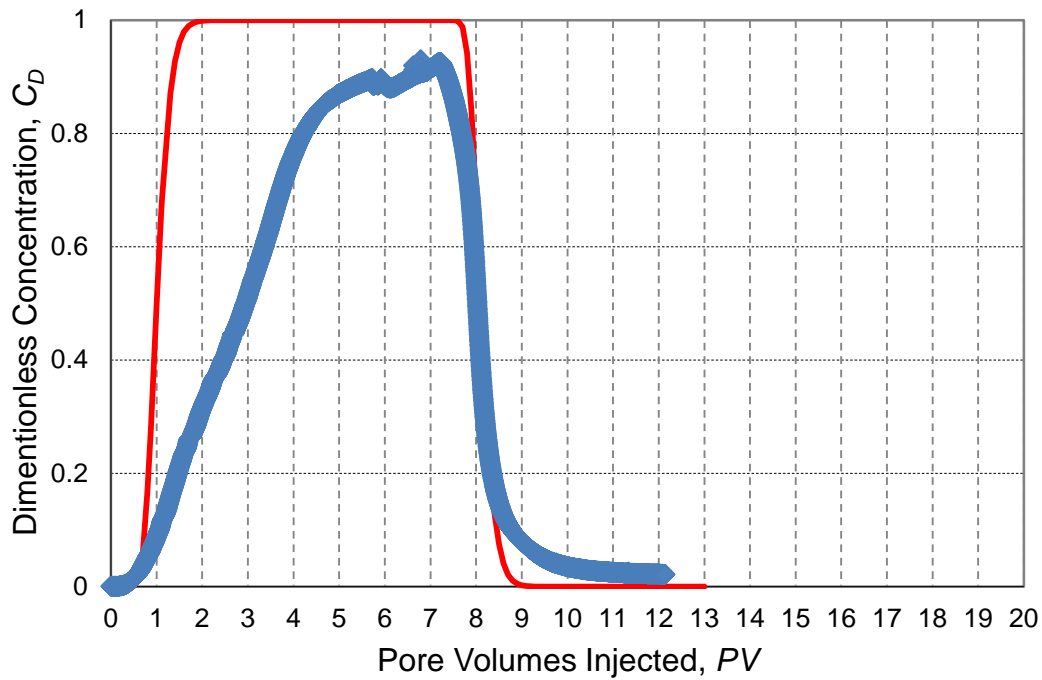


Figure A.49: Experiment 98 Effluent History

A.3.3.38 Experiment 99 (Part 1)

In experiment 99 part 1 7.4 PV of 0.1 wt% tagged fluorescent 3M nanoparticle dispersion was injected into a 100% Boise sandstone sandpack at 10 mL/min. At 5.65 PVI the pump was halted for 10 minutes and the fluid within the sandpack left stationary. The pump was then restarted and an additional 1.75 PV of 0.1 wt% tagged fluorescent 3M nanoparticle dispersion was injected followed by a brine postflush. This experiment is part of a flow rate sensitivity that included a 10 minute pump stop.

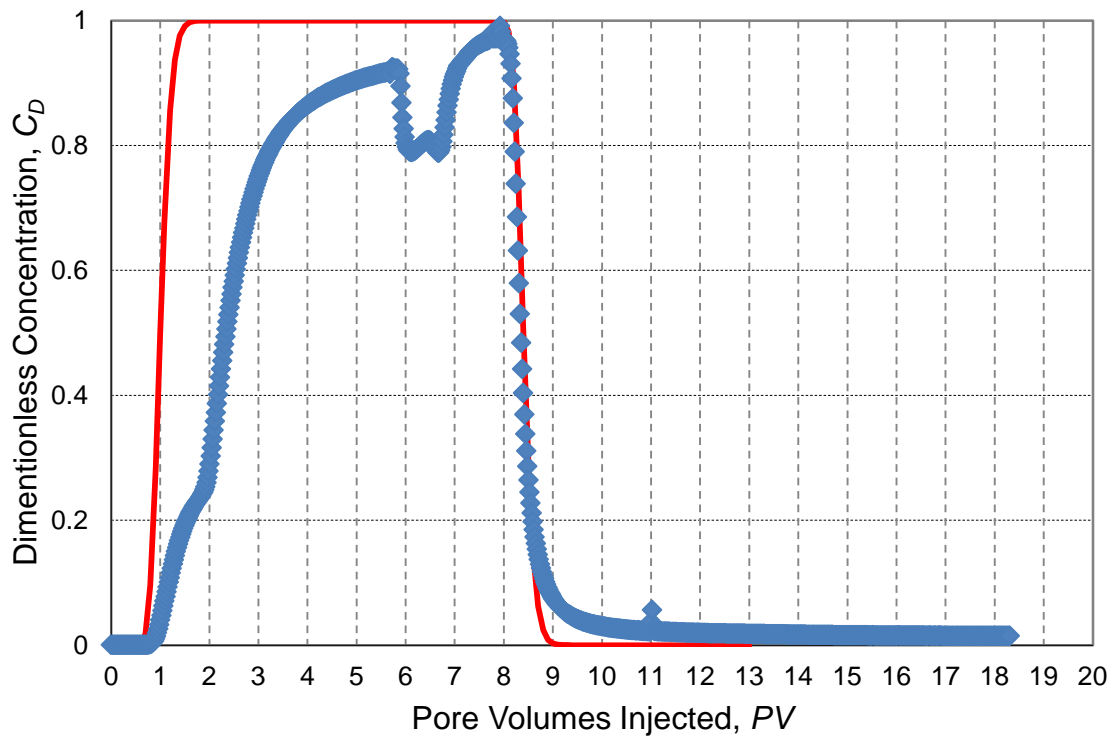


Figure A.50: Experiment 99 Part 1 Effluent History

A.3.3.39 Experiment 99 (Part 2)

In experiment 99 part 2 6 PV of 0.1 wt% tagged fluorescent 3M nanoparticle dispersion was injected into the sandpack from experiment 99 part 1 at 1 mL/min. The experiment was used to observe the additional retention that occurs when a second slug of nanoparticles is injected into a sandpack at a lower velocity.

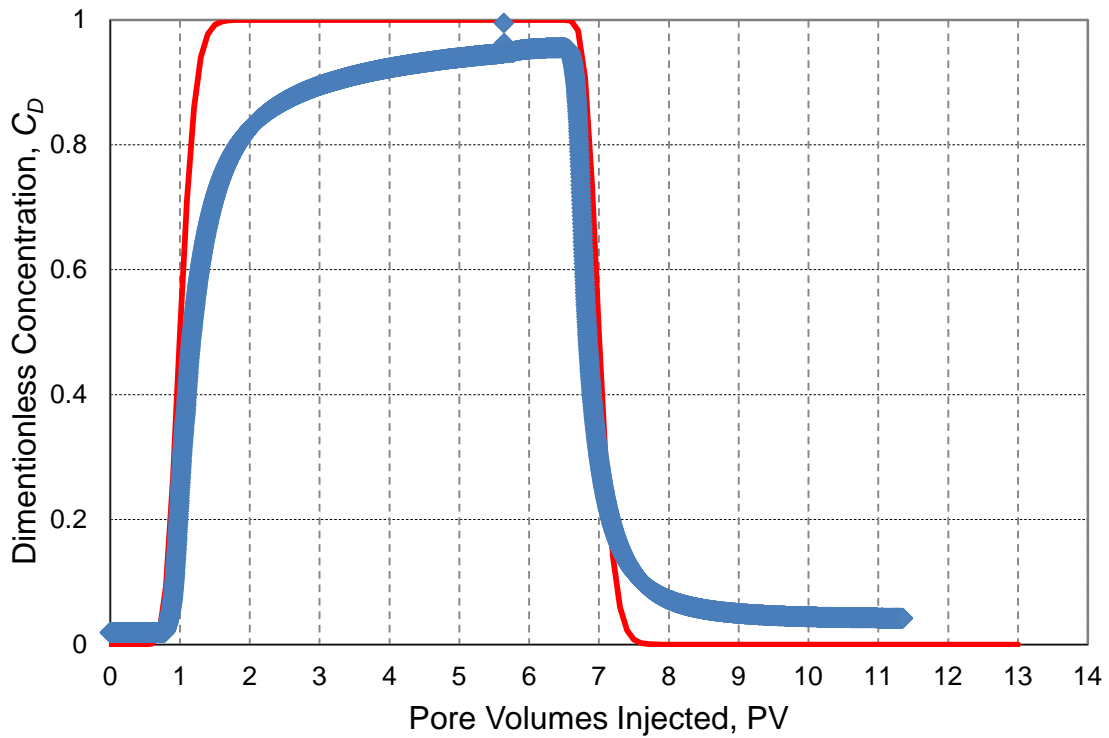


Figure A.51: Experiment 99 Part 2 Effluent History

A.3.3.40 Experiment 100

In experiment 100 7.23 PV of 0.1 wt% tagged fluorescent 3M nanoparticle dispersion was injected into a 100% Boise sandstone sandpack at 0.2 mL/min. At 5.95 PVI the pump was halted for 10 minutes and the fluid within the sandpack left stationary. The pump was then restarted and an additional 1.28 PV of 0.1 wt% % tagged fluorescent 3M nanoparticle dispersion was injected followed by a brine postflush. This experiment is part of a flow rate sensitivity that included a 10 minute pump stop.

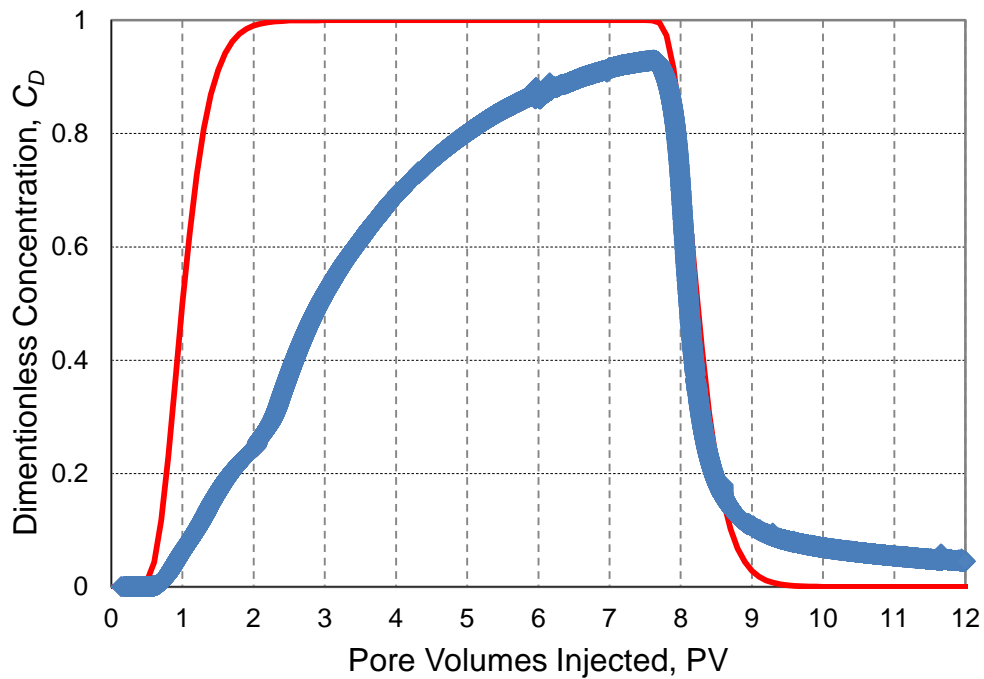


Figure A.52: Experiment 100 Effluent History

A.3.3.41 Experiment 101

In experiment 101 3.03 *PV* of 1 wt% tagged fluorescent 3M nanoparticle dispersion was injected into a 100% Boise sandstone sandpack at 10 mL/min. The experiment was run so that retention results could be compared with the 10 mL/min pump stop experiment (experiment 99 part 1) and discern whether the pump stop contributed to permanent nanoparticle retention. The results along with experiment 96 represent a flow rate sensitivity for 1 wt% Fluorescently Tagged 3M nanoparticles.

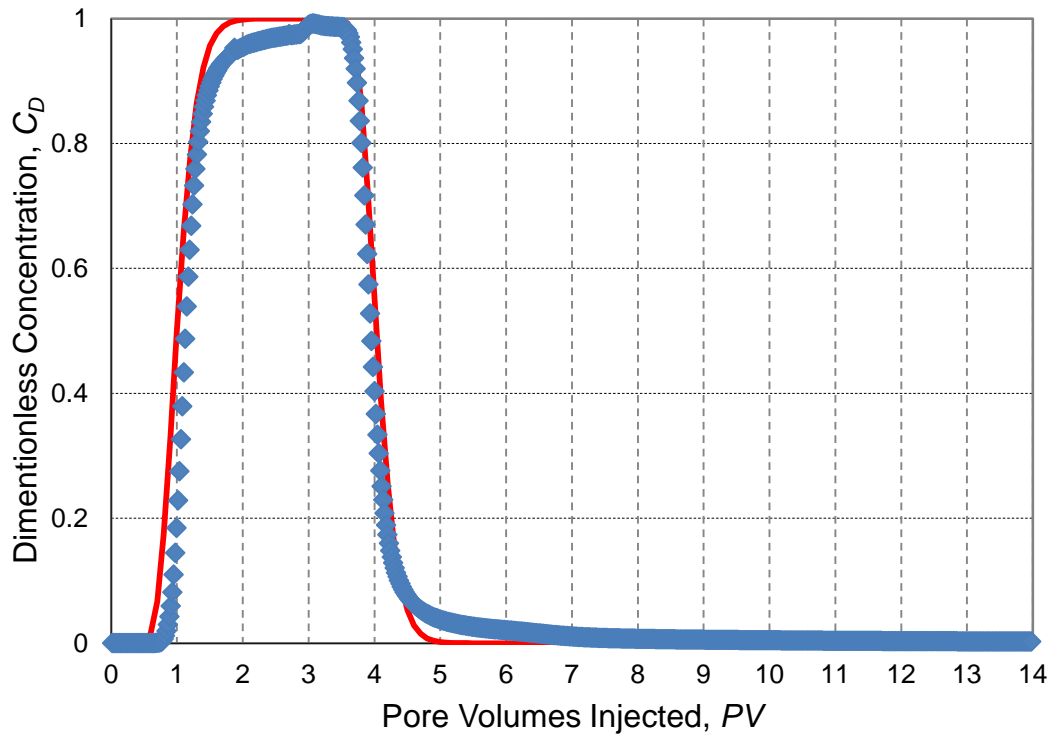


Figure A.53: Experiment 101 Effluent History

A.3.3.42 Experiment 102

In experiment 102 3.067 PV of 5 wt% tagged fluorescent 3M nanoparticle dispersion was injected into a 100% Boise sandstone sandpack at 1.02 mL/min. The experiment was run to test the retention of fluorescently tagged nanoparticles at high injected concentration. Results were used as part of an injected concentration sensitivity for Fluorescently Tagged 3M particles that included experiments 102, 103, 104 and 96.

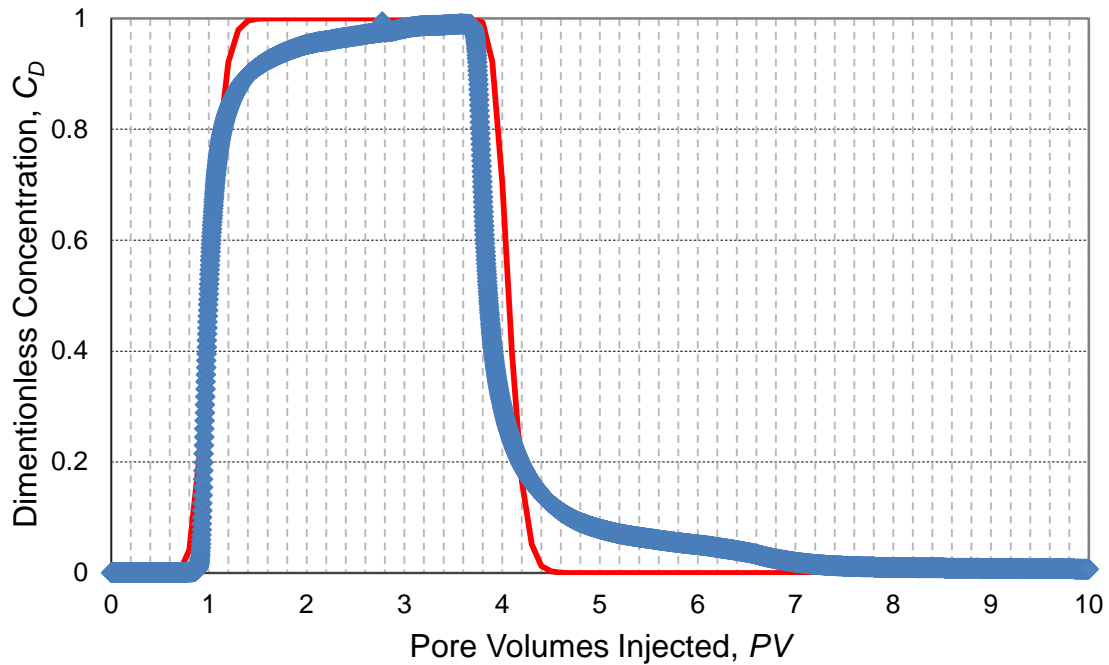


Figure A.54: Experiment 102 Effluent History

A.3.3.43 Experiment 103

In experiment 103 3.1 PV of 5 wt% tagged fluorescent 3M nanoparticle dispersion was injected into a 100% Boise sandstone sandpack at 1 mL/min. Experiment 103 is essentially a repeat of experiment 102. An electronic balance was employed to make frequent measurements of the effluent collected significantly increasing the accuracy of injection rate estimations. Results were used as part of an injected concentration sensitivity for Fluorescently Tagged 3M particles that included experiments 102, 103, 104 and 96.

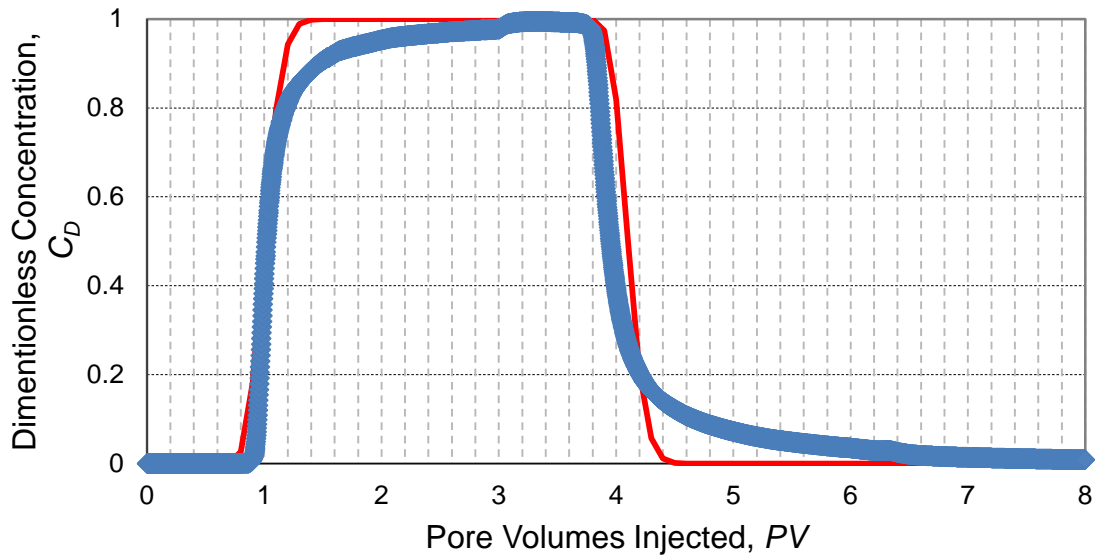


Figure A.55: Experiment 103 Effluent History

A.3.3.44 Experiment 104

In experiment 104 3 PV of 0.5 wt% tagged fluorescent 3M nanoparticle dispersion was injected into a 100% Boise sandstone sandpack at 1 mL/min. Results were used as part of an injected concentration sensitivity for Fluorescently Tagged 3M particles that included experiments 102, 103, 104 and 96.

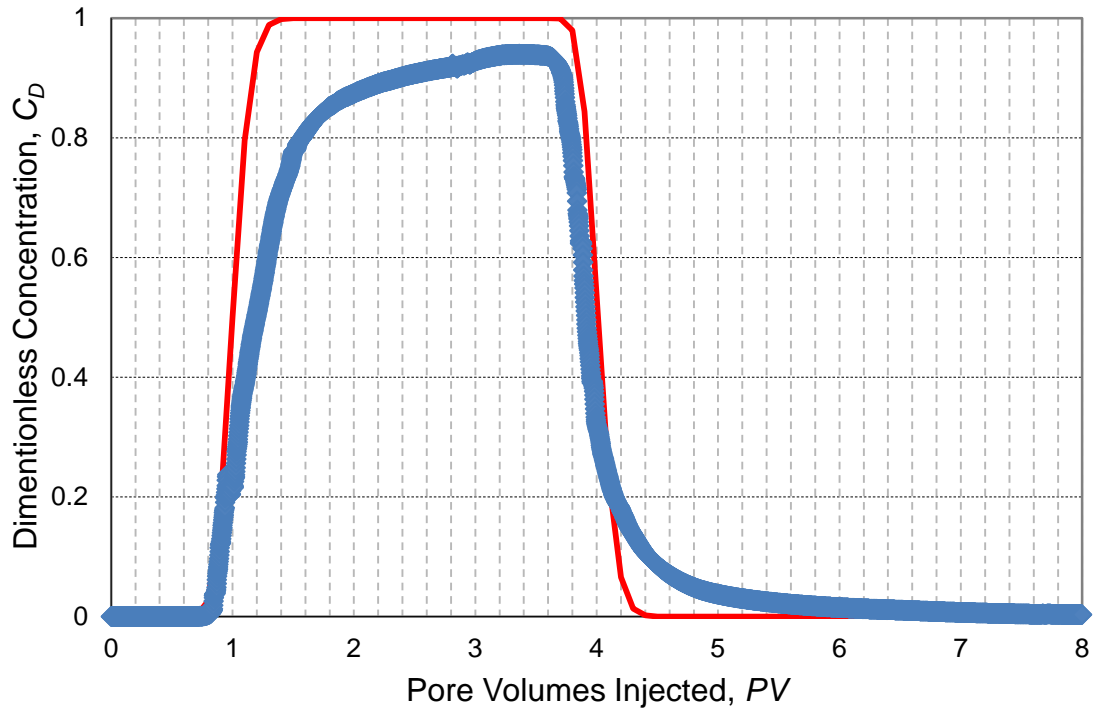


Figure A.56: Experiment 104 Effluent History

NOMENCLATURE

A	=	Sandpack cross-sectional area, cm^2
A_{BET}	=	Sample surface area measured with BET, m^2/g
C_0	=	Initial concentration, wt%
C_I	=	Injected concentration, wt%
C_F	=	Flush concentration, wt%
C_{NP}	=	Nanoparticle concentration, $\#/L$
C_D	=	Dimensionless nanoparticle concentration
C_{Di}	=	Dimensionless nanoparticle concentration of <i>ith</i> sample
D_p	=	Grain diameter, μm
ID	=	Inner diameter of sandpack tube, cm
L	=	Sandpack length, ft
ρ_{disp}	=	Dispersion Density, g/mL
N_{Pe}	=	Peclet number, dimensionless
PVI	=	Total pore volumes injected
PVI_i	=	Pore volumes injected at <i>ith</i> sample
q	=	Volumetric flow rate, cc/min
r	=	Grain size radius, μm
r_{NP}	=	Nanoparticle radius, nm
RI_0	=	Refractive index of flush fluid ($C_D = 0$)
RI_1	=	Refractive index of injected nanoparticle dispersion ($C_D = 1$)
R_M	=	Retained Mass, mg
$R_{M(Inc)}$	=	Incremental Retained Mass, mg
R_{Conc}	=	Retention Concentration, mg/m^2
$R_{Conc(Inc)}$	=	Incremental Retention Concentration, mg/m^2

$R_{monolayer}$	=	Monolayer Coverage
R_{NP}	=	Nanoparticle recovery, %
S_A	=	Total surface area, cm^2
$S_{A(Inc)}$	=	Incremental surface area, cm^2
v	=	Interstitial velocity, ft/day
V_b	=	Bulk volume, cc
V_p	=	Pore volume, cc
W_{Dry}	=	Weight of sandpack filled with dry sand, g
W_{Sat}	=	Weight of sandpack filled with brine saturated sand, g
W_{sand}	=	Weight of sand in sandpack, g
W_{brine}	=	Weight of brine saturating sandpack, g
ϕ_{brine}	=	Porosity calculated from brine weight, %
ϕ_{grain}	=	Porosity calculated from grain weight, %
μ_{app}	=	Apparent viscosity, cp
μ_w	=	Water viscosity, cp
ρ_{mix}	=	Nanoparticle dispersion density, g/cc
ρ_{sand}	=	Sand grain density, g/cc
$t_{arrival}$	=	Arrival time

REFERENCES

1. Rodriguez, E., Roberts, M. R., Yu, H., Huh, C., and Bryant, S. L., “Enhanced Migration of Surface-Treated Nanoparticles in Sedimentary Rocks”, **SPE 124418** presented at the **2009 SPE Annual Technical Conference and Exhibition**, New Orleans, LA, 4-7 October 2009.
2. Pourafshary, P., Azimipour, S. S., Motamedi, P., Samet, M., Taheri, S. A., Bargozin, H., and Hendi, S. S., “Priority Assessment of the Investment in Development of Nanotechnology in Upstream Petroleum Industry”, **SPE 126101** presented at the **2009 SPE Saudi Arabia Section Technical Symposium and Exhibition**, AlKhobar, Saudi Arabia, 9-11 May 2009.
3. Zhang, T., Davidson, A., Bryant, S. L., and Huh, C., “Nanoparticle-Stabilized Emulsions for Applications in Enhanced Oil Recovery”, **SPE 129885** presented at the **2010 SPE Improved Oil Recovery Symposium**, Tulsa, OK, 24-28 April 2010.
4. Saleh, N., Kim, H.-Y., Phenrat, T., Matuyjaszewski, K., Tildon, R. D., and Lowry, G. V., “Ionic Strength and Composition Affect the Mobility of Surface-Modified Fe⁰ Nanoparticles in Water-Saturated Sand Columns,” **Environmental Science and Technology**, Vol. 42, 3349 – 3355, 2008.
5. Krishanmoorti, R. 2006. “Extracting the Benefits of Nanotechnology for the Oil Industry.” **Journal of Petroleum Technology** (online) **58**:11.

6. Li, H., Xiao, H., Yuan, J., And Ou, J. 2004. "Microstructure of cement mortar with nano-particles." **Cement and Concrete Research** **34**: 435-438.
7. Agenet, N., Moradi-Tehrani, N., Tillement, T., "Fluorescent Nanobeads: A New Generation of Easily Detectable Water Tracers", **IPTC 15312** presented at the International Petroleum Technology Conference, Bangkok, Thailand, 7-9 February, 2012.
8. Greff, J. H., Babadagli, T., "Catalytic Effects of Nano-Size Metal Ions in Breaking Asphaltene Molecules During Thermal Recovery of Heavy-Oil", **SPE 146604** presented at the SPE Annual Technical Conference and Exhibition, Denver, CO, 30 October-2 November, 2011.
9. Huang, T., Crews, J., Willingham, J., "Nanoparticles for Formation Fines Fixation and Improving Performance of Surfactant Structure Fluids", **IPTC 12414** presented at the International Petroleum Technology Conference, Kuala Lumpur, Malaysia, 3-5 December, 2008.
10. Benamar, A., Ahfir, N-D., Wang, H.Q., and Alem, A., "Particle Transport in a Saturated Porous Medium: Pore Structure Effects", **C. R. Geoscience**, **339**, 674-681 (2007).
11. Wang, Y., Li, Y., Fortner, J.D., Hughes, J.B., Abriola, L.M., and Pennell, K.D., "Transport and Retention of Nanoscale C₆₀ Aggregates in Water-Saturated Porous Media", **Environ. Sci. Technol.**, **42**, 3588-3594, (2008a).
12. Shahavi, M.H., Jahanshahi, M., Najafpour, G.D., Ebrahimpour, M., and Hosenian, A.H., "Expanded Bed Retention of Biomolecules by NBG Contactor:

- Experimental and Mathematical Investigation”, **World Applied Sciences Journal**, **13(2)**, 181-187 (2011).
13. Alaskar, M., Ames, M., Connor, S., Liu, C., Cui, Y., Li, K., Horne, R., “Nanoparticle and Microparticle Flow in Porous and Fractured Media: An Experimental Study”, **SPE 146752** presented at the SPE Annual Technical Conference and Exhibition, Denver, CO, 30 October-2 November, 2011.
 14. Lecoanet, H., Wiesner, M., “Velocity Effects on Fullerene and Oxide Nanoparticle Deposition in Porous Media”, **Environ. Sci. Technol.**, **38**, 4377-4382, 2004.
 15. Caldelas, F., Murphy, M., Huh, C., Bryant, S., “Factors Governing Distance of Nanoparticle Propagation in Porous Media” **SPE 142305** presented at the SPE Production and Operations Symposium, Oklahoma City, OK, 27-29 March, 2011.
 16. Liu, X., Wazne, M., Christodoulatos, C., and Jasinkiewicz, K. L., “Aggregation and Deposition Behavior of Boron Nanoparticles in Porous Media”, **Journal of Colloid and Interface Science**, **330**, 90-96 (2009).
 17. Johnson, P.R., and Elimelech, M., “Dynamics of Colloid Deposition in Porous Media: Blocking Based on Random Sequential Retention”, **Langmuir**, **11**, 801-812 (1995).

VITA

Michael Murphy was born in Houston Texas, on August 25th of 1986. Upon graduating from Cypress Fairbanks Senior High School he enrolled at the University of Texas at Austin in 2005. He graduated with a Bachelor of Science in Petroleum Engineering in 2010. He chose to continue his education and work towards a Master of Science in Petroleum Engineering at the same university. He accepted a reservoir engineering position with Chevron in Houston, TX and expects to begin work the summer of 2012.

Permanent Address:

2803 Mid Lane, Unit F

Houston, TX, 77027

michaelmurphy@utexas.edu

This thesis was typed by the author.